



UNIVERSITÀ DEGLI STUDI DI TRIESTE

XXXII CICLO DEL DOTTORATO DI RICERCA IN FISICA

ASTRONOMIA E ASTROFISICA

Galactic Archaeology in the Era of Large Surveys

Dottorando:

Valeria GRISONI

Supervisore:

Prof. F. MATTEUCCI

F. Matteucci

Co-supervisore:

Dr. E. SPITONI

E. Spitoni

Coordinatore:

Prof. F. LONGO

F. Longo

ANNO ACCADEMICO 2018/2019



UNIVERSITÀ DEGLI STUDI DI TRIESTE

XXXII CICLO DEL DOTTORATO DI RICERCA IN FISICA

ASTRONOMIA E ASTROFISICA

Galactic Archaeology in the Era of Large Surveys

Dottorando:

Valeria GRISONI

Supervisore:

Prof. F. MATTEUCCI

Co-supervisore:

Dr. E. SPITONI

Coordinatore:

Prof. F. LONGO

ANNO ACCADEMICO 2018/2019

We are made of star-stuff.
We are a way for the universe to know itself.
(Carl Sagan)

Abstract

In this Thesis, we study Galactic Archaeology to understand the history of formation and chemical evolution of the Milky Way by means of new and detailed chemical evolution models in the light of the most recent data from Galactic surveys and missions. In recent years, many spectroscopic surveys and projects have been developed in order to study the formation and evolution of our Galaxy; moreover, Gaia mission is enhancing the value of these surveys. In this way, detailed stellar abundances of stars in the Milky Way can be measured. Then, by means of detailed chemical evolution models it is possible to predict the chemical abundances expected in the stars of each Galactic component: the halo, the thick and thin discs, and the bulge. The chemical evolution models follow the evolution of 34 chemical species from H up to Eu, and take into account detailed supernova progenitors and stellar nucleosynthesis. Infall and radial gas flows are also taken into account. From the comparison between data and model predictions, it is possible to reconstruct the history of star formation and in particular the timescales for the formation of each component, and thus the history of formation and evolution of the entire Galaxy, to which this Thesis is devoted.

In the first part of the Thesis, we study the Milky Way thick and thin discs in the solar neighbourhood, by developing detailed chemical evolution models and comparing them with data from the AMBRE Project. The evolution of the thick and thin discs is followed by means of two approaches: i) a two-infall approach where the thick disc forms via a fast episode of gas accretion and before the thin disc, whereas the thin disc forms by means of a second accretion episode on a longer timescale; ii) a new parallel approach,

where the two discs form in parallel but at different rates. By comparing our model results with the observed $[\text{Mg}/\text{Fe}]$ vs. $[\text{Fe}/\text{H}]$ and metallicity distribution functions in the two Galactic components, we conclude that both approaches can reproduce the observations, with the exception of a group of α -enhanced metal rich stars present in the data; in the parallel approach, these stars can be interpreted as metal-rich thick disc stars, whereas the two-infall approach cannot explain these stars unless they are the result of radial migration from the inner regions.

Then, we extend the analysis also to the other Galactocentric distances and we investigate abundance gradients along the Galactic thin disc. We consider the chemical evolution models for the Galactic disc developed in our previous work and we examine the processes which mainly influence the formation of abundance gradients: the inside-out scenario, a variable star formation efficiency, and radial gas flows. We compare our model results with recent abundance patterns obtained along the Galactic disc from the APOGEE survey and with abundance gradients observed from Cepheids, open clusters, HII regions and PNe. We conclude that the inside-out scenario is a key ingredient, but cannot be the only one to explain abundance patterns at different Galactocentric distances and abundance gradients. Further ingredients such as radial gas flows and variable star formation efficiency are needed to reproduce the observed features in the thin disc.

The formation and chemical evolution of the Galactic bulge is also discussed, with particular focus on the $[\text{Mg}/\text{Fe}]$ vs. $[\text{Fe}/\text{H}]$ relation, metallicity and age distribution functions. We first present a model assuming a fast and intense star formation. Then, we analyze the possibility of two distinct stellar populations in the bulge, as suggested by Gaia-ESO and APOGEE data. These two populations, one metal poor and the other metal rich, can have two different origins: i) the metal rich formed after a stop of ~ 250 Myr in the star formation rate of the bulge, or ii) the metal rich population is made of stars formed in the inner disc and brought into the bulge by the early secular evolution of the bar. We also examine the case of multiple star bursts in the bulge with consequent formation of multiple populations, as suggested by studies of microlensed stars. After comparing model results and observations, we suggest that the most likely scenario is that there are two

main stellar populations both made mainly by old stars (> 10 Gyr), with the metal rich and younger one formed from inner thin disc stars, in agreement with kinematical arguments. However, on the basis of dynamical simulations, we cannot completely exclude that the second population formed after a stop in the star formation during the bulge evolution, so that all the stars formed in situ.

Then, we investigate the Galactic evolution of lithium in the light of the most recent spectroscopic data from Galactic stellar surveys. We compare our model predictions with the most recent spectroscopic data for the Milky Way halo, discs and bulge. We analyse the various lithium producers and confirm that novae are the main source of lithium in the Galaxy, in agreement with other previous studies. We also focus on the decrease of lithium at high metallicity observed by several spectroscopic surveys, which still remains unexplained by theoretical models. By assuming that the fraction of binary systems giving rise to novae is lower at higher metallicity, we suggest a novel explanation to the lithium decline at super-solar metallicities: the above assumption is based on independent constraints on the nova system birthrate, that have been recently proposed in the literature. As regards to the thick disc, it is less lithium enhanced due to the shorter timescale of formation and higher star formation efficiency with respect to the thin disc and, therefore, we have a faster evolution and the reverse knee in the $A(\text{Li})$ vs. $[\text{Fe}/\text{H}]$ relation is shifted towards higher metallicities. We also present our predictions about lithium evolution in the Galactic bulge, that, however, still need further data to be confirmed or disproved.

Finally, we study the chemical evolution of Zr, La, Ce and Eu in the Galactic discs and bulge. We consider the chemical evolution models for the Galactic thick disc, thin disc and bulge, which have been already tested to reproduce the observed $[\alpha/\text{Fe}]$ vs. $[\text{Fe}/\text{H}]$ diagrams and metallicity distribution functions for the three different components, and we apply them to follow the evolution of neutron capture elements, which is still a topic of debate. In the $[\text{Eu}/\text{Fe}]$ vs. $[\text{Fe}/\text{H}]$ diagram, we observe and predict three distinct sequences corresponding to the thick disc, thin disc and bulge, similarly to what happens for the α -elements. We can nicely reproduce the three sequences by assuming different timescales of formation and star formation

efficiencies for the three different components, with the thin disc forming on a longer timescale of formation with respect to the thick disc and bulge. On the other hand, in the $[X/Fe]$ vs. $[Fe/H]$ diagrams for Zr, La and Ce, the three populations are mixed and also from the model point of view there is an overlapping between the predictions for the different Galactic components, but the observed behaviour can be also reproduced by assuming different star formation histories in the three components.

In conclusions, it is straightforward to see how different star formation histories can lead to different abundance patterns and looking at the abundance patterns of different chemical elements can help in constraining the history of formation and evolution of the main Galactic components. In particular, we suggest that the bulge formed the majority of its stars on a timescale of less than 1 Gyr, the thick disc formed also via a fast accretion episode and its timescale is irrespective of the Galactocentric distance, whereas the thin disc in the solar vicinity formed on a gas infall timescale of ~ 7 Gyr and inside-out.

Table of Contents

	Page
List of Tables	xi
List of Figures	xiii
List of Acronyms	xxiii
List of Publications	xxix
1 Introduction	1
1.1 The Milky Way	2
1.2 Galactic components	9
1.2.1 The halo	9
1.2.2 The bulge	11
1.2.3 The thin disc	12
1.2.4 The thick disc	13
1.3 Galactic archaeology	16
1.4 Goal and structure of the Thesis	21
2 Chemical evolution models	23
2.1 Fundamental ingredients	24

TABLE OF CONTENTS

2.1.1	Initial conditions	24
2.1.2	The stellar birthrate function	25
2.1.3	The stellar yields	27
2.1.4	Gas flows	29
2.2	Model equations	30
2.3	Models in literature	33
3	Chemical evolution of the thick and thin discs	45
3.1	Introduction	46
3.2	Observational data	49
3.3	The models	50
3.3.1	The revised two-infall model	50
3.3.2	The parallel model	52
3.3.3	Nucleosynthesis prescriptions	53
3.4	Results	54
3.4.1	Abundance patterns	57
3.4.2	Metallicity distribution functions	63
3.4.3	Solar abundances	65
3.4.4	Star formation history	65
3.4.5	Supernova rates	68
3.5	Conclusions	69
4	Abundance gradients along the Galactic disc	75
4.1	Introduction	76
4.2	Observational data	80
4.3	The models	81
4.3.1	Implementation of radial inflows	83
4.4	Model results	86

TABLE OF CONTENTS

4.4.1	Abundance patterns	90
4.4.2	Present-day gradients	93
4.4.3	Time evolution of the gradients	95
4.5	Conclusions	100
5	Chemical evolution of the Galactic bulge	103
5.1	Introduction	104
5.2	Observational data	107
5.3	The models	107
5.4	Results	109
5.4.1	Abundance patterns and MDFs	109
5.4.2	Multiple stops in the star formation	118
5.4.3	Age distribution	119
5.5	Conclusions	123
6	Galactic lithium evolution	129
6.1	Introduction	130
6.2	Observational data	133
6.3	Models	135
6.3.1	Model equations	135
6.3.2	Nucleosynthesis prescriptions	138
6.4	Results	140
6.4.1	The Galactic halo	141
6.4.2	The Galactic disc(s)	143
6.4.3	The Galactic bulge	148
6.5	Conclusions	150
7	Neutron capture elements	153
7.1	Introduction	154

TABLE OF CONTENTS

7.2	Observational data	156
7.3	The models	158
7.3.1	Model equations	159
7.3.2	Nucleosynthesis prescriptions	160
7.4	Comparison between data and model predictions	163
7.4.1	Comparison for Eu	164
7.4.2	Comparison for Zr, La and Ce	168
7.5	Conclusions	169
8	Final remarks	173
8.1	Summary and conclusions	174
8.2	Future prospects	185
	Bibliography	189
	Curriculum vitae	215
	Acknowledgements	217

List of Tables

Table	Page
1.1 Properties of the Galactic components.	10
3.1 Input parameters for the chemical evolution models of the Galactic thick and thin discs (Grisoni et al. 2017).	55
3.2 Solar abundances (Grisoni et al. 2017).	65
4.1 Input parameters for the models of the study on abundance gradients along the Galactic thin disc (Grisoni et al. 2018). . .	81
5.1 Input parameters for the chemical evolution models of the Galactic bulge (Matteucci, Grisoni et al. 2019).	110
6.1 Input parameters for the chemical evolution models of the study on Galactic lithium evolution (Grisoni et al. 2019).	137
7.1 Input parameters for the chemical evolution models of the study on neutron capture elements (Grisoni et al. 2020).	158

List of Figures

Figure	Page
1.1 The band of the Milky Way seen with the ESO 3.6-metre telescope at La Silla. Image credit to: Y. Beletsky (LCO)/ESO. . .	2
1.2 The Hubble sequence, originally suggested by Hubble (1926). Image credit to: http://www.physast.uga.edu	7
1.3 Schematic view of the main components of the Milky Way (Chiappini 2001).	8
1.4 <i>Upper panel:</i> Observed $[\alpha/\text{Fe}]$ vs. $[\text{Fe}/\text{H}]$ distribution for the solar neighbourhood from APOGEE Survey (Hayden et al. 2015). The left panel shows only 20% of the observed data points in the solar circle, whereas the right panel shows the entire sample in the solar neighbourhood with contours corresponding to 1, 2 and 3σ of the overall densities. The typical uncertainties in the abundances are shown at the bottom of the panel. <i>Lower panel:</i> Stellar distribution of stars in the $[\alpha/\text{Fe}]$ vs. $[\text{Fe}/\text{H}]$ plane as a function of R and $ z $ from APOGEE Survey (Hayden et al. 2015). The typical uncertainties in the abundances are shown as a function of metallicity across the bottom of each panel. . . .	15

LIST OF FIGURES

2.1	Star formation rate as a function of time in the two-infall model (Chiappini et al. 1997).	34
2.2	SN rates as functions of time in the two-infall model (Chiappini et al. 1997).	34
2.3	[X/Fe] vs. [Fe/H] relations for elements from C to Zn in the solar neighbourhood predicted by the two-infall model of Romano et al. (2010).	35
2.4	Star formation rate as a function of time in the three-infall model (Micali et al. 2013).	39
2.5	SN rates as functions of time in the three-infall model (Micali et al. 2013).	39
2.6	Predicted $[\alpha/\text{Fe}]$ vs. $[\text{Fe}/\text{H}]$ relations for the Galactic bulge (up- per curve), the solar neighbourhood (median curve) and irregular galaxies (lower curve). Data for the bulge are shown for com- parison. Data for the LMC and DLA systems are also reported. Figure from Matteucci (2012).	43

- 3.1 Predicted and observed $[\text{Mg}/\text{Fe}]$ vs. $[\text{Fe}/\text{H}]$ in the solar neighbourhood in the case of the two-infall model. The data are from the AMBRE Project and the different Galactic components are plotted: thin disc (grey dots), thick disc (red dots), metal-rich high- α sequence (blue dots), metal-poor low- α sequence (green dots), metal poor high- α sequence (magenta). *Upper left panel:* the effect of varying the IMF. The 2IM with Kroupa et al. (1993) IMF (green line) is compared with a model with Scalo (1986) IMF (light-blue line) and Salpeter (1955) IMF (orange line). *Lower left panel:* the effect of varying the star formation efficiency of the thick disc. The 2IM with $\nu_1 = 2 \text{ Gyr}^{-1}$ (green line) is compared with a model with $\nu_1 = 1 \text{ Gyr}^{-1}$ (light-blue line) and $\nu_1 = 3 \text{ Gyr}^{-1}$ (orange line). *Upper right panel:* the effect of varying the timescale of the thick disc. The 2IM with $\tau_1 = 0.1 \text{ Gyr}$ (green line) is compared with a model with $\tau_1 = 0.5 \text{ Gyr}$ (light-blue line) and $\tau_1 = 1 \text{ Gyr}$ (orange line). *Lower right panel:* the effect of varying the threshold. The 2IM with $\sigma_{th} = 7 \text{ M}_\odot \text{ pc}^{-2}$ (green line) is compared with a model with $\sigma_{th} = 4 \text{ M}_\odot \text{ pc}^{-2}$ (light-blue line) and $\sigma_{th} = 10 \text{ M}_\odot \text{ pc}^{-2}$ (orange line). 58
- 3.2 Predicted and observed $[\text{Mg}/\text{Fe}]$ vs. $[\text{Fe}/\text{H}]$ in the solar neighbourhood in the case of the two-infall model. The data are from the AMBRE Project and the different Galactic components are plotted: thin disc (grey dots), thick disc (red dots), metal-rich high- α sequence (blue dots), metal-poor low- α sequence (green dots), metal poor high- α sequence (magenta). The predictions are from model 2IM (green line). 59

3.3	Predicted and observed $[\text{Mg}/\text{Fe}]$ vs. $[\text{Fe}/\text{H}]$. The data are color-coded according to their guiding radius (inner, solar, outer) and the predictions are from model 2IM (both at 8 kpc and at 4 kpc).	59
3.4	Same as Fig. 3.2, but the predictions are for models 1IMT for the thick disc (black line) and 1IMt for the thin disc (magenta line).	60
3.5	<i>Left panel:</i> Predicted and observed metallicity distribution function of the thick disc in the case of the two-infall model. The data are from the AMBRE Project: MDF of thick disc stars (red) and MDF of MRHA stars (blue). The predictions are from model 2IM (green line). We notice that the two-infall model cannot reproduce the MRHA stars, as explained in the text. <i>Right panel:</i> Predicted and observed metallicity distribution function of the thin disc in the case of the two-infall model. The data are from the AMBRE Project: MDF of thin disc stars (grey). The predictions are from model 2IM (green line).	61
3.6	Same as Fig. 3.5, but the predictions are for models 1IMT for the thick disc (black line) and 1IMt for the thin disc (magenta line). We notice that in this case in the left panel the MDF of thick plus MRHA stars is considered, since the one-infall model of the thick disc can reproduce also the MRHA stars.	61
3.7	Temporal evolution of the SFR, as predicted by model 2IM.	66
3.8	Temporal evolution of the SFR. <i>Red line:</i> prediction of model 1IMT. <i>Green line:</i> prediction of model 1IMt.	66
3.9	Temporal evolution of the SN rates, as predicted by model 2IM. <i>Red line:</i> SNII rates predicted by model 2IM. <i>Green line:</i> SNIa rates predicted by model 2IM.	70

3.10	Temporal evolution of the SN rates. <i>Red line</i> : SNII rates predicted by model 1IMT. <i>Green line</i> : SNII rates predicted by model 1IMt. <i>Blue line</i> : SNIa rates predicted by model 1IMT. <i>Magenta line</i> : SNIa rates predicted by model 1IMt.	70
4.1	Scheme of the gas flow through the k -th shell (Portinari & Chiosi 2000).	84
4.2	Time evolution of the SFR, as predicted by the model 2IM A at various Galactocentric distances.	87
4.3	Predicted abundance patterns of $[\text{Mg}/\text{Fe}]$ vs. $[\text{Fe}/\text{H}]$ in the solar neighbourhood for the two scenarios, the two-infall (upper panel) and the parallel (lower panel).	88
4.4	Observed and predicted abundance patterns of $[\text{Mg}/\text{Fe}]$ vs. $[\text{Fe}/\text{H}]$. The data are from Hayden et al. (2015) and are divided as follows: 3-7 kpc (upper panel), 7-11 kpc (middle panel), 11-15 kpc (lower panel). The predictions are from model 2IM A (light-blue line), 1IM A (green line), 1IM B (blue line), 1IM C (red line) and 1IM D (magenta line) computed at different Galactocentric distances: 4 kpc (upper panel), 8 kpc (middle panel), 14 kpc (lower panel).	89
4.5	Observed and predicted radial abundance gradient for magnesium from Cepheids and young open clusters. The data are from Luck & Lambert 2011 (light-blue dots) and Genovali et al. 2015 (blue dots) for Cepheids, and from Magrini et al. 2017 (black squares) for young open clusters. The predictions are from model 1IM A (green line), 1IM B (blue line), 1IM C (red line) and 1IM D (magenta line), and also 1IM A0 which is the same as 1IM A but with a more extreme law for the inside-out, see text (black line).	93

4.6	Observed and predicted radial abundance gradient for oxygen from HII regions and young planetary nebulae. The data are from Deharveng et al. 2000 (gray dots), Esteban et al. 2005 (violet dots), Rudolph et al. 2006 (blue dots), Balser et al. 2015 (light-blue dots) for HII regions, and from Stanghellini & Haywood 2018 (black squares) for young PNe. The predictions are from model 1IM A (green line), 1IM B (blue line), 1IM C (red line) and 1IM D (magenta line).	96
4.7	Time evolution of the radial abundance gradient for magnesium. The data are from Anders et al. (2017) and are divided in age bins as follows: younger than 1 Gyr (upper panel), between 1 and 7.5 Gyr (middle panel), older than 7.5 Gyr (lower panel). The predictions are from model 2IM A (light-blue line), 1IM A (green line), 1IM B (blue line), 1IM C (red line) and 1IM D (magenta line) computed at the various times.	97
4.8	Time evolution of the radial abundance gradient for oxygen. The data are from Stanghellini & Haywood (2018) and are divided in age bins as follows: younger than 1 Gyr (upper panel) and older than 7.5 Gyr (lower panel). The predictions are from model 2IM A (light-blue line), 1IM A (green line), 1IM B (blue line), 1IM C (red line) and 1IM D (magenta line) computed at the various times.	98
5.1	<i>Upper panel:</i> Predicted $[\text{Mg}/\text{Fe}]$ vs. $[\text{Fe}/\text{H}]$ in the Galactic bulge, in the case of Model A (black continuous line), compared with Gaia-ESO data as in Rojas-Arriagada et al. (2017). <i>Lower panel:</i> Predicted MDF in the Galactic bulge for Model A compared with Gaia-ESO data.	111

- 5.2 *Upper left panel:* Predicted $[\text{Mg}/\text{Fe}]$ vs. $[\text{Fe}/\text{H}]$ in the Galactic bulge, in the case of Models A, B, C, D and E with no-stop and stops in the star formation of 50, 150, 250 and 350 Myr, respectively, compared to Gaia-ESO data. *Upper right panel:* Predicted MDF in the Galactic bulge for Models A, B, C, D and E compared with Gaia-ESO data. As one can see, longer is the stop in star formation and deeper is the dip between the two populations. The model which best reproduces the data is Model D with a stop of 250 Myr. *Lower panel:* a density plot for the Gaia-ESO data compared to the results of Model D. 112
- 5.3 Predicted MDF in the Galactic bulge for Models A (black continuous line) and H (inner disc population, blue dashed line) compared with Gaia-ESO data. The two peaks, in this case, should be due to the bulge and inner disc populations, respectively. 113
- 5.4 *Left panel:* Predicted MDF in the Galactic bulge for Model A* (black continuous line) compared with APOGEE data. *Right panel:* Density plot relative to the APOGEE data for $[\text{Mg}/\text{Fe}]$ vs. $[\text{Fe}/\text{H}]$ in the Galactic bulge. 113
- 5.5 *Left panel:* Predicted $[\text{Mg}/\text{Fe}]$ vs. $[\text{Fe}/\text{H}]$ in the Galactic bulge, in the case of Model A* (black continuous line) and Model H (blue dashed line) compared to APOGEE data. *Right panel:* Predicted MDF in the Galactic bulge for Model A* and Model H compared with APOGEE data. 114

5.6	<i>Left panel:</i> Predicted $[\text{Mg}/\text{Fe}]$ vs. $[\text{Fe}/\text{H}]$ in the Galactic bulge, in the case of Model A* (black continuous line) and Model G (Calamida et al. 2015 IMF, green line almost overlapping the black continuous line) and compared with APOGEE data. <i>Right panel:</i> Predicted MDF in the Galactic bulge for Model A* and G compared with APOGEE data.	114
5.7	<i>Upper left panel:</i> SFR as a function of time, predicted by Model F. <i>Upper right panel:</i> Predicted and observed MDF. The predictions are from Model F, the data are from Bensby et al. (2017). <i>Lower middle panel:</i> Predicted and observed $[\text{Mg}/\text{Fe}]$ vs. $[\text{Fe}/\text{H}]$ in the Galactic bulge, in the case of Model F compared to the data of Bensby et al. (2017). The data are shown as a density plot. . .	120
5.8	Age distribution predicted by the various models, compared to the observational data. <i>Upper panel :</i> we show the results of Model A with continuous star formation compared to the data of Schultheis et al. (2017)(deep green distribution): the pink distribution represents the theoretical predictions at a face value, while the light green distribution is the theoretical one after being convolved with the observational errors; <i>Middle panel:</i> we show the results of Model D, the colors of the distributions have the same meaning as described for the previous panel; <i>Lower panel:</i> we show the results of Model A and model H together, convolved with the observational errors. The colors of the distributions have the same meaning as described for the previous panels. . .	124
5.9	Age distribution as predicted by Model F and corrected by the age errors (light green histogram), as described in the text, compared with data of Bensby et al. (2017) (purple histogram).	125

6.1	<i>Left panel:</i> Observed and predicted lithium abundance as a function of metallicity in the solar neighbourhood. The predictions are from the two-infall model (blue line). The data are from Charbonnel & Primas (2005) (orange dots), Sbordone et al. (2010) (yellow dots) and from Gaia-ESO Survey (Fu et al. 2018) for the thick disc (green dots) and thin disc (purple dots). The meteoritic value is the one by Lodders et al. (2009) (light-blue square). <i>Right panel:</i> Same as the left panel, when a high-primordial Li abundance is adopted.	136
6.2	<i>Left-hand upper panel:</i> Observed and predicted lithium abundance as a function of metallicity for thick- and thin-disc stars in the solar neighbourhood. The predictions are from the parallel model for the thick (green line) and thin disc (purple line). The data are from Gaia-ESO Survey (Fu et al. 2018) for the thick disc stars (green dots) and thin disc stars (purple dots). The meteoritic value is the one by Lodders et al. (2009) (light-blue square). <i>Right-hand upper panel:</i> same as the left panel, but with AMBRE data (Guiglion et al. 2016) for the thick disc stars (green dots) and thin disc stars (purple dots). <i>Lower panels:</i> same as the corresponding upper panels, but when the contribution from massive stars is taken into account.	139
6.3	Predicted lithium abundance as a function of metallicity for the thin disc, where the various lithium sources are isolated. The predictions are from the parallel model for the thin disc with all the sources (purple line), only novae (blue line), only GCR (light blue line), only AGB (orange line) and only astration (red line). The meteoritic value is the one by Lodders et al. (2009) (light-blue square).	141

6.4	<i>Left panel:</i> Observed and predicted lithium abundance as a function of metallicity for the thin disc in the case with variable fraction of binary systems giving rise to novae. The predictions are from the parallel model for the thin disc with constant α (purple line) and with different variable α laws. The data are from Gaia-ESO Survey (Fu et al. 2018) for the thick disc stars (green dots) and thin disc stars (purple dots). The meteoritic value is the one by Lodders et al. (2009) (light-blue square). <i>Right panel:</i> same as the left panel, but with AMBRE data (Guiglion et al. 2016) for the thick disc stars (green dots) and thin disc stars (purple dots).	144
6.5	Observed and predicted lithium abundance as a function of metallicity in the Galactic bulge. The predictions are from the model of the Galactic bulge of Matteucci et al. (2019). The data of bulge stars are from Gonzalez et al. (2009) (orange dots) and Bensby et al. (2011) (blue dots, with the two bigger dots corresponding to the two stars which have $T_{eff} > 5900$ K). . .	149
7.1	Observed and predicted $[\text{Eu}/\text{Fe}]$ vs. $[\text{Fe}/\text{H}]$. The predictions are from the reference models for the Galactic thin disc (blue line), thick disc (red line) and bulge (green line). The data are for the Galactic thin disc stars (blue dots), thick disc stars (red dots) and bulge stars (green dots), and they are taken from Forsberg et al. (2019).	163
7.2	Same as Fig. 7.1, but for Zr.	164
7.3	Same as Fig. 7.1, but for La and Ce.	165

List of Acronyms

In this Thesis, many acronyms will be used. Here, I provide their complete list.

- 1IM (One-infall model)
- 2IM (Two-infall model)
- AGB (Asymptotic giant branch)
- AMBRE (Archéologie avec Matisse Basée sur les aRchives de l'ESO)
- APOGEE (Apache Point Observatory Galactic Evolution Experiment)
- B/P (Boxy/Peanut)
- CC SN (Core-collapse supernova)
- CMD (Colour-magnitude diagram)
- CoRoT (Convection, Rotation, and planetary Transits)
- CO WD (Carbon-oxygen white dwarf)
- DD (Double degenerate)
- DLA (Damped-Lyman Alpha)

LIST OF ACRONYMS

- DR (Data Release)
- DTD (Delay time distribution)
- EC SN (Electron-capture supernova)
- ESO (European Southern Observatory)
- ESPaDOnS (Echelle SpectroPolarimetric Device for the Observation of Stars)
- FEROS (Fiber-fed Extended Range Optical Spectrograph)
- FIES (Fiber-fed Echelle Spectrograph)
- FLAMES (Fibre Large Array Multi Element Spectrograph)
- Gaia (Global astrometric interferometer for astrophysics)
- GALAH (Galactic Archaeology with HERMES)
- GALEX (Galaxy evolution explorer)
- GCE (Galactic chemical evolution)
- GCR (Galactic cosmic ray)
- GIBS (GIRAFFE Inner Bulge Survey)
- HARPS (High Accuracy Radial velocity Planet Searcher)
- HST (Hubble space telescope)
- IMF (Initial mass function)
- ISM (Interstellar medium)

-
- LAMOST (Large sky area multi-object fibre spectroscopic telescope)
 - LIMS (Low and intermediate mass stars)
 - LMC (Large magellanic cloud)
 - LTE (Local thermodynamic equilibrium)
 - MCMC (Markov Chain Monte Carlo)
 - MDF (Metallicity distribution function)
 - MOONS (Multi Object Optical and Near-infrared Spectrograph for the VLT)
 - MP (Metal poor)
 - MR (Metal rich)
 - MRD SN (Magneto-rotationally driven supernova)
 - MRHA (Metal rich high alpha)
 - NLTE (Nonlocal thermodynamic equilibrium)
 - NOT (Nordic Optical Telescope)
 - NSM (Neutron star merger)
 - OC (Open cluster)
 - OPPNe (Planetary nebulae whose progenitor stars are older than 7.5 Gyr)
 - PN (Planetary nebula)

LIST OF ACRONYMS

- RAVE (Radial velocity experiment)
- RGB (Red giant branch)
- RVS (Radial velocity spectrometer)
- SBBN (Standard Big Bang nucleosynthesis)
- SD (Single degenerate)
- SEGUE (Sloan extension for galactic understanding and exploration)
- SMC (Small magellanic cloud)
- SME (Spectroscopy Made Easy)
- SFE (Star formation efficiency)
- SFR (Star formation rate)
- SN (Supernova)
- SNIa (Supernova Type Ia)
- SNII (Supernova Type II)
- TGAS (Tycho-Gaia Astrometric Solution)
- UVES (Ultraviolet and Visual Echelle Spectrograph)
- VLT (Very large telescope)
- VVV (Vista Variables in the Via Lactea)
- WD (White dwarf)

-
- WMAP (Wilkinson microwave anisotropy probe)
 - YPPNe (Planetary nebulae whose progenitor stars are younger than 1 Gyr)

List of Publications

This Thesis is the result of the research activity that I have carried out during my PhD at the University of Trieste, under the supervision of prof. Francesca Matteucci. The work accomplished during my PhD yielded the following publications, on which part of the Thesis is based.

REFEREED PUBLICATIONS

- **The AMBRE Project: chemical evolution models for the Milky Way thick and thin discs**
Grisoni, V., Spitoni, E., Matteucci, F., Recio-Blanco, A., de Laverny, P., Hayden, M., Mikolaitis, S., Worley, C. C. 2017, MNRAS, 472, 3637
- **Abundance gradients along the Galactic disc from chemical evolution models**
Grisoni, V., Spitoni, E., & Matteucci, F. 2018, MNRAS, 481, 2570
- **Evolution of lithium in the Milky Way halo, discs and bulge**
Grisoni, V., Matteucci F., Romano D., Fu X., 2019, MNRAS, 489, 3539
- **Galactic Archaeology with asteroseismic ages: evidence for delayed gas infall in the formation of the Milky Way disc**

LIST OF PUBLICATIONS

Spitoni, E., Silva Aguirre, V., Matteucci, F., Calura, F., & Grisoni, V. 2019, A&A, 623, A60

- **The origin of stellar populations in the Galactic bulge from chemical abundances**

Matteucci, F., Grisoni, V., Spitoni E., Zulianello A., Rojas-Arriagada A., Schultheis M., Ryde N., 2019, MNRAS, 487, 5363

- **Modelling the chemical evolution of Zr, La, Ce and Eu in the Galactic discs and bulge**

Grisoni, V., Cescutti G., Matteucci F., Forsberg R., Jönsson H., Ryde N., 2020, MNRAS, 492, 2828

CONFERENCE PROCEEDINGS

- **Highlights in the Milky Way**

Matteucci, F., Spitoni, E., & Grisoni, V. 2018, Rediscovering Our Galaxy, 334, 298

- **Lithium and the chemical evolution of the Milky Way**

Matteucci, F., Grisoni, V., Romano, D., 2020, to appear in Memorie della Società Astronomica Italiana

- **Evolution of lithium in the Galactic discs**

Grisoni, V., Matteucci, F., Romano, D., Fu, X., 2020, to appear in Memorie della Società Astronomica Italiana

Introduction

Galactic archaeology (or others say Galactic palaeontology) studies the history of formation and evolution of our Galaxy, the Milky Way. In this first Chapter, I outline the framework in which this Thesis fits. First, I give a general introduction about the Milky Way. Starting from the historical overview about our knowledge of the Milky Way, I will describe the Galaxy as we know it now and its main Galactic components: the halo, the thick disc, the thin disc, and the bulge. Finally, I present the goal of this Thesis in this context. In successive Chapters, I will deal with more technical details about the observational data considered in this work and the chemical evolution models developed, to finally deal with the results and the conclusions of the Thesis. Now, let us start with the introductory background.



Figure 1.1: The band of the Milky Way seen with the ESO 3.6-metre telescope at La Silla. Image credit to: Y. Beletsky (LCO)/ESO.

1.1 THE MILKY WAY

During the night, it may be possible to see a nebulous band of light arching across the sky: this is the Milky Way (see Fig. 1.1).

The name Milky Way comes from its appearance as a faint sparkling band stretching across the sky, whose individual stars cannot be distinguished by naked eye. The term is used both for the aforementioned phenomenon in the sky and for the large stellar system causing it. The Milky Way system is also called the Galaxy, with capital letter. The general term galaxy is used to refer to the other stellar systems, similar to our Milky Way. The

band of the Milky Way extends round the whole celestial sphere. It is a huge system consisting mostly of stars, among them the Sun. The stars of the Milky Way form a flattened disc-like system. In the direction of the plane of the disc, large numbers of stars are visible, whereas relatively few stars are seen in the perpendicular direction. The faint light of distant stars merges into a uniform glow, and for this reason the Milky Way appears as a nebulous band to the naked eye.

Throughout centuries, the sight of the Milky Way has inspired several interpretations. The first suggestions about its nature regards magical and mythological conceptions. The term Milky Way is a translation of the latin *Via Lactea*, from the ancient Greek γαλαξίας κύκλος (*galaxías kýklos*, i.e. milky circle). The word Galaxy comes from γάλα, which is the Greek word for milk, in reference to the myth according to which the Milky Way formed because of the milk lost by goddess Hera while she was breastfeeding Heracles. However, in ancient times, the Milky Way has been considered in different ways by many different cultures. For example, it was the Nile in the sky for ancient Egyptians, the heavenly river for the Incas or the tree of the world for the Mayan.

In 1610, the first scientific study of the physical nature of our Galaxy was done by Galileo, who performed the first telescopic observations of the Milky Way and discovered that it could be resolved into a myriad of faint stars. Consequently, it was clear that the diffuse light of the Milky Way could no longer be interpreted as due to a concentration of some sort of celestial fluid and the status of the Milky Way as a stellar system was definitively established.

In the eighteenth century, Thomas Wright and Immanuel Kant gave a description of our Galaxy consisting of a disc of stars in which the Sun is immersed. Kant pointed out also that our Galaxy might not be the only one

in the Universe and that similar systems, which he called island universes, might be distributed throughout space at large distances from our system. At the end of the eighteenth century, William Herschel performed telescopic observations in order to determine the spatial distribution of stars in the Milky Way. In particular, he counted the number of stars per magnitude interval in several directions of the sky. He assumed that all the stars have the same intrinsic luminosity, the stars are uniformly distributed in the Galaxy, all the stars are observable until the edges of the system and there is not any source of dimming of the star light, i.e. interstellar extinction. Thus, he proposed his famous map of the Milky Way stellar distribution. In his picture, the Galaxy is a flattened system with a diameter about five times larger than its thickness and with the Sun close to the center. He could not determine absolute dimensions for the system given the unavailability of distance standards to calibrate his method. Later on, he realized that there were some problems in his model. First, he was conscious of the possibility that the stars did not have an intrinsic constant luminosity, as assumed. A second problem arose when he repeated star counts with a larger telescope. In fact, the fainter he went, the more stars he counted. For these reasons, Herschel himself lost faith in his large scale star distribution model.

In 1922, Jacobus Cornelius Kapteyn proposed a new model of the distribution of stars in space. His approach was rather similar to the star-gaging of Herschel, and thanks to the advent of photography Kapteyn used photographic star counts of selected areas distributed over the sky. Moreover, he estimated distances based on parallaxes and proper motions of nearby stars. He concluded that the Galaxy is a flattened stellar system of 1500 pc thick and 8 times this size in the plane, with the Sun located slightly off from the center. He reached this conclusion from the fact that the star density was considered to decrease uniformly away from the center of the system.

However, he realized that there could also be an alternative explanation for his data for which the Sun was not near the center. In fact, if there was an absorbing interstellar medium, then the stellar light would suffer extra dimming. If this dimming is incorrectly interpreted as a distance effect, then the distances of stars would be wrong, leading to an artificial decrease of the star density in all directions away from the observer and thus producing the impression of being at the center. However, he was unable to give any evidence for such absorption, that remained to be discovered.

Around the same period, Harlow Shapley followed a different approach and focused on globular clusters. Globular clusters are compact spherical systems containing from 10^5 to 10^6 stars and thanks to their great brightness they can be observed at very great distance from the Sun. Furthermore, since they lie above the Galactic plane, they do not suffer much interstellar extinction. Shapley found that the globular clusters are distributed uniformly above and below the plane, but they are not distributed uniformly around the plane. Therefore, he concluded that, if these systems are major constituents of the Galaxy and are symmetrically distributed around the Galactic center, then the Sun should not be in that center. He estimated that the radius of the distribution of globular clusters should be 100 kpc from the Galactic center and that the Sun should be at about 18 kpc from the Galactic center. The conclusion that the Sun is located far away from the Galactic center is indeed correct as it has been shown by all subsequent studies, even if now we estimate that Sun's distance from the Galactic center is only about 8 kpc¹. However, by not considering the interstellar extinction, Shapley believed that the Galaxy was a unique system, at least in the part of Universe accessible to observations. In fact, the dimensions of the Galaxy found by Shapley were

¹Sun's distance from the Galactic center $R_0=8.2\pm0.1$ kpc (Bland-Hawthorn & Gerhard 2016, and references therein).

ten times larger than what Kapteyn had suggested and most astronomers had believed. If the spiral nebulae external to our Galaxy, whose nature was still unknown, had the same dimensions as Shapley's Galaxy, then they would have been unconceivably distant. For this reason, many astronomers did not believe in Shapley's ideas. In 1920, a famous debate on the size of the Galaxy and the nature of the spiral nebulae occurred between Heber Curtis and Harlow Shapley during the annual meeting at the National Academy of Sciences in Washington.

In the following years, between 1920 and 1930, the issue was finally settled thanks to Edwin Hubble, Jan Oort and Bertil Lindblad. The main discovery of Oort and Lindblad was Galactic rotation: the Sun belongs to a rapidly rotating system and moves on a circular orbit around the Galactic center at a velocity of the order of $200\text{-}300\text{ km s}^{-1}$. Moreover, Oort suggested that the Galactic rotation is differential: the rotation velocity changes with the distance from the Galactic center, with faster angular rotation near the center and slower near the edge. Meanwhile, Edwin Hubble resolved the outer regions of two nearby spirals M31 and M33, and showed that the distances to the spiral nebulae were about 285000 pc. These distances are large enough to conclude that the spirals must be stellar systems as large as our own Galaxy. Therefore, Kapteyn's Universe had been substituted and our Galaxy had become part of the spiral nebulae, showing that Kant's intuition about the island universes was indeed correct. In 1926, Hubble suggested its famous morphological classification scheme for galaxies and proposed the so-called Hubble sequence (see Fig. 1.2).

In 1944, Walter Baade gave new insights into the study of galaxies, when he resolved into stars the nucleus of M31, its companions M32 and NGC205, and the ellipticals NGC147 and NGC185. He found that the brightest stars in these systems were really different from the luminous blue

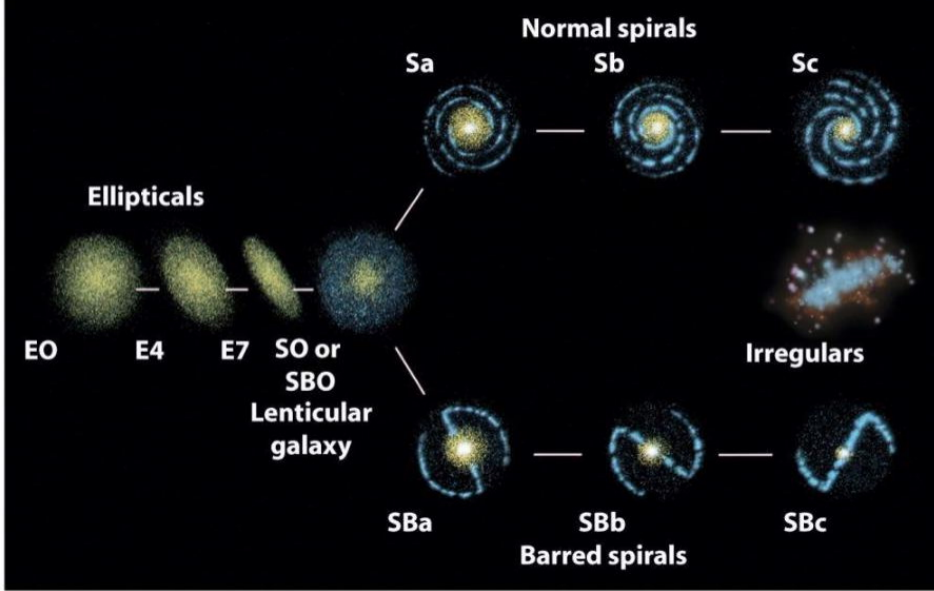


Figure 1.2: The Hubble sequence, originally suggested by Hubble (1926). Image credit to: <http://www.physast.uga.edu>.

stars in the spiral arms. Thus, he suggested that the stars in a galaxy could be categorized into different populations. He identified two different stellar populations: population I and population II. Population I represents the blue stars associated with spiral arms, whereas population II represents the red stars found in spheroidal components of galaxies such as bulges, halos and globular clusters. In 1978, another population known as population III has been added. At the present time, stellar populations are categorized as I, II and III, with each group having decreasing metal content Z^2 and increasing

² Z corresponds to the metallicity, i.e. the sum of all the abundances of the elements heavier than helium.

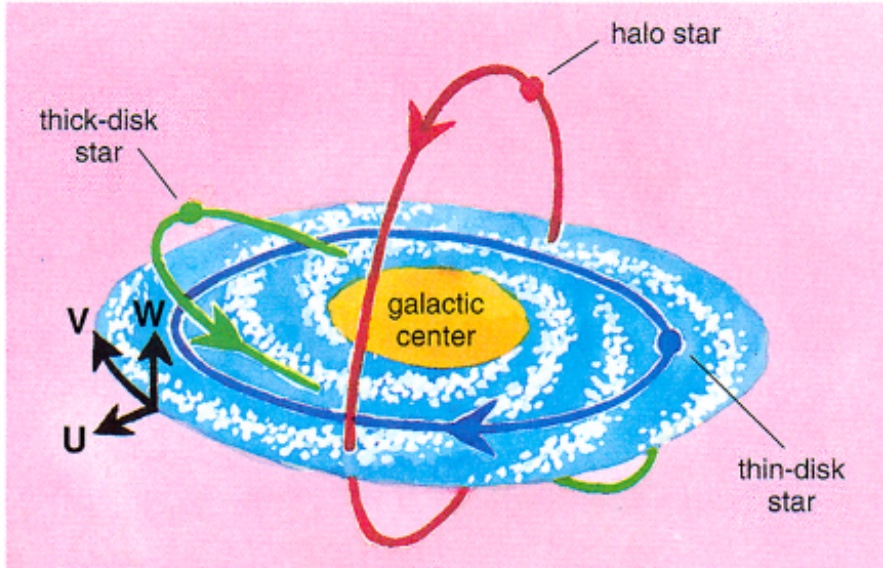


Figure 1.3: Schematic view of the main components of the Milky Way (Chiappini 2001).

age. The populations were named in the order they were discovered, which is the reverse of the order in which they were formed. Thus, the first stars in the Universe (zero metal content) are population III, the stars formed immediately after (low metal content) are population II, and recent stars (high metallicity) are population I. The concept of stellar populations has been fundamental because it inspired stellar evolution and star formation studies, which are tightly related to the studies of how galaxies form and evolve.

1.2 GALACTIC COMPONENTS

The Milky Way as we know it now is a gravitationally bound system of stars, gas, dust and dark matter. According to its global morphology, it is classified as a SBbc galaxy, namely a spiral barred galaxy in the Hubble classification (see Fig. 1.2). The Milky Way stellar content³ is given by the spatial arrangement of many different components, which were likely assembled into the system at different epochs and with different timescales during the formation and evolution of the Galaxy. The characteristics of the stellar content in each one of these components are closely related to the concept of stellar populations, that as mentioned in the previous Section was first introduced by Baade (1944). In Fig. 1.3, I show the main components of the Milky Way, which differ on the basis of chemical and kinematical criteria and they can be described as follows (see Table 1.1 for a summary of the main properties of the different Galactic components).

1.2.1 THE HALO

Here, I discuss the stellar halo, distinguishing it from the dark matter halo, which is supposed to surround and dominate the mass content of the Galaxy. The stellar halo comprehends about 1% of the Galactic stellar content, including globular cluster and field stars (the total stellar halo mass is $M = 4 - 7 \cdot 10^8 M_{\odot}$, Bland-Hawthorn & Gerhard 2016 and references therein). The halo stars constitute an extended spheroidal distribution, supported by random motions in eccentric orbits and with just a small possible net rotation. Essentially, all these stars are older than 10 Gyr (Snedden et al. 1996, Cayrel et al. 2001, Hill et al. 2002, Frebel et al. 2007, Helmi 2008). The halo stars are metal-poor (the local halo metallicity distribution is peaked

³The total stellar mass of the Galaxy is $M = 5 \pm 1 \cdot 10^{10} M_{\odot}$, Bland-Hawthorn & Gerhard 2016 and references therein.

CHAPTER 1. INTRODUCTION

Table 1.1: Properties of the Galactic components. In the first column, there is the considered Galactic component: the stellar halo, the thick and thin discs, and the bulge. In the second column, there is the stellar mass of each component in M_{\odot} (Bland-Hawthorn & Gerhard 2016 and references therein). In the third column, we write the age in Gyr (Helmi 2008 and references therein for the stellar halo, Haywood et al. 2013 for the discs, Barbuy et al. 2018 for the bulge). In the fourth, there is the metallicity (Helmi 2008 and references therein for the stellar halo, Hayden et al. 2015 for the discs, Barbuy et al. 2018 for the bulge). In the last column, we give information about the density profile of each Galactic component (Bland-Hawthorn & Gerhard 2016 and references therein).

	Mass (M_{\odot})	Age (Gyr)	[Fe/H] (dex)	Density profile
Stellar halo	$4 - 7 \cdot 10^8$	>10	<-3 to -0.5	$\rho \sim r^{-\beta}$, $r_{break} \sim 25$ kpc $\beta_{in} \sim 2.5, \beta_{out} \sim 3.7$
Thick disc	$6 \cdot 10^9$	$\gtrsim 8$	-1 to ~ 0	$\rho \sim \exp(-\frac{r}{R})\exp(-\frac{z}{Z})$ $R \sim 2.0$ kpc, $Z \sim 0.9$ kpc
Thin disc	$4 \cdot 10^{10}$	$\lesssim 8$	-0.6 to 0.5	$\rho \sim \exp(-\frac{r}{R})\exp(-\frac{z}{Z})$ $R \sim 2.6$ kpc, $Z \sim 0.3$ kpc
Bulge	$2 \cdot 10^{10}$	>10 (mostly)	-1.5 to 0.5	Boxy-peanut bulge

at a value of $[\text{Fe}/\text{H}]^4 \sim -1.6$ dex and it extends well below $[\text{Fe}/\text{H}] \sim -3$ dex, Ryan & Norris 1991, Helmi 2008 and references therein) and α -enhanced⁵ (Wheeler et al. 1989, Nissen et al. 1994, Carretta et al. 2000). Indications of a dual halo have been suggested from spatial distribution, kinematic and

⁴The bracket notation for chemical abundances is defined as: $[\text{X}/\text{H}] = \log(\text{X}/\text{H})_{\star} - \log(\text{X}/\text{H})_{\odot}$.

⁵ α -elements are all the elements produced by adding α -particles, i.e. O, Ne, Mg, Si, S, Ca...

chemical studies. Hartwick (1987) found that the spatial distribution of halo stars presented a duality, with a flattened inner component and a more spherical outer one. Further studies confirmed the presence of two broadly overlapping components: a high- α inner halo with slightly prograde rotation and mean metallicity of $[\text{Fe}/\text{H}] \sim -1.6$ dex, and a low- α outer halo with retrograde rotation and mean metallicity $[\text{Fe}/\text{H}] \sim -2.2$ dex (Carollo et al. 2007, Nissen & Schuster 2010, Hayes et al. 2018); the slope break of the radial density distribution between the two components is located at about 25 kpc (Bland-Hawthorn & Gerhard 2016, and references therein). In this context, the high- α stars would be formed in situ in the halo, whereas the low- α stars might correspond to an accreted component. Moreover, the stellar halo has a complex structure with a great variety of unrelaxed substructures, and it continues to accrete matter in the form of smaller galaxies which are then tidally disrupted in the gravitational field (Ibata et al. 1997, Belokurov et al. 2006).

1.2.2 THE BULGE

The bulge corresponds to the group of stars swelling out from the exponential profile of the disc star density at the Galactic center. It is a massive component comprising about a quarter of the Galactic stellar mass ($M = 2.0 \pm 0.3 \cdot 10^{10} M_{\odot}$, Valenti et al. 2013). The bulge stars have random motions and they span a metallicity range of $-1.5 \leq [\text{Fe}/\text{H}] \leq +0.5$ dex (Barbuy et al. 2018). Historically, studies of this region have been difficult due to the extreme dust absorption. In the last years, several studies looking at some regions where the extinction is lower, such as Baade’s window, and thanks to the exploitations of observations in near infrared wavelength have contributed to construct a new picture of the bulge and to reveal a very complex structure. In particular, Hill et al. (2011) by observing bulge

red clump stars concluded that their distribution is doubled-peaked, with one peak at $[\text{Fe}/\text{H}]=-0.30$ dex and the other at $[\text{Fe}/\text{H}]=+0.32$ dex, calling the two populations metal poor (MP) and metal rich (MR), confirmed by Uttenthaler et al. (2012). More recently, Rojas-Arriagada et al. (2017) with Gaia-ESO data and Schultheis et al. (2017) with APOGEE data, concluded that the metallicity distribution function in the bulge is indeed bimodal. Zoccali et al. (2017) also confirmed the existence of two main stellar populations with the MP one being more centrally concentrated. Bensby et al. (2017) by studying microlensed dwarfs and subgiant stars found that the bulge metallicity distribution is multi-modal, with at least four peaks corresponding to different star formation episodes occurred 12, 8, 6 and 3 Gyr ago, thus implying the existence of relatively young stars in the bulge. The existence of young bulge stars has been suggested also by Haywood et al. (2016), implying that these stars belong to the inner disc. On the other hand, Clarkson et al. (2011), Valenti et al. (2013), Renzini et al. (2018), Nogueras-Lara et al. (2018) and also Barbuy et al. (2018) concluded that most of the bulge stars are quite old (> 10 Gyr). In Renzini et al. (2018), from color-magnitude and luminosity functions of the MP and MR populations obtained from HST photometry, it is concluded that both MP and MR populations are similarly old. Bernard et al. (2018) inferred the history of star formation of the bulge from deep color-magnitude diagrams of four low reddening bulge regions and concluded that only 10% of bulge stars are younger than 5 Gyr, but this fraction rises to 20-25% in the metal rich peak.

1.2.3 THE THIN DISC

The thin disc is the Galactic component where we can find the majority of the stars, both field and open clusters (its stellar mass is $M = 4 \pm 1 \cdot 10^{10} M_{\odot}$,

Bland-Hawthorn & Gerhard 2016). The majority of the gas, atomic and molecular hydrogen, resides here too (even if there is a significant fraction of gas residing outside the Milky Way disc in the circumgalactic medium, Tumlinson et al. 2017). Thus, there is current active star formation (the present time star formation rate in the solar vicinity as measured with Gaia is $\sim 1.7 \text{ M}_\odot \text{ pc}^{-2} \text{ Gyr}^{-1}$, Bovy 2017). In structural terms, the thin disc constitutes a flat distribution with exponential number density profiles, both in the vertical direction (scaleheight of $Z \sim 300 \pm 50 \text{ pc}$ at R_0) and in the radial direction (scalelength of $R \sim 2.6 \pm 0.5 \text{ kpc}$) (Bland-Hawthorn & Gerhard 2016, and references therein). The thin disc is supported mainly by circular orbits, with small dispersion and mean rotational velocities of the order of 210 km s^{-1} (Recio-Blanco et al. 2014). The stars of the thin disc are young, with typical ages $\lesssim 8 \text{ Gyr}$ (Haywood et al. 2013). They are metal-rich stars of population I, and they have metallicities approximately from $-0.6 \leq [\text{Fe}/\text{H}] \leq +0.5 \text{ dex}$, with $[\alpha/\text{Fe}]$ enhancements going from slightly larger than solar to subsolar values (Hayden et al. 2015).

1.2.4 THE THICK DISC

The thick disc as a distinct structural component of galaxies was identified from the difficulty to account for the light profiles of some edge-on external galaxies with single exponential profile (Tsikoudi 1979, Burstein 1979). In the case of our Galaxy, the thick disc was first discovered by Yoshii (1982) and Gilmore & Reid (1983), as an overdensity of stars at large distances from the Galactic plane. Successively, it has been found that the thick disc differs from the thin disc also on the basis of its chemistry, age distribution and kinematics. It is less massive than the thin disc (the stellar mass of the thick disc is $M = 6 \pm 3 \cdot 10^9 \text{ M}_\odot$, Bland-Hawthorn & Gerhard 2016). In structural terms, the thick disc is more extended in the vertical direction

(scaleheight of $Z \sim 900 \pm 180$ pc at R_0), but more concentrated in the radial direction (scalelength $R \sim 2.0 \pm 0.2$ kpc) (Bland-Hawthorn & Gerhard 2016, and references therein). It is rotationally supported, although kinematically hotter than the thin disc. It is composed fundamentally by field stars with ages $\gtrsim 8$ Gyr (Haywood et al. 2013). The metallicity range spanned by its stars ranges from $[\text{Fe}/\text{H}] \sim -1.0$ dex to approximately solar values, with $[\alpha/\text{Fe}]$ enhancements systematically higher than those displayed by the thin disc at a given metallicity (Hayden et al. 2015).

MORE ON THE THICK AND THIN DISCS

Here, I would like to add more considerations on the chemical dichotomy between the thick and thin discs, which is of fundamental importance for the development of this Thesis work. In the upper panel of Fig. 1.4, the observed $[\alpha/\text{Fe}]$ vs. $[\text{Fe}/\text{H}]$ distribution for the solar neighbourhood from APOGEE Survey is shown (Hayden et al. 2015). It is evident that there are two distinct sequences in the distribution of stars in the $[\alpha/\text{Fe}]$ vs. $[\text{Fe}/\text{H}]$, one at high- $[\alpha/\text{Fe}]$ values, and one at solar- $[\alpha/\text{Fe}]$, which eventually merge at $[\text{Fe}/\text{H}] \sim +0.2$ dex. At subsolar metallicities, there is a gap between these two sequences. In the lower panel of Fig. 1.4, the stellar distribution of stars in the $[\alpha/\text{Fe}]$ vs. $[\text{Fe}/\text{H}]$ plane as a function of R and $|z|$ from APOGEE Survey is also shown (Hayden et al. 2015). The relative fraction of stars between the high- $[\alpha/\text{Fe}]$ and low- $[\alpha/\text{Fe}]$ sequences varies with disc height and radius. In the outer regions, the locus of the low- α sequence shifts towards lower metallicity. This can be well explained by inside-out formation: external Galactic regions are formed on longer timescales, hence the chemical enrichment is weaker and less efficient than the inner Galactic regions, leading to a lower metallicity. On the other hand, the high- $[\alpha/\text{Fe}]$ sequence appears similar at all locations in the Galaxy where it is observed

1.2. GALACTIC COMPONENTS

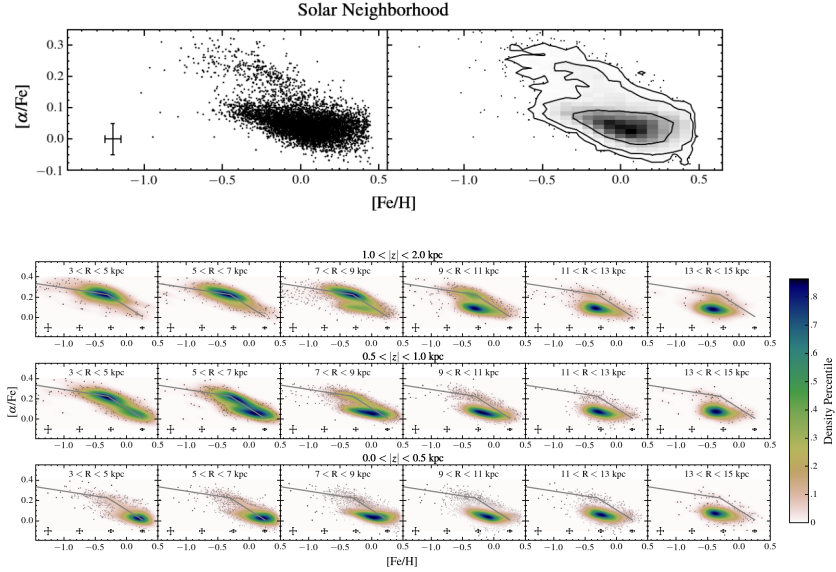


Figure 1.4: *Upper panel:* Observed $[\alpha/\text{Fe}]$ vs. $[\text{Fe}/\text{H}]$ distribution for the solar neighbourhood from APOGEE Survey (Hayden et al. 2015). The left panel shows only 20% of the observed data points in the solar circle, whereas the right panel shows the entire sample in the solar neighbourhood with contours corresponding to 1, 2 and 3σ of the overall densities. The typical uncertainties in the abundances are shown at the bottom of the panel. *Lower panel:* Stellar distribution of stars in the $[\alpha/\text{Fe}]$ vs. $[\text{Fe}/\text{H}]$ plane as a function of R and $|z|$ from APOGEE Survey (Hayden et al. 2015). The typical uncertainties in the abundances are shown as a function of metallicity across the bottom of each panel.

($3 < R < 13$ kpc). Stars with high- $[\alpha/\text{Fe}]$ values and the most metal-rich stars ($[\text{Fe}/\text{H}] > +0.2$ dex) have spatial densities that are consistent with short radial scalelengths or a truncation at larger radii, and have low number density in the outer disc. The abundance pattern of the inner Galaxy can be described as a single sequence, starting at high $[\alpha/\text{Fe}]$ and low metallicity, and ending at approximately solar $[\alpha/\text{Fe}]$ and $[\text{Fe}/\text{H}] \sim +0.5$ dex; the most metal-rich stars are confined to the midplane (Hayden et al. 2015). In this context, my Thesis is devoted to explain and interpret these observed features within a theoretical scenario.

1.3 GALACTIC ARCHAEOLOGY

Starting from the present properties of the main components of our Galaxy, for which detailed abundances can be measured, we can infer their past history, and this is the goal of Galactic archaeology, to which this Thesis is devoted.

The photospheric abundance of a given element X in a star is usually expressed as:

$$A(\text{X}) = 12 + \log(\text{X}/\text{H}), \quad (1.1)$$

where X/H is the abundance by number between the considered element and hydrogen. In studies of Galactic archaeology, photospheric abundances are often expressed in relation to the solar chemical composition with the so-called bracket notation:

$$[\text{X}/\text{H}] = \log(\text{X}/\text{H}) - \log(\text{X}/\text{H})_{\odot}, \quad (1.2)$$

where abundances can be expressed either by number or by mass. By definition, solar abundances are $[\text{X}/\text{H}] = 0$ dex.

In the abundance patterns of stars, a great amount of information can be

found, since they represent the fossil record of the detailed processes and relative timescales driving the formation and chemical evolution of different stellar populations. Each stellar atmosphere reflects the enrichment history of the interstellar medium from which it was formed; once a star is born, although its interior composition evolves, its atmosphere is negligibly polluted by the effects of stellar evolution. The interpretation of the information provided by the abundance patterns of stars belonging to different stellar populations has required the elaboration of models that follow the growth of metals with time, namely chemical evolution models.

Chemical evolution models are powerful tools to constrain the formation timescale of different stellar populations (see Pagel & Patchett 1975, Audouze & Tinsley 1976, Tinsley 1976 for the development of the first ideas in the field). Analytical and then numerical chemical evolution models have greatly evolved, allowing to interpret the abundance patterns of the different Milky Way components, as well as those of external galaxies. Generally, a good agreement between model predictions and observational data is obtained by assuming that the Milky Way formed by infall of gas, as first suggested by Larson (1976) and Chiosi (1980). In literature, many theoretical works have appeared concerning the chemical evolution of the Milky Way (Lacey & Fall 1985; Matteucci & Greggio 1986; Tosi 1988; Sommer-Larsen & Yoshii 1989, 1990; Matteucci & Francois 1989, 1992; Ferrini et al. 1992, 1994; Pardi & Ferrini 1994; Pardi et al. 1995; Tsujimoto et al. 1995; Prantzos & Aubert 1995; Chiappini et al. 1997, 1999; Chang et al. 1999; Portinari & Chiosi 1999, 2000; Boissier & Prantzos 1999; Goswami & Prantzos 2000; Cescutti 2008; Schönrich & Binney 2009; Romano et al. 2010; Kobayashi & Nakasato 2011; Haywood 2008, Haywood et al. 2013, 2015; Snaith et al. 2014, 2015).

From a conceptual point of view, chemical evolution models of the Milky

Way have passed through different phases that can be summarized as follows: i) Serial approach (e.g. Matteucci & Francois 1989); ii) Parallel approach (e.g. Ferrini et al. 1992, Pardi et al. 1995, Chiappini 2009); iii) Two-infall approach (e.g. Chiappini et al. 1997); iv) Stochastic approach (e.g. Argast et al. 2000, Cescutti 2008). In the serial scenario, the Galaxy is modelled by means of one accretion episode lasting for the entire Galactic lifetime, where halo, thick and thin disc form in sequence as a continuous process (e.g. Matteucci & Francois 1989). In the parallel scenario, the various Galactic components start forming at the same time and from the same gas, but evolve at different rates (e.g. Pardi et al. 1995). In the two-infall scenario, halo and disc formed out of two separate infall episodes. The first infall episode lasted no more than 1-2 Gyr, whereas the second, where the thin disc formed, lasted much longer with a timescale for the formation of the solar vicinity of 6-8 Gyr (Chiappini et al. 1997). In the stochastic approach, the hypothesis is that in the early halo phases ($[\text{Fe}/\text{H}] < -3.0$ dex) mixing was not efficient and, as a consequence, one should observe, in low metallicity halo stars, the effect of pollution from single SNe (e.g. Argast et al. 2000). Generally, these models predict a large spread for $[\text{Fe}/\text{H}] < -3.0$ dex in all the α -elements, which is not observed, as shown by data relative to metallicities down to -4.0 dex. However, inhomogeneities could explain the observed spread of s- and r-process elements at low metallicities (see Matteucci 2012 for a review on chemical evolution models).

Classical chemical evolution models are extremely useful, if their assumptions are then connected to a big picture of galaxy formation in the Universe; in fact, the cosmological growth of galaxies should also be considered. Thus, many chemo-dynamical models have been developed, such as chemical + dynamical models (e.g. Minchev et al. 2013, 2014), but also fully self-consistent simulations from cosmological initial conditions (see Vogelsberger et al. 2020

for a review on cosmological simulations). Recently, cosmological simulations have improved enough to study the formation and evolution of thick and thin discs (e.g. Kobayashi & Nakasato 2011, Loebman et al. 2011, Rahimi et al. 2011, Scannapieco et al. 2011, Miranda et al. 2016, Obreja et al. 2016, Buck et al. 2017, Navarro et al. 2017, Grand et al. 2018, Buck et al. 2020a,b). Such simulations suggest that thin discs form inside-out and upside-down (Bird et al. 2013, Stinson et al. 2013, Minchev et al. 2013, Grand et al. 2016); on the other hand, many scenarios have been proposed for centrally concentrated thick discs, for example violent gas-rich mergers (Brook et al. 2004, 2007), accretion of satellite stars (Kobayashi & Nakasato 2011), radial migration of kinematically hot stars from the inner to the outer disc (Loebman et al. 2011). In particular, Brook et al. (2004, 2007) showed that the infalling gas brought into the galaxy by violent gas-rich mergers can produce a compact centrally concentrated component, distinct from the subsequent formation of a younger and lower- $[\alpha/\text{Fe}]$ one. However, the presence of the chemical dichotomy still represents a matter of debate in the field of cosmological simulations; for example, Kobayashi & Nakasato (2011) and Brook et al. (2012) find signatures of two distinct sequences in the $[\alpha/\text{Fe}]$ vs. $[\text{Fe}/\text{H}]$ relation, whereas the evolution seems to be smooth and continuous in the case of Minchev et al. (2013), and in Grand et al. (2018) both the two possibilities can be realized. Therefore, the presence of a clear chemical dichotomy is not ubiquitous in simulations, and this fact raises interesting questions regarding the formation mechanisms of the observed bimodality. Cosmological simulations are rapidly improving and recently they have achieved significant resolution. However, due to the costs and challenges of these computations, they must make compromises in the implemented physics, the range in resolution and the number of simulated galaxies. Moreover, the long computational times of each simulation limits

a detailed exploration of variations in the parameters and in the physical processes involved in these cosmological simulations.

Another approach to study galaxy formation and evolution in the framework of the currently standard scenario for structure formation is represented by semi-analytic models. In order to follow the hierarchical nature of structure formation, these models use merger trees based on either the extended Press-Schechter formalism or on dark matter cosmological simulations. Then, the evolution of the baryonic component is modelled by following simple, but physically and observationally motivated prescriptions. The first development of this technique was suggested by the pioneering paper of White & Rees (1978), but recently many other works have appeared to extend and refine this approach (e.g. De Lucia & Blaizot 2007, Monaco et al. 2007, Somerville et al. 2008, Benson & Bower 2010, Guo et al. 2011, De Lucia 2012, see Somerville & Davé 2015 for a review on semi-analytic models). These models have been extensively used to study the chemical evolution of galaxies as a function of their mass (Yates et al. 2013, Fontanot et al. 2017) as well as the chemical evolution of specific galaxies, such as the Milky Way (Tumlinson 2006, 2010, Calura & Menci 2009, De Lucia 2012, Komiya et al. 2014, Crosby et al. 2016), local dwarf spheroidal and ultra-faint galaxies (Romano & Starkenburg 2013, Starkenburg et al. 2013, Romano et al. 2015, Côté et al. 2018). These models are less computationally expensive than cosmological simulations and thus it is possible to investigate more easily the relative role of the different physical processes involved. However, the significant amount of model parameters can lead to degeneracies and limits the predictivity of these models, in particular at high redshift.

In summary, many theoretical tools have been developed and can be used to study Galactic archaeology, from cosmological simulations to semi-analytic models and detailed chemical evolution models.

The aforementioned theoretical scenarios for the Milky Way must be constrained by reliable observational studies, which require the development of large, systematic and homogenous Galactic surveys, sampling all the stellar populations. In the last few years, many spectroscopic surveys have been planned and begun in order to investigate and constrain the formation and evolution of the Milky Way, such as RAVE (Steinmetz et al. 2006), SEGUE-1 (Yanny et al. 2009), SEGUE-2 (Rockosi et al. 2009), ARGOS (Freeman et al. 2013), LAMOST (Cui et al. 2012), Gaia-ESO (Gilmore et al. 2012), GALAH (Zucker et al. 2012), WEAVE (Dalton et al. 2014), 4MOST (de Jong et al. 2014), MOONS (Cirasuolo et al. 2014), APOGEE (Majewski et al. 2015) and the AMBRE Project (de Laverny et al. 2013). A huge amount of data is being collected by these surveys, and it is boosting the number of open questions that have to be solved by theoretical models.

1.4 GOAL AND STRUCTURE OF THE THESIS

In this context, this Thesis is devoted to the development of new and detailed chemical evolution models which best reproduce the characteristics of the main Galactic components in the light of the most recent data from Galactic stellar surveys in order to reconstruct the history of formation and evolution of our Galaxy. The Thesis is structured as follows. In Chapter 2, I describe in details the method used in this work, i.e. Galactic chemical evolution models with the fundamental ingredients and complete equations of chemical evolution. In successive Chapters, I show the original results of my work. In particular, in Chapter 3, I present the chemical evolution models that I developed for the Galactic thick and thin discs in the solar neighbourhood, both a revised two-infall model and the parallel one. In Chapter 4, I extend the study also to the other Galactocentric distances and explore abundance gradients along the Galactic thin disc, investigating

the main physical processes affecting them. In Chapter 5, I present the chemical evolution models implemented for the Galactic bulge and discuss the origin of different stellar populations in this Galactic component from chemical abundances. In Chapter 6 and 7, I apply the reference models developed for the Galactic discs and bulge to study the chemical evolution from lithium to europium, respectively. Finally, in Chapter 8, I summarize the main conclusions of this Thesis and discuss future perspectives arising from them.

CHAPTER 2

Chemical evolution models

In this Chapter, I present the fundamental background to the method used in this work, i.e. Galactic chemical evolution models. I start from the basic ingredients for chemical evolution models and then I describe the fundamental equations of chemical evolution. Then, I present some chemical evolution models present in the literature that have been relevant for the development of my Thesis work: the two-infall model developed by Chiappini et al. (1997) and then updated by Romano et al. (2010), the three-infall model of Micali et al. (2013) and the chemical evolution models for the Galactic bulge. For further details on the fundamental background, I address the interested reader to Mattuecci (2012).

2.1 FUNDAMENTAL INGREDIENTS

The basic ingredients for chemical evolution models can be summarized as follows.

- Initial conditions;
- The stellar birthrate function;
- The stellar yields;
- Gas flows.

In the next Sections, I provide details on these ingredients. Then, given all these ingredients, it would be possible to write a set of equations describing the evolution of the gas and its chemical abundances. These equations will follow the temporal and spatial variation of the gas content and its abundance by mass.

2.1.1 INITIAL CONDITIONS

The initial conditions for chemical evolution models consist of establishing whether:

- the chemical composition of the initial gas is primordial (which means H, He and Li only) or it is pre-enriched by a pre-galactic stellar generation;
- the studied system is a closed-box (without any interaction with the surrounding environment or between the different parts of the system itself) or an open system (with infall and/or outflow of gas).

2.1.2 THE STELLAR BIRTHRATE FUNCTION

The number of stars which were born in the mass interval $m, m+dm$ and in the time interval $t, t+dt$ is, by definition, the so-called stellar birthrate function $B(m, t)$. Usually, this quantity is separated into two independent functions and can be expressed as:

$$B(m, t) = \psi(t)\phi(m), \quad (2.1)$$

where the quantity $\psi(t)$ is the star formation rate, which represents the rate at which the interstellar gas is turned into stars per unit time, and the quantity $\phi(m)$ is the initial mass function, which represents the mass distribution of the stars at birth. In the following, detailed definitions of star formation rate and initial mass function are given.

2.1.2.1 THE STAR FORMATION RATE

The star formation rate (SFR) corresponds to the amount of mass within the interstellar medium which is converted into stars per unit time. Usually, it is expressed in units of $M_{\odot} \text{ pc}^{-2} \text{ yr}^{-1}$. The SFR is observed to correlate in galaxies with many fundamental physical quantities, such as the total galaxy stellar mass or the average metallicity of the galaxy interstellar medium. Nevertheless, the most common parametrization of the SFR is the so-called Schmidt-Kennicutt law (Schmidt 1959; Kennicutt 1998a,b):

$$\psi(t) = \nu \sigma_{gas}^k, \quad (2.2)$$

where σ_{gas} is the surface gas density, k is the index of the law and it lies in the interval $[1, 2]$, and ν corresponds to the so-called star formation efficiency, which is the SFR per unit mass of gas and it has the dimensions of the inverse of a time.

This law was first proposed by Schmidt (1959) to fit observational data. Later on, Kennicutt (1998a,b) derived $k=1.4\pm0.15$ for star-forming spiral and starburst galaxies. In literature, other parametrizations of the SFR have been explored; for example, they can refer to the dynamical timescale or the angular rotation speed (Boissier 2013).

2.1.2.2 THE INITIAL MASS FUNCTION

The initial mass function (IMF) is the mass distribution of stars at their birth. In literature, most of the IMF which have been proposed to fit observational data in the solar neighbourhood are defined as a one-slope or a multi-slope power law. An example of a one-slope power law is given by:

$$\phi(m) = am^{-(1+x)}, \quad (2.3)$$

usually defined in the mass range of 0.1-100 M_{\odot} , where a is the normalization constant derived by imposing that:

$$\int_{0.1}^{100} m\phi(m)dm = 1. \quad (2.4)$$

The most common value for x is 1.35, as given by Salpeter (1955).

An example of a multi-slope power law is the one of Scalo (1986):

$$\begin{aligned} x &= 1.35 \text{ for } M \leq 2M_{\odot} \\ x &= 1.70 \text{ for } M > 2M_{\odot} \end{aligned} \quad (2.5)$$

Another parametrization for the IMF is the one of Kroupa et al. (1993):

$$\begin{aligned} x &= 0.3 \text{ for } M \leq 0.5M_{\odot} \\ x &= 1.2 \text{ for } 0.5M_{\odot} < M \leq 1.0M_{\odot} \\ x &= 1.7 \text{ for } M > 1.0M_{\odot} \end{aligned} \quad (2.6)$$

Another IMF is the one suggested by Chabrier (2003) who proposed a log-normal form for the low-mass part of the IMF ($m < 1M_{\odot}$):

$$\begin{aligned}\phi(\log m) &\propto e^{-\frac{(\log m - \log m_c)^2}{2\sigma^2}} \text{ for } M \leq 1.0M_{\odot} \\ \phi(m) &= am^{-(1+x)} \text{ for } M > 1.0M_{\odot}\end{aligned}\tag{2.7}$$

with $x=1.3$ which is basically the index of the Salpeter (1955), $m_c = 0.079M_{\odot}$ and $\sigma_c = 0.69$.

Assuming different IMFs can strongly affect the predictions of chemical evolution models, since the IMF determines the relative numbers of stars lying in different mass ranges, and thus the amount of restitution of chemical elements by stars.

2.1.3 THE STELLAR YIELDS

The stellar yields correspond to the amount of both newly formed and pre-existing elements ejected by stars of all masses at their death. They represent a fundamental ingredient for chemical evolution models and they can be calculated by means of stellar evolutionary models.

All the elements with mass number A from 12 to 60 have been formed in stars during quiescent burnings in stellar evolution. Stars convert H into He, and then He into heavier atoms until Fe-peak elements, where the binding energy per nucleon reaches a maximum and the nuclear fusion reactions stop. H is converted into He through the proton-proton chain (pp chain) or through the Carbon-Nitrogen-Oxygen cycle (CNO cycle), depending on stellar mass. Then, ${}^4\text{He}$ is converted into ${}^{12}\text{C}$ through the triple- α reaction. Elements heavier than ${}^{12}\text{C}$ are then produced by synthesis of α -particles: they are called α -elements (O, Ne, Mg, Si, S and Ca). The last main burning in stars is the ${}^{28}\text{Si}$ -burning, which produces ${}^{56}\text{Ni}$, which then β -decays into ${}^{56}\text{Co}$ and ${}^{56}\text{Fe}$. Si-burning can be quiescent or explosive, according to the temperature.

Explosive nucleosynthesis occurring during supernova explosions mainly produces Fe-peak elements. Elements heavier than Fe cannot be produced by exoenergetic fusion reactions in stars. Instead, they must be the result of neutron capture on Fe-peak nuclei. The neutron capture process can be rapid (r-process) or slow (s-process) with respect to the β -decay timescale and these elements are called r- and s-process elements, according to which of the two processes has contributed more to the production at solar metallicity. In chemical evolution models, stars are usually divided into two main classes, according to their mass and thus their final fate:

- low and intermediate mass stars (LIMS, $0.8 M_{\odot}$ - $8 M_{\odot}$), which are divided into single stars and binary systems which can give rise to Type Ia SNe,
- massive stars ($M > 8 M_{\odot}$).

I remind that stars with mass $< 0.8 M_{\odot}$ have lifetimes larger than the Hubble time, and thus they play a marginal role in chemical evolution models, since they do not contribute to the Galactic chemical enrichment. Single stars in the mass range $0.8 M_{\odot}$ - $8 M_{\odot}$ contribute to the Galactic chemical enrichment through planetary nebula ejection and quiescent mass loss along the giant branch. They enrich the interstellar medium mainly in He, C, and N, but they can also produce some amounts of ^7Li , Na and s-process elements. These stars end their lives as white dwarfs. Type Ia SNe are considered to originate from carbon deflagration in carbon-oxygen white dwarfs (CO WD) in binary systems. These stars contribute a substantial amount of iron ($0.6 M_{\odot}$ per event) and non negligible quantities of Si and S, and also Mn (see Kobayashi et al. 2019). They also contribute to other elements, such as O, C, Ne, Ca, and Mg, but in negligible amounts with

respect to the masses of such elements ejected by Type II SNe. Massive stars with masses $M > 8 M_{\odot}$ are the progenitors of Type II, Ib and Ic SNe: if the explosion energies are much higher than 10^{51} erg, hypernova events can occur (SNe Ic). Massive stars produce not only α -elements, but also odd-Z elements such as Na and Al, some iron-peak elements, light s-process elements ($A < 90$) and perhaps r-process elements.

The most important factor governing the nucleosynthesis production is certainly the stellar mass, even if the chemical composition can be very important in affecting the yields. In fact, stellar yields show a sharp dependence on the initial metallicity and the assumed mass loss. Moreover, including stellar rotation has shown to play an important role to explain the abundance of some elements in massive stars.

Romano et al. (2010) explored the impact of different sets of yields in chemical evolution models and concluded that the best agreement with the observations was provided by the following nucleosynthesis prescriptions: for single stars in the mass range $0.8 M_{\odot}$ - $8 M_{\odot}$ the yields of Karakas (2010), for SNe Ia Iwamoto et al. (1999), and for massive stars with mass $M > 8 M_{\odot}$ the yields of Kobayashi et al. (2006) and Geneva models. Throughout the Thesis, I will provide details of the datasets of stellar yield used in my chemical evolution models.

2.1.4 GAS FLOWS

Gas flows are key ingredients in chemical evolution models and they can be:

- incoming (namely, infall or inflow);
- outcoming (galactic winds or outflow);
- radially flowing along the disc (radial flows).

Generally, a good agreement with the observational properties of the Galaxy, such as the metallicity distribution function of G-dwarfs in the solar neighbourhood and the abundance patterns, is obtained by assuming that the disc formed by infall of gas (see for example Chiosi 1980; Matteucci & Francois 1989; Ferrini et al. 1994; Chiappini et al. 1997, 2001; Colavitti et al. 2009; Chiappini 2009; Magrini et al. 2009; Spitoni & Matteucci 2011; Mott et al. 2013). In particular, a good assumption for reproducing abundance gradients is that the timescale for the formation of the Galactic thin disc increases with Galactocentric radius according to the inside-out scenario (Matteucci & Francois 1989; Chiappini et al. 2001). Then, to maintain consistency with the dynamical consequence of infall, also radial gas flows should be taken into account (Spitoni & Matteucci 2011; Bilitewski & Schönrich 2012; Wang & Zhao 2013; Spitoni et al. 2013; Mott et al. 2013; Cavichia et al. 2014; Pezzulli et al. 2017).

2.2 MODEL EQUATIONS

Once we have these fundamental ingredients, we can write a complete set of equations. A complete chemical evolution model can be described by a number of equations equal to the number of the chemical elements. The fundamental equations that follow the time evolution of G_i , namely the mass fraction of the element i in the gas, are (see Matteucci 2012):

$$\dot{G}_i(r, t) = -\psi(r, t)X_i(r, t) + R_i(r, t) + \dot{G}_i(r, t)_{flows} \quad (2.8)$$

where $\psi(r, t)$ is the SFR, $X_i(r, t)$ indicates the abundance by mass of the element i , $R_i(r, t)$ represents the rate of matter restitution from stars with different masses into the interstellar medium (ISM), and $\dot{G}_i(r, t)_{flows}$ takes into account the gas flows.

The first term in the right hand side of Eq. (2.8) represents the rate at which

the chemical elements are subtracted from the ISM to be included in stars. The second term represents the rate of restitution of matter from the stars with different masses into the ISM and it corresponds to:

$$\begin{aligned}
R_i(r, t) = & \int_{M_L}^{M_{Bm}} \psi(t - \tau_m) Q_{mi}(t - \tau_m) \phi(m) dm + \\
& + A \int_{M_{Bm}}^{M_{BM}} \phi(m) \left[\int_{\mu_{Bmin}}^{0.5} f(\mu_B) \psi(t - \tau_{m2}) Q_{mi}(t - \tau_{m2}) d\mu_B \right] dm + \\
& + (1 - A) \int_{M_{Bm}}^{M_{BM}} \psi(t - \tau_m) Q_{mi}(t - \tau_m) \phi(m) dm + \\
& + \int_{M_{BM}}^{M_U} \psi(t - \tau_m) Q_{mi}(t - \tau_m) \phi(m) dm
\end{aligned} \tag{2.9}$$

where $\psi(t)$ is the SFR, $\phi(m)$ is the IMF and $\tau_m(m)$ is a function describing stellar lifetimes. The quantity $Q_{mi}(t - \tau_m)$ corresponds to $\Sigma_j Q_{ij}(m) X_j(t - \tau_m)$, where $Q_{ij}(m)$ is the production matrix (Talbot & Arnett 1973) that takes into account both the newly formed element i (originating from the element j) and the already present element i in the star of mass m at birth. $X_j(t - \tau_m)$ is the abundance of the element j originally present in the star at its birth and later transformed into the element i and ejected. Let us describe each integral in detail.

The first integral regards the stars in the mass range $M_L - M_{Bm}$, where $M_L = m(t)$ is the minimum mass dying at the time t (its minimum value is $\simeq 0.8M_\odot$ with a lifetime corresponding to the age of the Universe).

The second integral corresponds to the contribution of SNe Ia, as first introduced by Matteucci & Greggio (1986). Here, the rate is calculated by assuming the single degenerate (SD) scenario for the progenitor of these SNe, i.e. a CO WD plus a red giant companion; in Matteucci et al. (2009), it has been demonstrated that this scenario is equivalent to the double degenerate (DD) one as the effects on Galactic chemical evolution are concerned. The

extremes of the second integral represent the minimum (M_{Bm}) and the maximum (M_{BM}) mass allowed for the whole binary systems giving rise to Type Ia SNe. The maximum mass is constrained by the requirement that the mass of each component cannot exceed $M_{up} = 8M_{\odot}$, which is the assumed maximum mass giving rise to a CO WD; hence, $M_{BM} = 16M_{\odot}$. The minimum mass M_{Bm} is more uncertain and it has been considered as a free parameter. In the original formulation of the Type Ia SN rate, $M_{Bm} = 3M_{\odot}$ in order to ensure that both the primary and the secondary star would be massive enough to allow the WD to reach the Chandrasekhar mass M_{Ch} , after accretion from the companion. The function $f(\mu_B)$ describes the distribution of the mass ratio of the secondary ($\mu_B = \frac{M_2}{M_B}$) of the binary system. The quantity A is a free parameter which represents the fraction in the IMF of binary systems with the right properties to give rise to SNe Ia and it is obtained by fitting the present time Type Ia SN rate in the studied galaxy (for the Milky Way, we assume $A=0.035$, Grisoni et al. 2017). The time τ_{m2} is the lifetime of the secondary star in the binary system giving rise to a SN Ia, and represents the clock of the system in the SD scenario. The third integral represents the mass restored by single stars with masses in the range $M_{Bm} - M_{BM}$ (namely, $3M_{\odot} - 16M_{\odot}$). They can be either stars ending their lives as CO WDs or as Type II SNe (those with $M > M_{up}$ which is normally assumed to be $8 M_{\odot}$).

The fourth integral refers to the material restored into the ISM by core-collapse SNe.

Finally, the quantity $\dot{G}_i(r, t)_{flows}$ takes into account possible gas flows, which can be incoming (in this case, we have to add a quantity corresponding to the rate at which the element i is accreted through infall), outcoming (in this case, we have to subtract a quantity corresponding to the rate at which the element i is lost through a galactic wind) and radially flowing (in this

case, we have to consider the possible rate of radial gas flows along the disc).

2.3 MODELS IN LITERATURE

In this Section, I review some chemical evolution models in literature, which are fundamental for the development of my Thesis. First, I introduce the two-infall model of Chiappini et al. (1997), which has been the starting point of my study. Secondly, I present the three-infall model of Micali et al. (2013). Then, I introduce the parallel approach. Finally, I discuss the models for the bulge.

THE TWO-INFALL MODEL

The two-infall model was first proposed by Chiappini et al. (1997). This model assumes that the Galaxy forms as a result of two main infall episodes. During the first one, the halo and the thick disc form, and the gas lost by the halo quickly accumulates in the center of the Galaxy with the consequent formation of the Galactic bulge. During the second episode, a much slower infall of gas gives rise to the thin disc, with the gas accumulating in the inner regions faster than in the outer ones. This mechanism for the disc formation is known as inside-out scenario (Matteucci & Francois 1989; Chiappini et al. 2001). The origin of the gas in the two infall episodes is extragalactic and its composition is assumed to be primordial. The Galactic disc is approximated by several independent rings, 2 kpc wide, without exchange of matter between them. The basic equations for the evolution of chemical elements in the gas are given by Eq. (2.8). The main assumptions of the two-infall model as updated by Romano et al. (2010) can be summarized as follows.

As this model assumes two main infall episodes, the gas infall is given by:

$$\dot{G}_i(r, t)_{inf} = A_{01}(r)(X_i)_{inf}e^{-\frac{t}{\tau_{01}}} + B(r)(X_i)_{inf}e^{-\frac{t-t_{max}}{\tau_2}}, \quad (2.10)$$

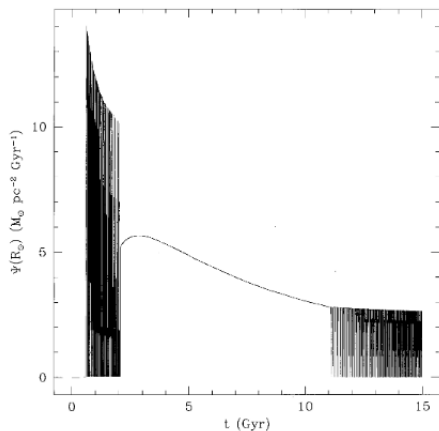


Figure 2.1: Star formation rate as a function of time in the two-infall model (Chiappini et al. 1997).

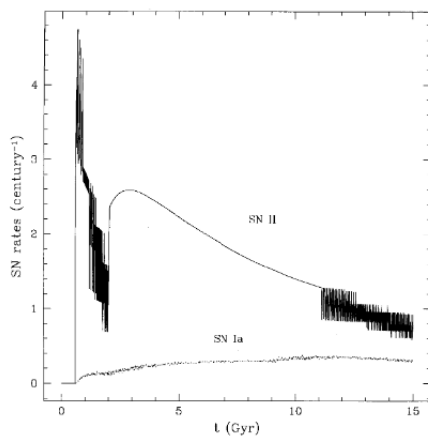


Figure 2.2: SN rates as functions of time in the two-infall model (Chiappini et al. 1997).

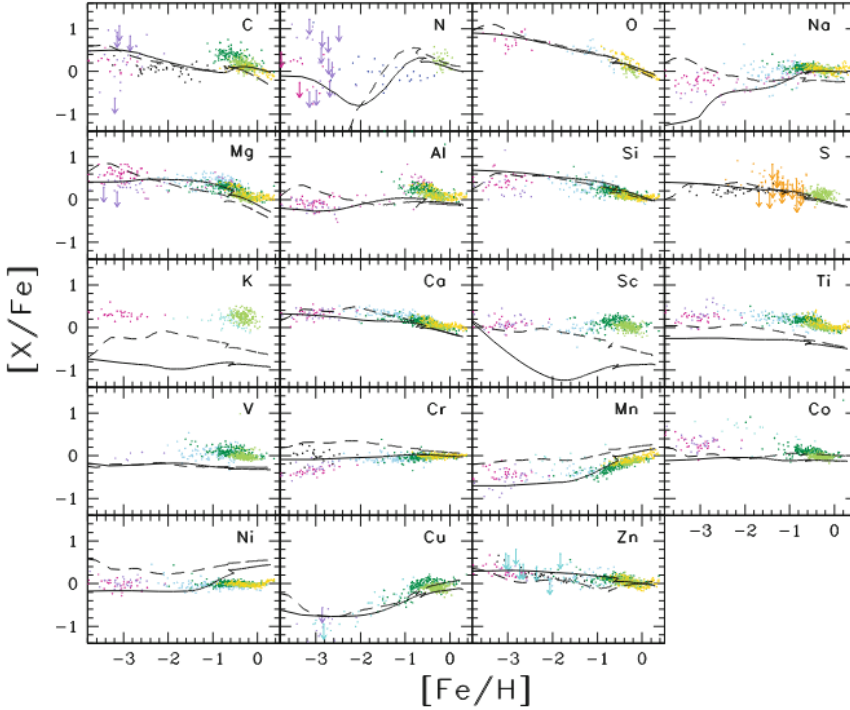


Figure 2.3: $[X/Fe]$ vs. $[Fe/H]$ relations for elements from C to Zn in the solar neighbourhood predicted by the two-infall model of Romano et al. (2010).

where $G_i(r, t)_{inf}$ is the infalling material in the form of element i and $(X_i)_{inf}$ is the composition of the infalling gas, which is assumed to be primordial. The quantities $A_{01}(r)$ and $B(r)$ are two parameters fixed by reproducing the total present time surface mass density in the solar neighbourhood, as given by Kuijken & Gilmore (1991). The parameter t_{max} is the time for the maximum mass accretion onto the disc; it is set equal to 1 Gyr and it roughly corresponds to the end of the halo-thick disc phase. The parameters

τ_{01} and τ_2 are the timescales for mass accretion in the halo-thick disc and thin disc components, respectively. These timescales are free parameters of the model and they are constrained mainly by comparison with the observed metallicity distribution of long-lived stars in the solar vicinity. In particular, τ_{01} is set equal to 1 Gyr, whereas $\tau_2(r)$ is considered as a function of the Galactocentric distance, according to the inside-out scenario (Chiappini et al. 2001); the relation for $\tau_2(r)$ is constructed in order to obtain a timescale for the bulge formation ($r \leq 2$ Kpc) of 1 Gyr in agreement with the results of Matteucci & Brocato (1990), and a timescale of formation of 7 Gyr at the solar neighbourhood, which best reproduces the G-dwarf metallicity distribution.

The IMF is Kroupa IMF (Kroupa et al. 1993). The SFR is the Schmidt-Kennicutt law (Kennicutt 1998a). The exponent of the surface gas density k is set equal to 1.5. The parameter ν is the efficiency of the star formation process expressed in units of Gyr^{-1} . In the best model of Romano et al. (2010), the efficiency of star formation is equal to $\nu_{01}=2 \text{ Gyr}^{-1}$ during the halo-thick disc phase, while it is equal to $\nu_2=1 \text{ Gyr}^{-1}$ during the thin disc formation, and becomes zero when the gas surface density drops below a critical threshold. The existence of such a threshold for the star formation is quite uncertain since it has been suggested by optical studies, but its existence has been challenged by UV results (GALEX). Theoretical arguments (Elmegreen 1999) have suggested that a gas density threshold for star formation should exist also in some objects suffering bursts of star formation, but it should be lower than in discs. For this reason, the adopted threshold gas densities in the halo-thick disc and thin disc phases are different and the threshold is lower during the halo-thick disc phase where the star formation was stronger than in the thin disc. In the best model of Romano et al. (2010), the thresholds are 4 and $7 \text{ M}_{\odot} \text{ pc}^{-2}$ during

the halo-thick and thin disc phases, respectively. The predicted behaviour of the SFR with the assumed thresholds in the gas density is shown in Fig. 2.1. As we can see, the SFR is higher during the halo-thick disc phase, while it is lower during the thin disc formation. The SFR is also characterized by an oscillating behaviour during all the halo-thick disc phase, and at the end of the thin disc phase. These oscillations are due to the adopted thresholds. The most important feature of this plot is the gap in the SFR between the halo-thick disc and the thin disc formation. This is clearly due to the fact that the star formation in the thin disc occurs only after a density of $7 \text{ M}_{\odot} \text{ pc}^{-2}$ has been accumulated.

The assumed Type Ia SN model is the SD scenario. The minimum time for the explosion of the first Type Ia SN is 30 Myr, whereas the timescale for restoring the bulk of Fe is $\sim 1 \text{ Gyr}$, for the SFR adopted in the solar vicinity. This timescale is not universal, since it depends on the assumed SNIa progenitor model, but also on the assumed star formation history. The choice of the SD scenario for the progenitors of Type Ia SNe is dictated by the fact that it reproduces at best the abundance patterns. The predicted behaviour of the SN rates as a function of time is shown in Fig. 2.2. As we can see in Fig. 2.2, the gap between the end of the halo-thick disc phase and the beginning of the thin disc phase, due to the adopted threshold, is also responsible for the trend of Type II SN rate. In fact, the trend shows a peak around $\sim 0.5 \text{ Gyr}$, which roughly corresponds to the timescale of formation of the halo-thick disc phase, and then goes to zero at a time of about 1 Gyr, which corresponds to the end of the halo-thick disc phase. The explanation of this feature is that the SNe Type II are created by stars with high mass and short lifetime, thus closely track the SFR and, hence, the number of this type of SNe per century is higher in the first gigayears of the formation of the Milky Way. Once the halo-thick disc formation ends, star formation

starts again and the number of supernovae per century increases until 3 Gyr, and then decreases until the achievement of the present rate. On the other hand, the SNe Type Ia are produced by progenitors with long lifetime, thus they are very little influenced by the existence of a threshold in the star formation and, as showed in Fig. 2.2, the SNe Type Ia rate increases with time and remains almost constant until the achievement of the present value.

In Fig. 2.3, I show abundance patterns predicted by Romano et al. (2010) compared to observational data. The behaviour of the $[X/Fe]$ vs. $[Fe/H]$ relation can be well-interpreted in terms of the so-called time-delay model (Matteucci 2012). The time-delay refers to the delay with which Fe is ejected into the interstellar medium by SNe Ia relative to the fast production of α -elements by core-collapse SNe (where α -elements are those formed by subsequent addition of α -particles, such as O, Mg, Si, Ca). Therefore, the supersolar value of the $[\alpha/Fe]$ ratios for low $[Fe/H]$ values is due to the core-collapse SNe which restore the α -elements on short timescales. When SNe Ia, originating from CO WDs which have longer lifetimes, start restoring the amount of Fe, then the $[\alpha/Fe]$ ratios start decreasing. By means of the time-delay model, we can interpret any abundance ratio. In particular, the time-delay model allows us to derive the timescales for the formation of different stellar populations, since the $[Fe/H]$ axis can be read as a time axis (Matteucci 2001, 2012).

THE THREE-INFALL MODEL

A natural development of the two-infall model is the three-infall model (Micali et al. 2013). In fact, in order to impose constraints on the formation and the chemical evolution of the thick disc, the three-infall model has been developed. In the case of this model, there are three main infall episodes: the

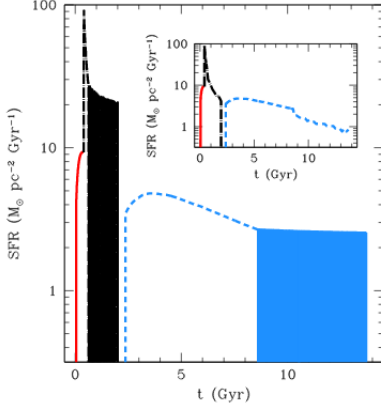


Figure 2.4: Star formation rate as a function of time in the three-infall model (Micali et al. 2013).

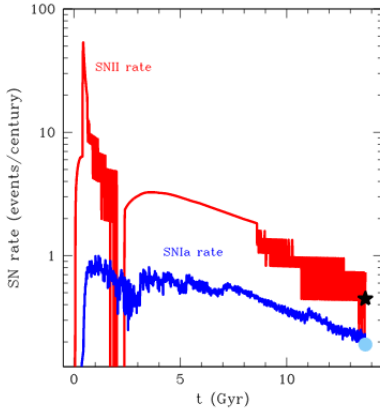


Figure 2.5: SN rates as functions of time in the three-infall model (Micali et al. 2013).

first is responsible for the formation of the halo, the second one gives rise to the thick disc and the third one to the thin disc. As in the previous model, the origin of the gas is extragalactic and its composition is assumed to be primordial; the Galactic disc is approximated by several independent rings, 2 kpc wide, without exchange of matter between them. The basic equation is the same discussed before, i.e. Eq. (2.8). The main assumptions of the three-infall model of Micali et al. (2013) can be summarized as follows.

As this model assumes three main infall episodes, the rate for mass accretion has to be changed into:

$$\begin{aligned} \dot{G}_i(r, t)_{inf} = & A_0(r)(X_i)_{inf}e^{-\frac{t}{\tau_0}} + A(r)(X_i)_{inf}e^{-\frac{t-t_{max0}}{\tau_1}} + \\ & + B(r)(X_i)_{inf}e^{-\frac{t-t_{max1}}{\tau_2}}, \end{aligned} \quad (2.11)$$

where $G_i(r, t)_{inf}$ is the infalling material in the form of element i and $(X_i)_{inf}$ is the composition of the infalling gas, which is assumed to be primordial. The quantities $A_0(r)$, $A(r)$ and $B(r)$ are three parameters fixed by reproducing the current total surface mass density distribution (halo+thick+thin disc), taken from Kuijken & Gilmore (1991). The parameter τ_{max0} is the time of maximum accretion onto the halo and roughly corresponds to the end of the halo phase, τ_{max1} represents the time of maximum accretion onto the thick disc and roughly corresponds to the end of the thick disc phase, τ_0 is the timescale for mass accretion in the halo, τ_1 is the timescale for mass accretion in the thick disc component and finally τ_2 is the timescale for mass accretion in the thin disc component. In the best model of Micali et al. (2013), $\tau_{max0}=0.4$ Gyr, $\tau_{max1}=2.0$ Gyr, $\tau_0=0.2$ Gyr, $\tau_1=1.25$ Gyr and finally $\tau_2=6.0$ Gyr at the solar radius.

The IMF is Scalo IMF (Scalo 1986). The SFR is the Schmidt-Kennicutt law (Kennicutt 1998a). The novelty introduced in the three-infall models concerns the efficiency of the SFR. In the best model of Micali et al. (2013),

$\nu_0=2 \text{ Gyr}^{-1}$ for the halo phase, $\nu_1=10 \text{ Gyr}^{-1}$ for the thick disc and finally $\nu_2=1 \text{ Gyr}^{-1}$ for the thin disc. Moreover, a threshold in the SFR has been introduced also in the thick disc component, in addition to that for the halo and that for the thin disc present in the two-infall model. In the best model of Micali et al. (2013), the thresholds are $4, 5$ and $7 \text{ M}_\odot \text{ pc}^{-2}$ during the halo, thick and thin disc phases, respectively. The predicted behaviour of the adopted SFR with a threshold in the gas density is shown in Fig. 2.4. In this plot, we see that, during the halo formation, the gas density never goes below the threshold, at variance with the two-infall model, in which the SFR during the halo formation was oscillating because of the gas density threshold. In the case of the three-infall model, this occurs because a time of maximum accretion for the halo has been assumed, namely the time at which the halo formation ends, of 0.4 Gyr . This time is shorter than assumed in the two-infall model and the infall rate is stronger, therefore it is more difficult to go below the threshold gas density of $4 \text{ M}_\odot \text{ pc}^{-2}$ during this time interval. Then, the thick disc formation starts and the star formation efficiency changes from 2 Gyr^{-1} to 10 Gyr^{-1} . This change in the star formation efficiency is responsible for the spike in the SFR. After this spike, the star formation trend presents an intermittent behaviour regulated by the surface gas density in the thick disc. This intermittent behaviour ends at 2 Gyr , which corresponds to the time of maximum accretion of gas density in the thick disc. At this time, we can see a star formation gap (like the gap in the two-infall model between the end of the halo-thick disc and the beginning of the thin disc phase), which lasts for 0.4 Gyr . The star formation changes again to the value of 1 Gyr^{-1} , which is appropriate for the thin disc. At this point, the formation of the thin disc starts and in this case the threshold of $7 \text{ M}_\odot \text{ pc}^{-2}$ is reached roughly at 8.5 Gyr , thus there are oscillations in the star formation from that epoch until the present time.

The assumed Type Ia SN model is the SD scenario. The predicted behaviour of the SN rates as a function of time is shown in Fig. 2.5. We can see that the gap between the end of the thick disc and the beginning of the thin disc due to the adopted gas density threshold is present in the predicted SNII rate as well (this gap was present also in the predictions of the two-infall model). The duration of the gap is 0.4 Gyr. The SNII rate shows a peak at around 0.4 Gyr, which roughly corresponds to the end of the halo phase, and then it reaches the value of 50 SNe per century because of the increased star formation efficiency during the thick disc formation. After this spike, the SNII rate goes to zero at a time of about 2 Gyr, this time corresponding to the end of the thick disc and the beginning of the gap in the SFR. Once the thick disc formation ends, star formation starts again and the number of supernovae per century increases until 4 Gyr, and then it decreases until the achievement of the present-time rate. On the other hand, Type Ia SNe, which are produced by progenitors with long lifetimes, show a smaller effect caused by the threshold in the star formation. First, their rate increases with time and then it remains almost constant until it decreases and reaches the present-time value.

BULGE MODELS

Matteucci & Brocato (1990) first suggested that to reproduce the metallicity distribution function in the bulge, one should assume a strong and short burst of star formation with the bulk of stars formed in the first 0.5 Gyr. Therefore, the bulge forms by fast gas infall and the assumed gas accretion law is:

$$\dot{G}_i(r, t)_{inf} = C(r)(X_i)_{inf}e^{-\frac{t}{\tau_3}}, \quad (2.12)$$

where $G_i(r, t)_{inf}$ is the infalling material in the form of the element i , $(X_i)_{inf}$ the composition of the infalling gas which is assumed to be primordial and

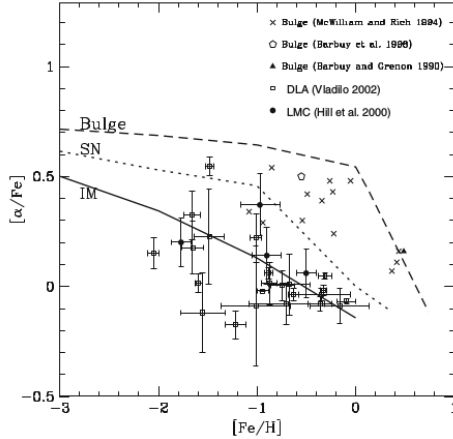


Figure 2.6: Predicted $[\alpha/\text{Fe}]$ vs. $[\text{Fe}/\text{H}]$ relations for the Galactic bulge (upper curve), the solar neighbourhood (median curve) and irregular galaxies (lower curve). Data for the bulge are shown for comparison. Data for the LMC and DLA systems are also reported. Figure from Matteucci (2012).

the parameter τ_3 corresponds to the timescale for mass accretion in this Galactic component and it is of the order of $\tau_3 = 0.1$ Gyr. Moreover, they assumed an IMF more top-heavy than the one in the solar neighbourhood. As a consequence of these assumptions, they predicted a plateau in the $[\alpha/\text{Fe}]$ ratios in bulge stars longer than in the solar vicinity, with a knee close to $[\text{Fe}/\text{H}] = 0.0$ dex. Their prediction was somewhat confirmed by the first data on $[\alpha/\text{Fe}]$ ratios by McWilliam & Rich (1994) (see Fig. 2.6).

As a general rule, the $[\text{X}/\text{Fe}]$ vs. $[\text{Fe}/\text{H}]$ relation of the solar vicinity should be shifted towards right if the star formation is more intense than in the solar region, whereas it should be shifted towards left if the star formation is less intense. This rule is a consequence of the time-delay model (Matteucci 2012).

Wyse & Gilmore (1992) considered various possibilities for the bulge formation, including the model of Matteucci & Brocato (1990): i) the bulge formed by accretion of extant stellar systems, which by dynamical friction eventually settled in the center of the Galaxy; ii) the bulge formed by accumulation of gas at the center of the Galaxy and evolved independently of the other components of the Galaxy, with either rapid or slow star formation; iii) the bulge formed by accumulation of metal-enriched gas from the thick or thin disc.

Later on, Ballero et al. (2007) presented an updated version of the model by Matteucci & Brocato (1990) and again concluded that the bulge formed on a very short timescale, of the order of 0.1 Gyr, that the star formation was much more efficient than in the solar vicinity by a factor of ~ 20 , and that the IMF was flatter than the one adopted for the solar neighbourhood. These conclusions were also supported by the paper of Cescutti & Matteucci (2011), where it was suggested that either a Salpeter or a flatter IMF were required to reproduce the bulge abundance patterns.

Then, Grieco et al. (2012) aimed at explaining the existence of the two main stellar populations observed in the bulge. They concluded that a stellar population forming by means of a classical gravitational gas collapse can be mixed with a younger stellar population created perhaps by the bar evolution.

Several other works have considered that the bulge formed as a result of secular evolution of the inner disc through bar formation and its subsequent buckling into a pseudo-bulge boxy/peanut (B/P) structure (Combes et al. 1990; Norman et al. 1996; Athanassoula 2005; Bekki & Tsujimoto 2011; Shen et al. 2010; Debattista et al. 2017; Buck et al. 2017; Fragkoudi et al. 2018), or a mixed scenario where the secular and spheroidal components coexist (Samland & Gerhard 2003; Tsujimoto & Bekki 2012).

CHAPTER 3

Chemical evolution of the thick and thin discs

In this Chapter, I present the results on the formation and chemical evolution of the Galactic thick and thin discs. The fundamental question that I would like to address in this Chapter can be summarized as follows. How can we explain the dichotomy of the Galactic discs? How did the thick and thin disc form? What is the origin of the metal-rich high- α stars? The Chapter is organized as follows. In Section 3.1, I give a brief introduction to the context to which this Chapter belongs. In Section 3.2, I present the data which have been used to make a comparison with the predictions of the chemical evolution models. In Section 3.3, I describe the chemical evolution models adopted. In Section 3.4, I show the comparison between model predictions and observations. Finally, Section 3.5 summarizes the results and conclusions. The results presented in this Chapter are described in the published paper Grisoni et al. (2017).

CHAPTER 3. CHEMICAL EVOLUTION OF THE THICK AND THIN DISCS

3.1 INTRODUCTION

As described in Chapter 1, we are in a golden era for Galactic Archaeology. In fact, recently many spectroscopic surveys and projects have been developed in order to study the formation and evolution of the Milky Way, such as for example Gaia-ESO (Gilmore et al. 2012), APOGEE (Majewski et al. 2015) and the AMBRE Project (de Laverny et al. 2013). Furthermore, the arrival of Gaia data is enhancing the value of these surveys. For instance, the Gaia/RVS data will provide abundances data for several tenths of millions of stars (Recio-Blanco et al. 2016). In this way, detailed stellar abundances of stars in the Milky Way can be measured.

In particular, the latest observational data reveal a clear distinction between the abundance patterns of the thick and thin disc stars, especially for the α -elements. In fact, Gaia-ESO data (Recio-Blanco et al. 2014; Rojas-Arriagada et al. 2017), APOGEE data (Hayden et al. 2015) and AMBRE data (Mikolaitis et al. 2017) indicate two distinct sequences corresponding to thick and thin disc stars, and the presence of these two sequences still has to be interpreted in terms of Galactic chemical evolution models.

As pointed out in Matteucci (2012), Galactic chemical evolution models have passed through different phases that can be summarized as follows: i) Serial approach (e.g. Matteucci & Francois 1989); ii) Parallel approach (e.g. Ferrini et al. 1992, Pardi et al. 1995, Chiappini 2009); iii) Two-infall approach (e.g. Chiappini et al. 1997, Romano et al. 2010); iv) Stochastic approach (e.g. Argast et al. 2000, Cescutti 2008). In the serial approach, one assumes that the halo, thick and thin-disc form in sequence. In this framework, the thick disc is simply a later phase relative to the halo and the thin disc is a later phase relative to the thick disc. In the parallel approach, the various Galactic stellar components start forming at the same time but evolve in parallel at

different rates. The two-infall model belongs to the serial approach, but it assumes that the halo-thick disc formed out of a completely independent gas accretion episode relative to the thin disc. This latter formed out of different extragalactic gas on a much longer timescale. In the stochastic approach, the early phases of the evolution are characterized by inhomogeneities of the ISM, in the sense that the early supernovae (SNe) pollute only nearby regions and the mixing is not efficient.

In this work, we will model the thick and thin disc evolution by adopting both the two-infall and the parallel approach.

The parallel approach was first introduced by Ferrini et al. (1992) and Pardi et al. (1995). In their model, they consider the three phases (halo, thick and thin discs) to evolve separately and in parallel. However, a limitation of this model is that the three phases are connected to one another through the infalling gas and this fact prevents to obtain a good agreement with the stellar metallicity distribution functions in the three phases. In fact, the three observed metallicity distribution functions are different, indicating that each component cannot have formed out of gas shed by the other two (see Matteucci 2001). An advantage of their approach is that they can explain the observed spread in the data and the observed overlapping in metallicity of stars belonging to different components. A more recent parallel approach was suggested by Chiappini (2009), Anders et al. (2017). The main difference between Chiappini (2009) and Pardi et al. (1995) is that in Chiappini's approach the thick and thin disc evolutions are completely disentangled.

On the other hand, the two-infall approach assumes two main infall episodes: during the first one, the halo-thick disc formed, whereas the second one gave rise to the thin disc. On this line, Chang et al. (1999) applied the two-infall model of Chiappini et al. (1997) to the thick and thin discs, although the

CHAPTER 3. CHEMICAL EVOLUTION OF THE THICK AND THIN DISCS

data at that time were much less and sparse. In the original two-infall model the thick disc was assumed to form fast on a timescale no longer than 2 Gyr and it was considered together with the halo. Micali et al. (2013) extended the two-infall model into a three infall model where the formation of the thick disc was assumed to have occurred by means of a gas accretion episode totally independent from the episodes forming the halo and the thin disc. In their model, the thick disc formed faster than the thin disc and on a timescale of 1 Gyr. They were able to reproduce the stellar metallicity distribution functions of the thick and thin discs. However, for what concerns the $[\alpha/\text{Fe}]$ ratios the available data were too sparse to identify different trends between the thick and thin disc stars. Recently, on the basis of the data of Adibekyan et al. (2012), Haywood et al. (2015) studied the evolution of the thick disc and concluded that the star formation history was uniform throughout the thick disc. They also concluded that the thick disc did not form inside-out in the first 3-5 Gyr of the evolution of the Galaxy. Later on, Haywood et al. (2016) by considering APOGEE data concluded that there was a quenching in the star formation at the end the thick phase. Kubryk et al. (2015a) suggested instead that the thick disc is the result of stellar migration: they concluded that the thick disc is the early part of the Milky Way disc. They explained the sequences of $[\alpha/\text{Fe}]$ ratios of the thick and thin discs by analyzing the data of Bensby et al. (2014). Masseron & Gilmore (2015) by studying the APOGEE data concluded that the majority of thick disc stars formed earlier than the thin disc ones and that the star formation rate in the thick disc was more efficient than in the thin disc. The aim of this work is to reproduce the chemical characteristics of the thick and thin disc stars as observed by the most recent data of the AMBRE Project (Mikolaitis et al. 2017). The AMBRE abundances come from high resolution data, similarly to those of Adibekyan et al. (2012), but they

belong to a much larger sample. The AMBRE resolution is also higher than APOGEE data. In order to study these data, we test the two-infall and parallel scenarios, by means of improved and updated Galactic chemical evolution models. Our chemical models are based on the two-infall model (Chiappini et al. 1997, Romano et al. 2010) revisited and applied to the thick and thin discs and a new parallel model adopting two one-infall models for the thick and thin discs, respectively. In this way, the evolution of the thick and thin discs are completely disentangled.

3.2 OBSERVATIONAL DATA

The observational data used in this work for comparison with the chemical evolution models are issued from the AMBRE Project (de Laverny et al. 2013). We remind that AMBRE has been defined in order to homogeneously determine stellar atmospheric parameters and chemical abundances for the archived spectra of the ESO spectrographs for Galactic archaeology purposes. Up to now, more than 200,000 high resolution spectra (including several repeats for several stars) have already been analysed. The corresponding atmospheric parameters have been derived thanks to the MATISSE algorithm (Recio-Blanco et al. 2006) and a large grid of FGKM synthetic spectra (de Laverny et al. 2012). In the present work, we have adopted the magnesium and iron chemical abundances presented in Mikolaitis et al. (2017). These abundances have been derived owing to an automatic line-fitting technique for the AMBRE FEROS and HARPS spectra, which have been previously parametrized by Worley et al. (2012) and de Pascale et al. (2014), respectively. We also point out the AMBRE sample is not complete and is characterized by different observational biases inherent to the content of the ESO archive. The present sample consists in 4,666 individual slow-rotating stars, most of them ($\sim 11\%$) being dwarfs of the solar neighbourhood for

CHAPTER 3. CHEMICAL EVOLUTION OF THE THICK AND THIN DISCS

which accurate Mg and Fe are available. All of these targets have been classified owing to their Mg and Fe properties into five different Galactic components (thin and thick discs, metal-poor high/low α , and metal-rich high α , MRHA hereafter). We remind that it has been possible to conduct such a chemical labelling thanks to the small uncertainties of the derived abundances and also because magnesium is one of the best specy to separate the two Galactic discs (Mikolaitis et al., 2014).

Finally, we have recently analysed the kinematical and dynamical properties of the stars in the AMBRE catalogue (Hayden et al. 2017). Those stars are also part of the TGAS catalogue (Brown et al. 2016, Lindegren et al. 2016) included in the first data release of the Gaia mission (Prusti et al. 2016). Thanks to the Gaia precise astrometry, we have been able to derive reliable orbital parameters for the stars using the galpy code (Bovy 2015). In particular, the perigalacticon points of the orbits, derived by Hayden et al. (private communication) will be used in this work.

3.3 THE MODELS

The chemical evolution models adopted here are:

- the two-infall model (Chiappini et al. 1997, Romano et al. 2010) revisited and applied to the thick and thin discs;
- a parallel model adopting two one-infall models for the thick and thin discs, respectively.

3.3.1 THE REVISED TWO-INFALL MODEL

The two-infall model adopted here is a revision of the model developed by Chiappini et al. (1997) and Romano et al. (2010), described in Chapter 2. The revised two-infall model assumes that the Galaxy forms as a result

of two main infall episodes: during the first one, the thick disc formed, whereas during the second one a much slower infall of gas, delayed with respect to the first one, gives rise to the thin disc. Here, we do not take into account the evolution of the halo, but we focus on the evolution of the thick and thin discs. The origin of the gas in the infall episodes is extragalactic and its composition is assumed to be primordial. The Galactic thin disc is approximated by several independent rings, 2 kpc wide, without exchange of matter between them whereas the evolution of the thick disc is fixed with radius.

The basic equations that follow the time evolution of G_i , namely the mass fraction of the element i in the gas, are described by Eq. (2.8). In particular, here we assume that the gas infall term is given by:

$$\dot{G}_i(r, t)_{inf} = A(r)(X_i)_{inf}e^{-\frac{t}{\tau_1}} + B(r)(X_i)_{inf}e^{-\frac{t-t_{max}}{\tau_2}}, \quad (3.1)$$

where $G_i(r, t)_{inf}$ is the infalling material in the form of element i and $(X_i)_{inf}$ is the composition of the infalling gas which is assumed to be primordial. The parameter t_{max} is the time for the maximum mass accretion onto the disc and roughly corresponds to the end of the thick disc phase. The parameters τ_1 and τ_2 are the timescales for mass accretion in the thick and thin disc components, respectively: they are the e-folding times of the mass accretion law and represent the times at which each component accumulated roughly half of its mass. These timescales are free parameters of the model and they are constrained mainly by comparison with the observed metallicity distribution of long-lived stars in the solar vicinity. The quantities $A(r)$ and $B(r)$ are two parameters fixed by reproducing the present time total surface mass density in the solar neighbourhood as taken from Nesti & Salucci (2013). In particular, this is equal to $65 \text{ M}_\odot \text{pc}^{-2}$ for the thin disc and $6.5 \text{ M}_\odot \text{pc}^{-2}$ for the thick disc. Other studies suggest slightly different values

CHAPTER 3. CHEMICAL EVOLUTION OF THE THICK AND THIN DISCS

for the total local surface mass density (Bovy & Rix 2013; Zhang et al. 2013; McKee et al. 2015): we tested also these values and found negligible difference in the results. What really matters here is the ratio between the total surface mass density of the thick and thin discs, which is considered to be 1:10.

The SFR is parametrized according to the Schmidt-Kennicutt law (Kennicutt 1998a), as introduced in Chapter 2. The star formation efficiency ν is assumed to become zero when the surface gas density goes below a critical threshold σ_{th} (Kennicutt 1998a,b; Martin & Kennicutt 2001). For the IMF, we adopt the Kroupa et al. (1993) one, but we also test the Scalo (1986) and the Salpeter (1955) ones.

3.3.2 THE PARALLEL MODEL

Secondly, we consider the possibility of abandoning a sequential scenario like the one of the two-infall, in favour of a picture which treats the thick disc and the thin disc stars as two truly distinct evolutionary phases, which start at the same time but evolve independently, as suggested by Chiappini (2009). In the light of these considerations, we develop two distinct one-infall models: one for the thick disc and the other for the thin disc.

As in the previous model, the material accreted by the Galactic discs comes mainly from extragalactic sources, and the basic equation is the same discussed before, i.e. Eq. (2.8).

Since this model assumes two distinct infall episodes, the gas infall is described as:

$$(\dot{G}_i(r, t)_{inf})|_{thick} = A(r)(X_i)_{inf}e^{-\frac{t}{\tau_1}}, \quad (3.2)$$

$$(\dot{G}_i(r, t)_{inf})|_{thin} = B(r)(X_i)_{inf}e^{-\frac{t}{\tau_2}}, \quad (3.3)$$

for the thick disc and for the thin disc, respectively. The quantities $A(r)$ and $B(r)$ and the parameters τ_1 and τ_2 have the same meaning as discussed

for Eq. (3.1). Actually, the exponential form is similar to the case of the two-infall model, but the novelty introduced here concerns the fact that the infall rate of the thick and thin discs are now totally disentangled. In fact, as mentioned above, we want to treat the thick and the thin disc as two truly distinct evolutionary phases. For the SFR and the IMF, the functional forms are the same of the two-infall model.

3.3.3 NUCLEOSYNTHESIS PRESCRIPTIONS

The nucleosynthesis prescriptions and the implementation of the yields in the model are fundamental ingredients for chemical evolution models. In this work, we adopt the same nucleosynthesis prescriptions of model 15 of Romano et al. (2010), where an exhaustive description of the adopted yields can be found.

For the computation of the stellar yields, one has to distinguish between different mass ranges as well as single stars versus binary systems:

- low and intermediate mass stars ($0.8 M_{\odot}$ - $8 M_{\odot}$), which are divided into single stars and binary systems which can give rise to Type Ia SNe,
- massive stars ($M > 8 M_{\odot}$).

Single stars in the mass range $0.8 M_{\odot}$ - $8 M_{\odot}$ contribute to the Galactic chemical enrichment through planetary nebula ejection and quiescent mass loss along the giant branch. They enrich the interstellar medium mainly in He, C, and N, but they can also produce some amounts of ${}^7\text{Li}$, Na and *s*-process elements. For these stars, which end their lives as white dwarfs, the adopted nucleosynthesis prescriptions are from Karakas (2010).

Type Ia SNe are considered to originate from carbon deflagration in CO WDs in binary systems. These stars contribute a substantial amount of iron

CHAPTER 3. CHEMICAL EVOLUTION OF THE THICK AND THIN DISCS

($0.6 M_{\odot}$ per event) and non negligible quantities of Si and S, and also Mn. They also contribute to other elements, such as O, C, Ne, Ca, and Mg, but in negligible amounts with respect to the masses of such elements ejected by Type II SNe. The adopted nucleosynthesis prescriptions for SNe Ia are from Iwamoto et al. (1999).

Massive stars with masses $M > 8 M_{\odot}$ are the progenitors of Type II, Ib and Ic SNe: if the explosion energies are much higher than 10^{51} erg, hypernova events can occur (SNe Ic). For these stars, the adopted nucleosynthesis prescriptions are from Kobayashi et al. (2006) for the following elements: Na, Mg, Al, Si, S, Ca, Sc, Ti, Cr, Mn, Co, Ni, Fe, Cu and Zn. As for the He and CNO elements, we consider the results of Geneva models for rotating massive stars (see Romano et al. 2010). However, for Mg which is one the relevant element in this study we adopted yields multiplied by a factor 1.2 in order to obtain a better agreement with the data. It is well known, in fact, that Mg yields have been underestimated in many nucleosynthesis studies (see François et al. 2004 for a discussion of this point), and although the most recent ones have improved nonetheless the Mg production in massive stars is still underestimated.

3.4 RESULTS

Good models of Galactic chemical evolution should reproduce the majority of the observational features and always a number of observational constraints that is larger than the number of free parameters. In this work, the observational constraints considered are the following ones:

- Abundance patterns of the most common chemical elements, in particular the $[\text{Mg}/\text{Fe}]$ vs. $[\text{Fe}/\text{H}]$ abundance pattern recently observed by the AMBRE Project;

Table 3.1: Input parameters for the best chemical evolution models. 2IM corresponds to the two-infall model, whereas 1IMT and 1IMt correspond to the one-infall models for the thick and thin discs, respectively. In the second column, we show the adopted initial mass function. In the third and fourth columns, there are the star formation efficiencies for the thick and thin discs, respectively. In the fifth and sixth columns, we give the timescales for mass accretion in the thick and thin discs, respectively. Finally, in last column, we show the adopted threshold in the star formation rate.

Model	IMF	ν_1 [Gyr ⁻¹]	ν_2 [Gyr ⁻¹]	τ_1 [Gyr]	τ_2 [Gyr]	σ_{th} [M _⊙ pc ⁻²]
2IM	Kroupa	2	1	0.1	7	7
1IMT	Kroupa	2	-	0.1	-	-
1IMt	Kroupa	-	1	-	7	7

- Metallicity distribution function of long-lived stars belonging to the thick and thin disc components as recently observed by the AMBRE Project;
- Solar abundances;
- Present-time SFR;
- Present-time Type Ia and Type II supernova rates.

Our best models have been selected after running several numerical simulations by varying one at the time the most important input parameters. The input parameters of the best models are summarized in Table 3.1. In the first column, we give the names of the models: 2IM corresponds to

CHAPTER 3. CHEMICAL EVOLUTION OF THE THICK AND THIN DISCS

the two-infall model, whereas 1IMT and 1IMt correspond to the one-infall models for the thick and thin discs, respectively. In the second column, we show the adopted IMF. In the third and fourth columns, there are the star formation efficiencies for the thick and thin discs, respectively. In the fifth and sixth columns, we give the timescales for mass accretion in the thick and thin discs, respectively. Finally, in last column, we show the adopted threshold in the SFR.

In Fig. 3.1, we show the effect of varying one at the time the most important input parameters of the two-infall model.

In the upper left panel of Fig. 3.1, we show the effect of varying the IMF. We can see the prediction of the two-infall model in the solar vicinity for which we consider Kroupa et al. (1993) IMF, compared to the case with Scalo (1986) IMF and Salpeter (1955) IMF. We can see that Scalo (1986) IMF predicts too few massive stars, and so the corresponding track in the $[\text{Mg}/\text{Fe}]$ vs. $[\text{Fe}/\text{H}]$ lies below the data. On the other hand, Salpeter (1955) IMF predicts too many massive stars, and so the corresponding track in the $[\text{Mg}/\text{Fe}]$ vs. $[\text{Fe}/\text{H}]$ is above the data.

In the lower left panel of Fig. 3.1, we show the effect of varying the star formation efficiency of the thick disc. We can see the prediction of the two-infall model in the solar vicinity for which the star formation efficiency of the thick disc is $\nu_1 = 1, 2$ and 3 Gyr^{-1} . We can see that a higher star formation efficiency implies a higher track in the $[\text{Mg}/\text{Fe}]$ vs. $[\text{Fe}/\text{H}]$, even if the effect is less strong than in the case of varying the IMF. Furthermore, we can see that a higher star formation efficiency means a more rapid evolution for the thick disc, and this extends the range of $[\text{Mg}/\text{Fe}]$ values for the thick disc stars.

In the upper right panel of Fig. 3.1, we show the effect of varying the timescale for mass accretion in the thick disc. We can see the prediction of

the two-infall model in the solar vicinity for which the timescale of the thick disc is $\tau_1 = 0.1, 0.5$ and 1 Gyr. We can see that a shorter timescale for the thick disc formation extends the range of $[\text{Mg}/\text{Fe}]$ values for the thick disc stars, because the evolution is more rapid.

In the lower right panel of Fig. 3.1, we show the effect of varying the threshold in the SFR. We can see the prediction of the two-infall model in the solar vicinity for which the threshold is $\sigma_{th} = 4, 7$ and $10 \text{ M}_\odot \text{ pc}^{-2}$. The gap in the model prediction is due to the assumed threshold in the star formation process. Varying the threshold means varying the extension of this gap, and the gap increases with increasing threshold.

On the other hand, the two parameters regarding the star formation efficiency and the timescale for mass accretion in the thin disc are well constrained by reproducing the G-dwarf distribution and correspond to $\nu_2 = 1 \text{ Gyr}^{-1}$ and $\tau_2 = 7$ Gyr, as found in previous studies (Chiappini et al. 1997; Romano et al. 2010).

Similarly, we chose also the various input parameters for the one-infall models, as summarized in Table 3.1.

In the following, we focus on our best models and we show the predictions concerning the abundance patterns, the metallicity distribution functions of the thick and thin discs, the solar abundances, the star formation history and the supernova rates.

3.4.1 ABUNDANCE PATTERNS

The first observational constraint considered is the $[\text{Mg}/\text{Fe}]$ vs. $[\text{Fe}/\text{H}]$ relation, as observed by the AMBRE Project. We consider Mg, since it is the best specy to separate the two Galactic discs (Mikolaitis et al. 2014), but the interpretation of the formation of the Galactic components would be unchanged when considering other α -elements, such as Si and Ca.

CHAPTER 3. CHEMICAL EVOLUTION OF THE THICK AND THIN DISCS

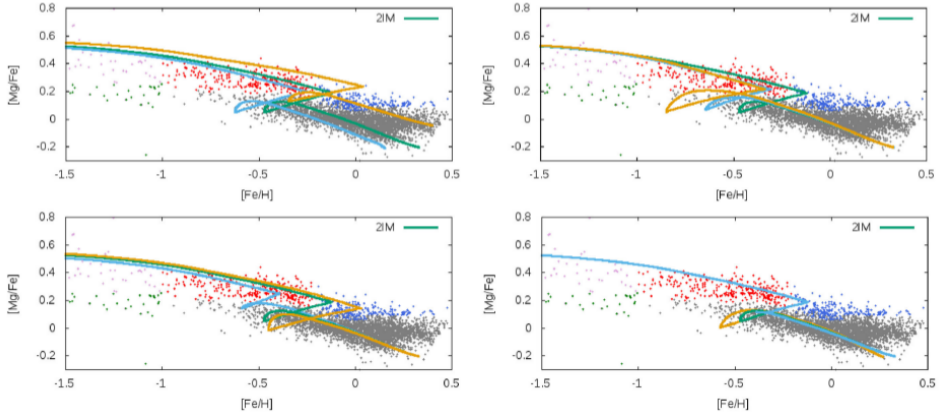


Figure 3.1: Predicted and observed $[Mg/Fe]$ vs. $[Fe/H]$ in the solar neighbourhood in the case of the two-infall model. The data are from the AMBRE Project and the different Galactic components are plotted: thin disc (grey dots), thick disc (red dots), metal-rich high- α sequence (blue dots), metal-poor low- α sequence (green dots), metal-poor high- α sequence (magenta). *Upper left panel:* the effect of varying the IMF. The 2IM with Kroupa et al. (1993) IMF (green line) is compared with a model with Scalo (1986) IMF (light-blue line) and Salpeter (1955) IMF (orange line). *Lower left panel:* the effect of varying the star formation efficiency of the thick disc. The 2IM with $\nu_1 = 2 \text{ Gyr}^{-1}$ (green line) is compared with a model with $\nu_1 = 1 \text{ Gyr}^{-1}$ (light-blue line) and $\nu_1 = 3 \text{ Gyr}^{-1}$ (orange line). *Upper right panel:* the effect of varying the timescale of the thick disc. The 2IM with $\tau_1 = 0.1 \text{ Gyr}$ (green line) is compared with a model with $\tau_1 = 0.5 \text{ Gyr}$ (light-blue line) and $\tau_1 = 1 \text{ Gyr}$ (orange line). *Lower right panel:* the effect of varying the threshold. The 2IM with $\sigma_{th} = 7 \text{ M}_\odot \text{ pc}^{-2}$ (green line) is compared with a model with $\sigma_{th} = 4 \text{ M}_\odot \text{ pc}^{-2}$ (light-blue line) and $\sigma_{th} = 10 \text{ M}_\odot \text{ pc}^{-2}$ (orange line).

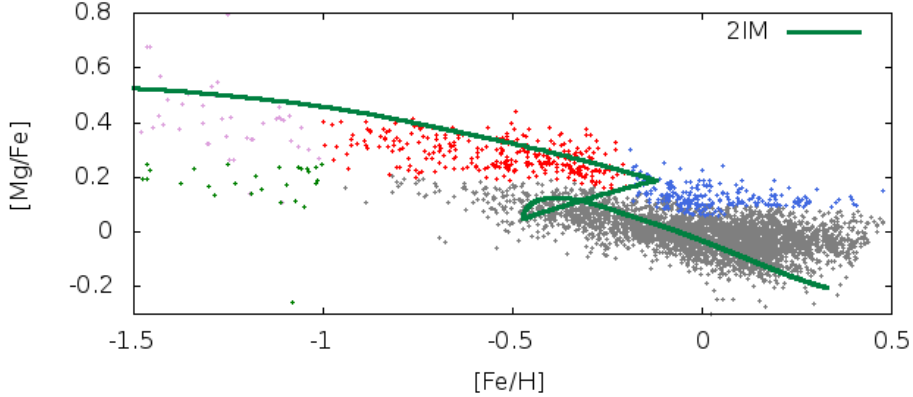


Figure 3.2: Predicted and observed $[\text{Mg}/\text{Fe}]$ vs. $[\text{Fe}/\text{H}]$ in the solar neighbourhood in the case of the two-infall model. The data are from the AMBRE Project and the different Galactic components are plotted: thin disc (grey dots), thick disc (red dots), metal-rich high- α sequence (blue dots), metal-poor low- α sequence (green dots), metal poor high- α sequence (magenta). The predictions are from model 2IM (green line).

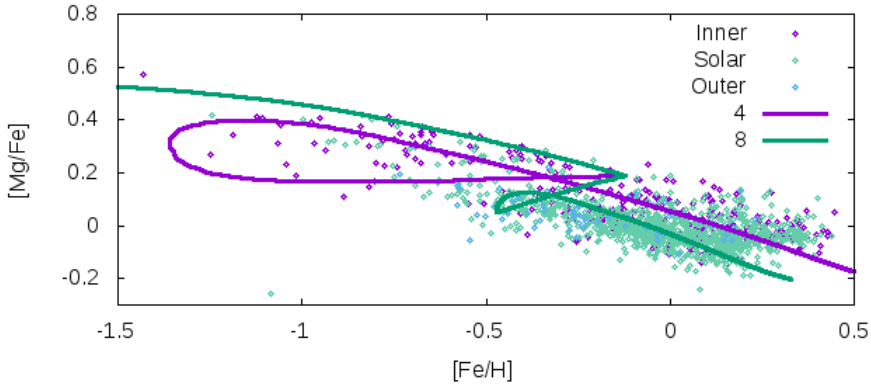


Figure 3.3: Predicted and observed $[\text{Mg}/\text{Fe}]$ vs. $[\text{Fe}/\text{H}]$. The data are color-coded according to their guiding radius (inner, solar, outer) and the predictions are from model 2IM (both at 8 kpc and at 4 kpc).

CHAPTER 3. CHEMICAL EVOLUTION OF THE THICK AND THIN DISCS

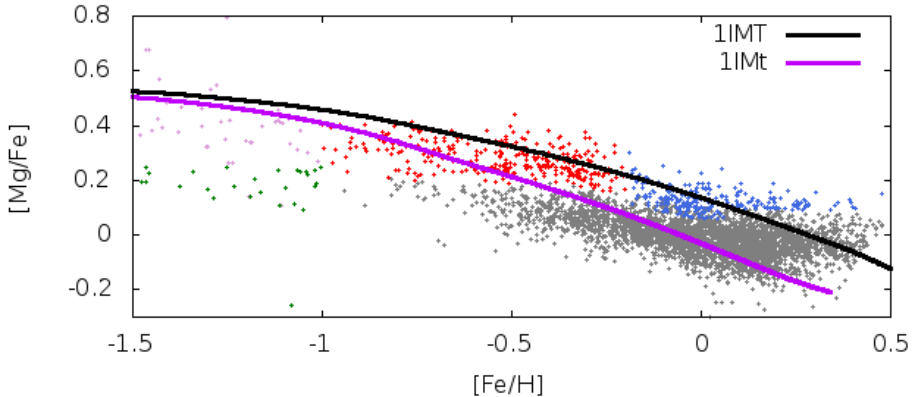


Figure 3.4: Same as Fig. 3.2, but the predictions are for models 1IMT for the thick disc (black line) and 1IMt for the thin disc (magenta line).

In Fig. 3.2, we show the predicted and observed $[\text{Mg}/\text{Fe}]$ vs. $[\text{Fe}/\text{H}]$ in the solar neighbourhood in the case of the two-infall model 2IM. The model predicts an overabundance of Mg relative to Fe almost constant until $[\text{Fe}/\text{H}] < -1.5$ dex and then for $[\text{Fe}/\text{H}] \sim -1.5$ dex the trend shows a slight decrease due to the delayed explosion of Type Ia SNe. This behaviour of the abundance patterns of α -elements such as Mg is well-interpreted in terms of the time-delay model (see Matteucci 2001; 2012): the time-delay refers to the delay of iron ejection from Type Ia SNe relative to the faster production of α -elements by core-collapse SNe. The effect of the delayed iron production is to create an overabundance of α -elements relative to iron at low $[\text{Fe}/\text{H}]$ values, and a continuous decline of the $[\alpha/\text{Fe}]$ ratio until the solar value is reached. A peculiar feature of the 2IM is that at $[\text{Fe}/\text{H}] \sim -0.2$ dex we have a gap of 700 Myr duration due to the assumed threshold in the star formation process, which marks the transition between the thick and

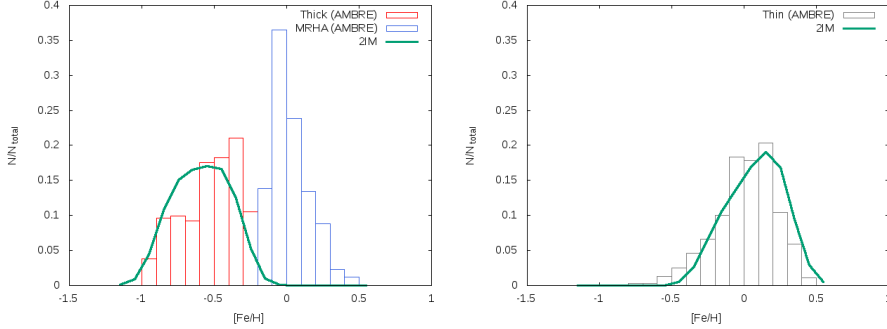


Figure 3.5: *Left panel:* Predicted and observed metallicity distribution function of the thick disc in the case of the two-infall model. The data are from the AMBRE Project: MDF of thick disc stars (red) and MDF of MRHA stars (blue). The predictions are from model 2IM (green line). We notice that the two-infall model cannot reproduce the MRHA stars, as explained in the text. *Right panel:* Predicted and observed metallicity distribution function of the thin disc in the case of the two-infall model. The data are from the AMBRE Project: MDF of thin disc stars (grey). The predictions are from model 2IM (green line).

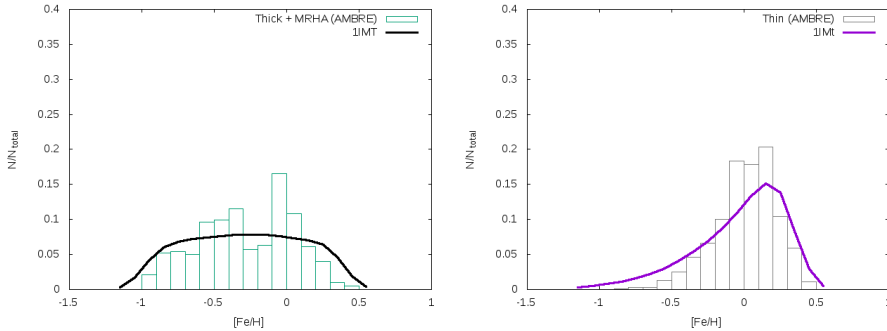


Figure 3.6: Same as Fig. 3.5, but the predictions are for models 1IMT for the thick disc (black line) and 1IMt for the thin disc (magenta line). We notice that in this case in the left panel the MDF of thick plus MRHA stars is considered, since the one-infall model of the thick disc can reproduce also the MRHA stars.

CHAPTER 3. CHEMICAL EVOLUTION OF THE THICK AND THIN DISCS

thin disc phases, where the star formation stops until the gas density in the thin disc reaches the threshold. A similar gap was found in the two-infall model of Chiappini et al. (1997), but between the halo-thick and thin disc phases, whereas here we focus on the disc (thick plus thin). It is worth noting that the 2IM model does not reproduce the metal rich α -enhanced stars (MRHA) (blue dots). If they are thick disc stars, this model cannot reproduce them since the thick disc does not extend far enough in $[\text{Fe}/\text{H}]$. However, these stars have shorter R_p (perigalacticon) values and we could suppose that we see them now in the solar neighbourhood thanks to stellar migration from the inner thin disc.

In Fig. 3.3, we show the predictions of the 2IM also in a slice that is more internal than the solar neighbourhood, i.e. 4 kpc from the Galactic center. What differ from the 2IM for the solar neighbourhood are the timescale of the thin disc (which is shorter and at 4kpc is equal to 0.5 Gyr in the framework of an inside-out scenario) and the surface mass density (which changes with radius and at 4 kpc is equal to $303 \text{ M}_{\odot}\text{pc}^{-2}$ as in Nesti & Salucci 2013). According to the 2IM at 4 kpc, a large loop is evident in the abundance pattern: this is due to the fact that the initial gas infall in the inner disc is more efficient than in the solar ring, and this produces a large $[\text{Fe}/\text{H}]$ dilution between the thick and thin disc formation. In this case, the track in the abundance pattern is higher at higher metallicities and the MRHA stars can be fitted. Hence, these stars could be interpreted as stars that have migrated from the inner thin disc.

Then, in Fig. 3.4, we show the predicted and observed $[\text{Mg}/\text{Fe}]$ vs. $[\text{Fe}/\text{H}]$ in the solar neighbourhood in the case of the parallel models 1IMT and 1IMt for the thick and thin discs, respectively. In the case of a parallel model, the thick and thin discs are treated as two truly distinct evolutionary phases and so we have two distinct tracks in the abundance pattern. Both the

tracks show an overabundance of Mg relative to Fe almost constant until $[\text{Fe}/\text{H}] < -1.5$ dex and then the trends show the decrease due to the delayed explosion of Type Ia SNe. However, the $[\alpha/\text{Fe}]$ ratios in the thick disc stars are higher than in the thin disc, as a consequence of the assumed faster evolution of the thick disc (a timescale of the order of 0.1 Gyr, as shown in Table 3.1). Indeed, the fit to the data requires that the formation of the thick disc occurs on shorter timescales than the formation of the thin disc. In fact, a fast SFR and a short timescale of gas accretion are required to form the thick disc, whereas a much slower SFR and longer accretion timescale (7 Gyr, see Table 3.1) are necessary to reproduce the features of the thin disc. In Figure 3.2 it is evident that with the parallel model we are able to reproduce the MRHA stars as metal rich thick disc stars, since in the parallel approach the thick disc can extend up to high $[\text{Fe}/\text{H}]$, at variance with the 2IM model.

3.4.2 METALLICITY DISTRIBUTION FUNCTIONS

A fundamental constraint that we have to analyze is the metallicity distribution function (MDF), both in the thick and thin discs. Thanks to our models, we are able to create two different MDFs, one for the thick and one for the thin disc.

First, let us consider the case of the two-infall model. Since the two-infall model predicts a gap in the star formation between the thick and thin discs, we consider as stars of the thick disc all those formed before the gap in the star formation and as stars of the thin disc all those formed afterwards.

In the left panel of Fig. 3.5, we show the predicted and observed MDF of the thick disc in the case of the two-infall model: the data are from the AMBRE Project and the predictions are from model 2IM. From the data, we can see that the metallicity of the thick disc goes from $[\text{Fe}/\text{H}] \sim -1.0$ dex

CHAPTER 3. CHEMICAL EVOLUTION OF THE THICK AND THIN DISCS

to $[\text{Fe}/\text{H}] \sim -0.2$ dex, and the mean value is $\langle [\text{Fe}/\text{H}] \rangle \sim -0.5$ dex. The 2IM well reproduces the observations. In fact, we have a tail of metal-poor stars and the same relative number for higher-metallicity stars, and the relative number of stars with $[\text{Fe}/\text{H}] \sim -0.5$ dex predicted by the model is equal to $\sim 15\%$. Therefore, as regards to the thick disc, the model is good from the chemical point of view, as it predicts a relative number of stars in agreement with the observations, in the right $[\text{Fe}/\text{H}]$ range. However, we notice that the 2IM model cannot reproduce the MRHA stars, because in the two-infall approach the thick disc phase does not extend so far in metallicity.

In the right panel of Fig. 3.5, we show the predicted and observed MDF of the thin disc in the case of the two-infall model: the data are from the AMBRE Project and the predictions are from model 2IM. From the data, we can see that the metallicity of the thin disc goes from $[\text{Fe}/\text{H}] \sim -0.5$ dex to $[\text{Fe}/\text{H}] \sim 0.5$ dex, and the mean value is around the solar metallicity. Also in the case of the thin disc, the model is in good agreement with observations. Secondly, let us consider the case of the parallel model.

In the left panel of Fig. 3.6, we show the predicted and observed MDF of the thick disc in the case of the parallel model: the data are from the AMBRE Project and the predictions are from model 1IMT. To have a good agreement with the data, we have to consider the MDF of thick plus MRHA stars, which can be reproduced in the framework of the 1IMT model. In fact, the MDF predicted by model 1IMT is very broad and includes also the MRHA stars.

In the right panel of Fig. 3.6, we show the predicted and observed MDF of the thin disc in the case of a parallel model: the data are from the AMBRE Project and the predictions are from model 1IMt. Concerning the thin disc, the model is in quite good agreement with the data of the thin disc stars.

Table 3.2: Solar abundances in dex.

Elem.	Observations	2IM	1IMt
O	8.66 ± 0.05	8.95	8.96
Mg	7.53 ± 0.09	7.58	7.59
Si	7.51 ± 0.04	7.71	7.72
S	7.14 ± 0.04	7.34	7.36
Fe	7.45 ± 0.05	7.64	7.66

3.4.3 SOLAR ABUNDANCES

In Table 3.2, the solar abundances predicted by the models 2IM and 1IMt are compared with observations of Grevesse et al. (2007).

The abundances are expressed as $12 + \log(X/H)$. These abundances correspond to the composition of the interstellar medium at the time of the formation of the Sun, 4.5 Gyr ago. Since we assume a Galactic lifetime of 13.7 Gyr, we have calculated the solar abundances at 9.2 Gyr after the Big Bang. Given the uncertainties, we can say that the predictions are in reasonable agreement with the observations. However, our predicted solar O is always a bit overestimated and the good agreement with the Mg solar abundance is due to the fact that we did increase the Mg yields from massive stars by multiplying them by a factor 1.2.

3.4.4 STAR FORMATION HISTORY

In Fig. 3.7, we show the SFR versus time as predicted by model 2IM. As we can see, the SFR is higher during the thick disc phase, while it is lower during the thin disc formation. A peculiar feature of this plot is the gap in

CHAPTER 3. CHEMICAL EVOLUTION OF THE THICK AND THIN DISCS

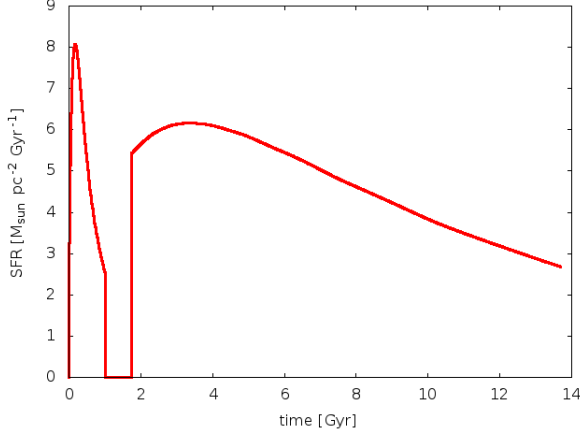


Figure 3.7: Temporal evolution of the SFR, as predicted by model 2IM.

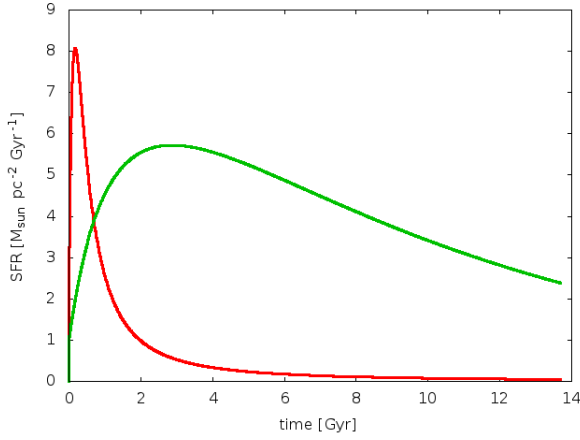


Figure 3.8: Temporal evolution of the SFR. *Red line*: prediction of model 1IMT. *Green line*: prediction of model 1IMt.

the SFR between the thick disc and the thin disc formation. This is clearly due to the fact that the star formation in the thin disc occurs only after a density of $7 \text{ M}_\odot \text{ pc}^{-2}$ has been accumulated. This gap was already predicted by Chiappini et al. (1997) for the 2IM model applied to the halo-thick disc and thin disc. The duration of the predicted gap between the thick and thin disc formation here is roughly 1 Gyr. An important constraint is represented by the present time SFR in the solar vicinity, and according to Bovy (2017) the present time SFR as measured with Gaia is:

$$\psi_0 \sim 1.7 \text{ M}_\odot \text{ pc}^{-2} \text{ Gyr}^{-1},$$

with an e-folding time of $\sim 7 \text{ Gyr}$. The value predicted by our best model is:

$$\psi_0 = 2.7 \text{ M}_\odot \text{ pc}^{-2} \text{ Gyr}^{-1},$$

in good agreement with observations.

In Fig. 3.8, we show the SFR versus time as predicted by models 1IMT and 1IMt for the thick and thin discs, respectively. The two SFRs are now separate, since we have assumed a distinct evolution for the two components of the disc, and there is no gap in star formation between the thick and thin disc phases. The star formation history of the thick disc is very different from the star formation history of the thin disc. In fact, the star formation history of the thick disc is peaked at earlier times, because it forms more rapidly than the thin disc (in fact, the thick disc has a higher star formation efficiency and a shorter timescale of formation with respect to the thin disc). On the other hand, the SFR of the thin disc has a peak shifted to a later time and has still an active star formation at the present time. The value predicted for the present time SFR in the solar vicinity by model 1IMt is:

$$\psi_0 = 2.4 \text{ M}_\odot \text{ pc}^{-2} \text{ Gyr}^{-1},$$

CHAPTER 3. CHEMICAL EVOLUTION OF THE THICK AND THIN DISCS

also in this case, in agreement with observations. On the other hand, for the thick disc there is no constraint available, since there is no active star formation at the present time.

3.4.5 SUPERNOVA RATES

In Fig. 3.9, we show the predicted behaviour of the SN rates as a function of time as predicted by the two-infall model. As we can see, the gap between the end of the thick disc phase and the beginning of the thin disc phase, due to the adopted threshold, is also responsible for the trend of Type II SN rate. In fact, the trend shows a peak around ~ 0.1 Gyr, which roughly corresponds to the timescale of formation of the thick disc phase, and then goes to zero at a time of about 1 Gyr, which corresponds to the end of the thick disc phase. The explanation of this feature is that the SNe Type II originate from stars with high mass and short lifetime, thus closely track the SFR and, hence, the number of this type of SNe per century is higher in the first gigayears of the formation of the Milky Way. Once the thick disc formation ends, star formation starts again and the number of supernovae per century increases until 3 Gyr, and then decreases until the achievement of the present rate. On the other hand, the SNe Type Ia are produced by progenitors with long lifetimes, thus they are very little influenced by the existence of a threshold in the star formation and the SNe Type Ia rate increases with time and remains almost constant until the achievement of the present value. An important constraint is represented by the present time SN rates in the solar vicinity, and according to Cappellaro & Turatto (1997) we have that:

$$\text{SNII} = 1.2 \pm 0.8 \text{ century}^{-1},$$

$$\text{SNIa} = 0.3 \pm 0.2 \text{ century}^{-1},$$

or more recently according to Li et al. (2011):

$$\text{SNCC} = 2.30 \pm 0.48 \text{ century}^{-1},$$

$$\text{SNII} = 1.54 \pm 0.32 \text{ century}^{-1},$$

$$\text{SNIa} = 0.54 \pm 0.12 \text{ century}^{-1}.$$

The values predicted by the model 2IM are respectively:

$$\text{SNII} = 1.4 \text{ century}^{-1},$$

$$\text{SNIa} = 0.3 \text{ century}^{-1},$$

in good agreement with observations.

On the other hand, in Fig. 3.10, we show the predicted behaviour of the SN rates as a function of time as predicted by the parallel model. The values of the present time SN rates in the solar vicinity predicted by the 1IMt are:

$$\text{SNII} = 1.2 \text{ century}^{-1},$$

$$\text{SNIa} = 0.3 \text{ century}^{-1},$$

also in this case, in agreement with observations.

3.5 CONCLUSIONS

In this work, we have studied the formation and evolution of the Milky Way thick and thin discs on the basis of detailed chemical evolution models to compare with the recent AMBRE [Mg/Fe] vs. [Fe/H] (Mikolaitis et al. 2017).

In particular, we have explored two different approaches for modelling Galactic chemical evolution: the two-infall and the parallel approach. In the two-infall scenario, the Galaxy formed by means of two infall episodes:

CHAPTER 3. CHEMICAL EVOLUTION OF THE THICK AND THIN DISCS

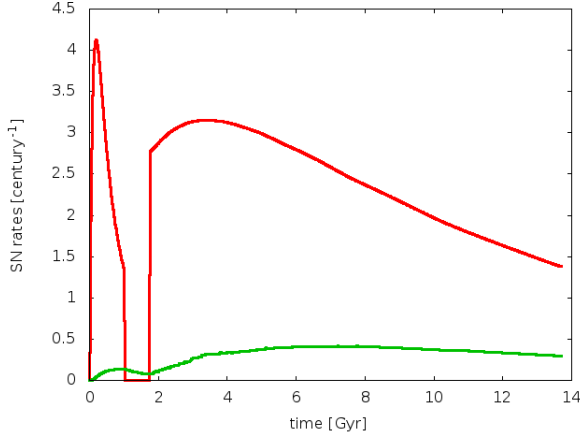


Figure 3.9: Temporal evolution of the SN rates, as predicted by model 2IM. *Red line*: SNII rates predicted by model 2IM. *Green line*: SNIa rates predicted by model 2IM.

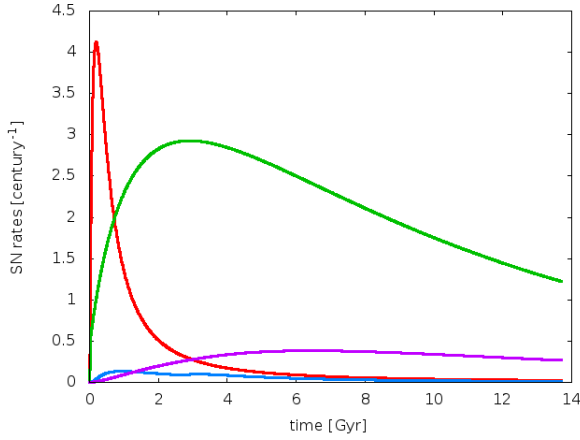


Figure 3.10: Temporal evolution of the SN rates. *Red line*: SNII rates predicted by model 1IMT. *Green line*: SNII rates predicted by model 1IMt. *Blue line*: SNIa rates predicted by model 1IMT. *Magenta line*: SNIa rates predicted by model 1IMt.

during the first one, the thick disc formed whereas the second one gave rise to the thin disc. On the other hand, the parallel scenario assumes that the various Galactic components started forming at the same time but at different rates.

Our best models have been selected after performing several numerical simulations by varying one at the time the most important input parameters. The input parameters of the best models are: $\tau_1=0.1$ Gyr for the timescale of formation of the thick disc and $\tau_2=7$ Gyr for the timescale of formation of the thin disc, $\nu_1=2$ Gyr $^{-1}$ for the star formation efficiency of the thick disc and $\nu_2=1$ Gyr $^{-1}$ for the star formation efficiency of the thin disc, $\sigma_{th}=7$ M $_{\odot}$ pc $^{-2}$ for the assumed threshold in the star formation rate, and a Kroupa et al. (1993) IMF.

Our conclusions are as follows.

- As regard to the abundance patterns, we have focused on the α -element for which there is a clear distinction between thick and thin disc stars. The two-infall model can reproduce the thick and thin disc stars, but not the MRHA stars unless we assume that these stars have migrated from the inner thin disc. On the other hand, the parallel model treats the thick and thin discs as two truly distinct and parallel evolutionary phases and so we have two distinct tracks in the abundance pattern. With the parallel model, we are able to reproduce the MRHA stars as the metal rich thick disc stars, since in the parallel approach the thick disc can extend up to high [Fe/H], at variance with the two-infall sequential model.
- For the metallicities distribution functions, the two-infall model can reproduce the MDF of the thick and thin disc stars, whereas it cannot

CHAPTER 3. CHEMICAL EVOLUTION OF THE THICK AND THIN DISCS

reproduce the MRHA stars. On the other hand, with the parallel model the MDF of the thick disc is very broad and includes also the MRHA stars. We underline that the MDF represents a fundamental constraint for chemical evolution models because it is strongly dependent on the mechanism of disc formation. In particular, for our best models in the parallel scenario the timescale for the formation of the thick disc is equal to 0.1 Gyr, whereas the timescale for the formation of the thin disc at solar position is much longer and it is equal to 7 Gyr. Both these timescales are dictated by reproducing the MDF of each Galactic component.

- Concerning the solar abundances, the predictions of all models are in reasonable agreement with the observations of Grevesse et al. (2007), but for Mg we had to increase the canonical yields from massive stars by a factor 1.2.
- The predicted present-time SFR is $\psi_0 = 2.7 \text{ M}_\odot \text{ pc}^{-2} \text{ Gyr}^{-1}$ (for the two-infall model) and $\psi_0 = 2.4 \text{ M}_\odot \text{ pc}^{-2} \text{ Gyr}^{-1}$ (for the one-infall model of the thin disc), both in good agreement with observations. The predicted present-time SNII rate is 1.4 century^{-1} (for the two-infall model) and 1.2 century^{-1} (for the one-infall model of the thin disc), whereas the predicted present-time SNIa rate is 0.3 century^{-1} (for the two-infall model) and 0.3 century^{-1} (for the one-infall model of the thin disc), in good agreement with the observations.
- In the two-infall approach, there is a gap in star formation between the thick and thin disc formation of several hundreds of Myr (~ 700 Myr), at variance with the parallel approach where no gap is present.

To summarize, a sequential approach like the one of the two-infall model can reproduce the chemical properties of thick and thin disc stars, but not those of the MRHA stars; in this case, these stars can be explained only by stellar migration from the inner disc. On the other hand, in order to reproduce the chemical properties of the MRHA stars without invoking stellar migration, it is better to consider a parallel scenario where the evolution of the thick and thin discs are separated; in this way, the MRHA stars can be interpreted as metal rich thick disc stars. In particular, the parallel approach can be very useful to follow the evolution of the Galactic thick and thin discs separately, to explore the dichotomy between the two discs in different abundance patterns (see for example Chapter 6 on lithium and Chapter 7 on neutron capture elements).

Abundance gradients along the Galactic disc

In this Chapter, I discuss the results on the formation of abundance gradients along the Galactic disc. The fundamental question that I would like to address here can be summarized as follows. How did abundance gradient form? What are the main ingredients that shape the present-time abundance gradient? What is the time evolution of abundance gradients? The Chapter is organized in the following way. In Section 4.1, I outline the context in which this Chapter fits. In Section 4.2, we show the observational data which have been considered to make a comparison with the predictions of the chemical evolution models. In Section 4.3, we describe the chemical evolution models used in this work. In Section 4.4, we present the comparison between observations and model predictions. Finally, in Section 4.5, we summarize our results and conclusions. The results presented in this Chapter are described in the published paper Grisoni et al. (2018).

CHAPTER 4. ABUNDANCE GRADIENTS ALONG THE GALACTIC DISC

4.1 INTRODUCTION

In order to study the formation and chemical evolution of our Galaxy, a fundamental constraint is represented by abundance gradients along the Galactic thin disc. Furthermore, recent observational data of abundance patterns at various Galactocentric distances represent another important constraint for understanding the formation and evolution of the Milky Way disc. In this context, it is important to have several elements, produced by stars with different masses and timescales (Adibekyan et al. 2012; Bensby et al. 2014; Hayden et al. 2015; Magrini et al. 2017), to gain information about the nucleosynthesis channels, sites of production and timescales of enrichment of each chemical element, but also about the star formation history of the Galactic disc.

Abundance gradients have been observed in many spiral galaxies and show that the abundances of metals decrease outward from the Galactic center. Generally, a good agreement between observational properties of the Galaxy and model predictions is obtained by assuming that the disc formed by infall of gas (Chiosi 1980; Matteucci & Francois 1989; Ferrini et al. 1994; Chiappini et al. 1997, 2001; Cescutti et al. 2007; Colavitti et al. 2009; Chiappini 2009; Magrini et al. 2009; Spitoni & Matteucci 2011; Mott et al. 2013; Haywood et al. 2013; Snaith et al. 2015; Kubryk et al. 2015a,b; Prantzos et al. 2018). In particular, a good assumption for reproducing abundance gradients is that the timescale for the formation of the Galactic thin disc increases with Galactocentric radius according to the inside-out scenario (Matteucci & Francois 1989; Chiappini et al. 2001). Cescutti et al. (2007) showed that a two-infall model with inside-out scenario gives a very good agreement with the data of Cepheids for many elements (Andrievsky et al. 2002a,b,c, 2004; Luck et al. 2003). Colavitti et al. (2009) showed that it is fundamental

to assume an inside-out scenario, but also other ingredients, such as a threshold in the gas density for the star formation rate or a variable star formation efficiency (higher in the inner region than in the outer ones), in order to reproduce the present day gradients in the outer disc. More recently, Pilkington et al. (2012) have supported the conclusion that spiral discs form inside-out. To maintain consistency with the dynamical consequence of infall, also radial gas flows have to be taken into account (Spitoni & Matteucci 2011; Bilitewski & Schönrich 2012; Wang & Zhao 2013; Spitoni et al. 2013; Mott et al. 2013; Cavichia et al. 2014; Pezzulli et al. 2017). The infalling gas has a lower angular momentum than the circular motions in the disc, and mixing with the gas in the disc induces a net radial inflow. Lacey & Fall (1985) found that the gas inflow velocity (v_R) is up to a few km s^{-1} and at 10 kpc is $v_R = -1 \text{ km s}^{-1}$. Goetz & Koeppen (1992) developed numerical and analytical models including radial gas flows and they concluded that radial flows alone cannot explain the abundance gradients, but they are an efficient process to amplify the existing ones. Portinari & Chiosi (2000) implemented radial gas flows in a detailed chemical evolution model characterized by a single infall episode. More recently, Spitoni & Matteucci (2011) and Spitoni et al. (2013) have taken into account inflows of gas in detailed one-infall models for the Milky Way and M31 respectively, treating the evolution of the thin disc independently from the halo and thick disc. Spitoni & Matteucci (2011) tested also the radial flows in a two-infall model, but only for oxygen. They found that the observed gradient of oxygen can be reproduced if the gas inflow velocity increases in modulus with the Galactocentric distance, in both the one-infall and two-infall models. A similar approach was followed also by Mott et al. (2013), who studied also the evolution with time of the gradients. At variance with the previous papers where the velocity patterns of the inflow were chosen to produce a best-fit model, Bilitewski &

CHAPTER 4. ABUNDANCE GRADIENTS ALONG THE GALACTIC DISC

Schönrich (2012) presented a chemical evolution model where the flow of gas is directly linked to physical properties of the Galaxy like the angular momentum budget. The resulting velocity patterns of the flows of gas are time dependent and show a non linear trend, always decreasing with decreasing Galactocentric distance. At a fixed Galactocentric distance, the velocity flows decrease with time.

The time evolution of abundance gradients has been studied in several works and in literature various predictions have been made by chemical evolution models. Some authors predicted that the gradient steepens with time (Chiappini et al. 2001; Mott et al. 2013), whereas others suggested that the gradient flattens in time (Prantzos & Boissier 2000; Mollá & Díaz 2005; Vincenzo & Kobayashi 2018; Minchev et al. 2018). The discrepancy between different model predictions is due to the fact that chemical evolution is very sensitive to the prescriptions of the physical processes that lead to the differential enrichment of inner and outer discs, and the flattening or steepening of gradients with time depends on the interplay between infall rate, star formation rate along the disc and also on the presence of a threshold in the gas density for the star formation (Kennicutt 1998a,b). Different recipes of star formation or gas accretion mechanisms can provide different abundance gradients predictions. From the observational point of view, there have been some studies to infer the time evolution of gradients from planetary nebulae (PNe) of different ages (Maciel & Costa 2009, 2013; Stanghellini & Haywood 2010, 2018). In particular, Maciel & Costa (2009) found a time flattening of the gradients during the last 6-8 Gyr, whereas Maciel & Costa (2013) concluded that the radial gradient has not changed appreciably during the Galactic lifetime. On the other hand, Stanghellini & Haywood (2010) found that the Galactic PN gradient may steepen with Galaxy evolution, and this conclusion has been confirmed by Stanghellini

& Haywood (2018). Xiang et al. (2015) studied the evolution of stellar metallicity gradients of the Milky Way disk from main sequence turn-off stars from LAMOST Spectroscopic Survey of the Galactic Anticentre (LSS-GAC), and concluded that the radial gradients, after being essentially flat at the earliest epochs of disc formation, steepen with time, reaching a maximum at age 7-8 Gyr, and then they flatten again, suggesting a two-phase disc formation history (see also Huang et al. 2015, Xiang et al. 2017). Furthermore, Anders et al. (2017) measured the age dependence of the radial metallicity distribution in the Galactic thin disc over cosmic time from CoRoT and APOGEE red giants, and concluded that the slope of the radial iron gradient was compatible with a flat distribution for older ages, then it steepens and finally flattens again. These results are in agreement with the one of the Geneva-Copenhagen survey (Nordström et al. 2004; Casagrande et al. 2011), but there are differences with the LAMOST study of Xiang et al. (2015), possibly due to systematic shifts in the distance and age scales. Furthcoming data from asteroseismic and spectroscopic observations will be fundamental to further constrain the time evolution of the radial abundance gradients.

The aim of this work is to study the abundance ratios and abundance gradients in the Galactic thin disc at the present time and their evolution on the basis of detailed chemical evolution models. We consider the recent chemical evolution models for the Galactic thin disc developed by Grisoni et al. (2017) for the solar neighbourhood and we extend our analysis to other Galactocentric distances. In particular, we examine the processes which mainly influence the formation of abundance gradients: i) the inside-out scenario for the formation of the Galactic thin disc, ii) a variable star formation efficiency, and iii) radial gas flows along the Galactic disc.

CHAPTER 4. ABUNDANCE GRADIENTS ALONG THE GALACTIC DISC

4.2 OBSERVATIONAL DATA

Abundance gradients can be studied by using several tracers, such as HII regions, planetary nebulae (PNe), Cepheids and open clusters (OCs).

In this work, we adopt the Cepheids data by Luck & Lambert (2011) and Genovali et al. (2015), and the OCs data from Magrini et al. (2017). We adopt the HII region data by Deharveng et al. (2000), Esteban et al. (2005), Rudolph et al. (2006) and Balser et al. (2015), and the PNe data by Stanghellini & Haywood (2018). Since PNe and OCs, due to their age spread, are not representative of a single epoch in the Galaxy lifetime, when comparing with the present-time gradient we consider only young PNe and young OCs; in particular, we consider only YPPNe, i.e. PNe whose progenitor stars are younger than 1 Gyr (Stanghellini & Haywood 2018), and also the young OCs with ages less than 1 Gyr of Magrini et al. (2017). The observational data are plotted with their typical errors (see references for further details on the typical errors both in abundances, distances, and ages as well). Regarding the systematic errors affecting the distance estimation of the used stellar populations, we note that the distance scale of PNe is much more uncertain of those of the other tracers.

For comparison with the time evolution of the radial metallicity gradient, we adopt the recent APOGEE data by Anders et al. (2017) and the PNe data by Stanghellini & Haywood (2018).

We also look at how the abundance patterns of $[\alpha/\text{Fe}]$ vs. $[\text{Fe}/\text{H}]$ vary with Galactocentric distance and we consider the APOGEE data of Hayden et al. (2015) for comparison with our models; in particular, among the α -elements, here we focus on magnesium and we compare our predictions with the observed $[\text{Mg}/\text{Fe}]$ vs. $[\text{Fe}/\text{H}]$ at various Galactocentric distances.

Table 4.1: Input parameters for the chemical evolution models. In the first column, we write the name of the model. In the second column, there is the star formation efficiency of the thin disc at different radii (4-6-8-10-12-14-16 kpc from the Galactic center). Finally, in the last column, we indicate the presence or the absence of radial flows. In each model, we adopt Kroupa et al. (1993) IMF.

Model	$\nu_2(4-6-8-10-12-14-16 \text{ kpc})$ [Gyr ⁻¹]	Radial flows
2IM A	const	no
1IM A	const	no
1IM B	8.0-4.0-1.0-0.5-0.2-0.1-0.05	no
1IM C	const	yes
1IM D	8.0-4.0-1.0-0.5-0.2-0.1-0.05	yes

4.3 THE MODELS

The chemical evolution models adopted here are the ones developed in Grisoni et al. (2017) for the solar neighbourhood, that now we extend to the other Galactocentric distances. The models are as follows.

- The two-infall model (Chiappini et al. 1997, Romano et al. 2010) revisited and applied to the thick and thin discs. This model assumes that the discs form as a result of two main infall episodes: during the first infall episode, the thick disc formed, whereas during the second one a much slower infall of gas, delayed with respect to the first one, gives rise to the thin disc.
- The parallel model, adopting two separate one-infall approaches for

CHAPTER 4. ABUNDANCE GRADIENTS ALONG THE GALACTIC DISC

the thick and thin discs, respectively; in this model, we consider the thick and the thin disc stars as formed in two distinct evolutionary phases, which evolve independently.

In this work, the Galactic thin disc is approximated by several independent rings, 2 kpc wide, whereas the evolution of the thick disc evolves as a one-zone with radius of 8 kpc (see Haywood et al. 2018). The basic equations that follow the time evolution of G_i , i.e. the mass fraction of the element i in the gas, are described by Eq. (2.8).

The SFR is parametrized according to the Schmidt-Kennicutt law (Kennicutt 1998a). The parameter ν is the star formation efficiency (SFE), which is tuned to reproduce the present time SFR; in particular, ν_1 and ν_2 represent the star formation efficiencies in the thick and thin discs, respectively. Here, the adopted IMF is the Kroupa et al. (1993) one.

Concerning the gas infall law, in the revised two-infall model (Grisoni et al. 2017) it is described by Eq. (3.1). The parameters τ_1 and τ_2 represent the timescales for mass accretion in the thick and thin discs, respectively. These timescales are free parameters of the model and they are constrained mainly by comparison with the observed metallicity distribution function of long-lived stars in the solar vicinity. In the solar vicinity, Grisoni et al. (2017) found that the best values for these timescales are $\tau_1 = 0.1$ Gyr and $\tau_2 = 7$ Gyr. In this work, we assume that the timescale for mass accretion in the Galactic thin disc changes with the Galactocentric distance according to the inside out scenario (see Chiappini et al. 2001), in particular:

$$\tau_2[\text{Gyr}] = 1.033r[\text{kpc}] - 1.267, \quad (4.1)$$

whereas the timescale of the thick disc is fixed and so there is no inside-out scenario for the thick disc (see also Haywood et al. 2018). The quantities

$A(r)$ and $B(r)$ are two parameters fixed by reproducing the present time total surface mass density in the solar neighbourhood. In particular, the surface mass density is equal to $65 \text{ M}_\odot \text{pc}^{-2}$ for the thin disc, and $6.5 \text{ M}_\odot \text{pc}^{-2}$ for the thick disc (Nesti & Salucci 2013). In this work, we assume that the surface mass density in the Galactic thin disc changes with the Galactocentric distance according to:

$$\sigma(r) = \sigma_0 e^{-\frac{r}{r_D}}, \quad (4.2)$$

where $\sigma_0 = 1413 \text{ M}_\odot \text{pc}^{-2}$ is the central total surface mass density and $r_D = 2.6 \text{ kpc}$ is the scale length (Nesti & Salucci 2013). In the case of the thick disc, it is constant and equal to $6.5 \text{ M}_\odot \text{pc}^{-2}$ up to 8 kpc and then it decreases with the inverse of the Galactocentric distance (see Chiappini et al. 2001).

On the other hand, in the parallel model, since we assume two distinct infall episodes, the gas infall is described by Eq. (3.2) and Eq. (3.3) for the thick and thin discs, respectively. The parameters τ_1 and τ_2 represent the timescales for mass accretion in the thick and thin discs, respectively, and they have the same meaning as discussed in the case of the revised two-infall model.

4.3.1 IMPLEMENTATION OF RADIAL INFLOWS

We implement radial inflows of gas in our chemical evolution models following the prescriptions of Spitoni & Matteucci (2011).

In Fig. 4.1, we show the k -th shell defined in terms of the Galactocentric radius r_k , where its inner and outer edge are labeled as $r_{k-\frac{1}{2}}$ and $r_{k+\frac{1}{2}}$. Through these edges, gas inflow occurs with velocity $v_{k-\frac{1}{2}}$ and $v_{k+\frac{1}{2}}$, respectively. The flow velocities are assumed to be positive outward and negative inward.

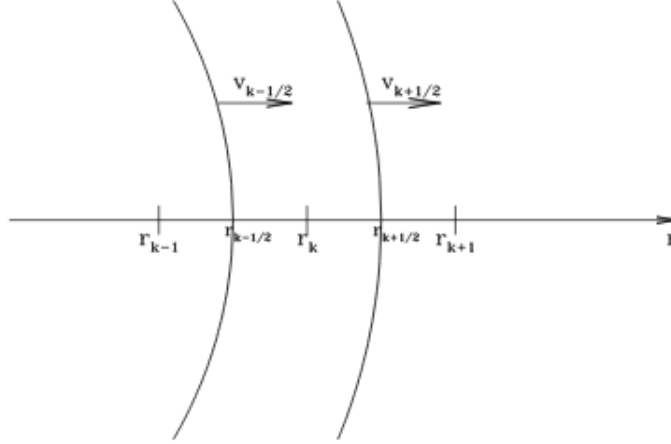


Figure 4.1: Scheme of the gas flow through the k -th shell (Portinari & Chiosi 2000).

Radial inflows with a flux $F(r)$ alter the gas surface density σ_{gk} in the k -th shell according to:

$$\left[\frac{d\sigma_{gk}}{dt} \right]_{rf} = - \frac{1}{\pi(r_{k+\frac{1}{2}}^2 - r_{k-\frac{1}{2}}^2)} [F(r_{k+\frac{1}{2}}) - F(r_{k-\frac{1}{2}})], \quad (4.3)$$

where

$$F(r_{k+\frac{1}{2}}) = 2\pi r_{k+\frac{1}{2}} v_{k+\frac{1}{2}} [\sigma_{g(k+1)}], \quad (4.4)$$

and

$$F(r_{k-\frac{1}{2}}) = 2\pi r_{k-\frac{1}{2}} v_{k-\frac{1}{2}} [\sigma_{g(k-1)}]. \quad (4.5)$$

We take the inner edge of the k -shell, $r_{k-\frac{1}{2}}$, at the midpoint between the characteristic radii of the shells k and $k-1$, and similarly for the outer edge

$r_{k+\frac{1}{2}}$:

$$r_{k-\frac{1}{2}} = \frac{r_{k-1} + r_k}{2}, \quad (4.6)$$

and

$$r_{k+\frac{1}{2}} = \frac{r_k + r_{k+1}}{2}, \quad (4.7)$$

We get that:

$$(r_{k+\frac{1}{2}}^2 - r_{k-\frac{1}{2}}^2) = \frac{r_{k+1} - r_{k-1}}{2} \left(r_k + \frac{r_{k-1} + r_{k+1}}{2} \right). \quad (4.8)$$

Therefore, by inserting these quantities into Eq. 4.3, we obtain the radial flow term to be added in the fundamental equation of chemical evolution (Eq. (2.8)):

$$\left[\frac{dG_i(r_k, t)}{dt} \right]_{rf} = -\beta_k G_i(r_k, t) + \gamma_k G_i(r_{k+1}, t), \quad (4.9)$$

where

$$\beta_k = -\frac{2}{r_k + \frac{r_{k-1} + r_{k+1}}{2}} \left[v_{k-\frac{1}{2}} \frac{r_{k-1} + r_k}{r_{k+1} - r_{k-1}} \right], \quad (4.10)$$

and

$$\gamma_k = -\frac{2}{r_k + \frac{r_{k-1} + r_{k+1}}{2}} \left[v_{k+\frac{1}{2}} \frac{r_k + r_{k+1}}{r_{k+1} - r_{k-1}} \right] \frac{\sigma_{(k+1)}}{\sigma_k}, \quad (4.11)$$

where $\sigma_{(k+1)}$ and σ_k are the present time total surface mass density profile at the radius r_{k+1} and r_k , respectively. We assume that there are no flows from the outer parts of the disc where there is no star formation. In our implementation of the radial inflow of gas, only the gas that resides inside the Galactic disc within the radius of 16 kpc can move inward by radial

CHAPTER 4. ABUNDANCE GRADIENTS ALONG THE GALACTIC DISC

inflow.

We adopt a variable velocity for the radial gas flows. In particular, the modulus of the radial inflow velocity as a function of the Galactocentric distance is assumed to be:

$$|v_R| = \frac{R_g}{4} - 1, \quad (4.12)$$

where the range of the velocities span the range 0-3 km s⁻¹, in accordance with previous works (Wong et al. 2004; Schönrich & Binney 2009; Spitoni & Matteucci 2011; Mott et al. 2013). Furthermore, our radial inflow patterns are in agreement with the ones computed by Bilitewski & Schönrich (2012), imposing the conservation of the angular momentum.

4.4 MODEL RESULTS

We consider the chemical evolution models for the Galactic disc developed by Grisoni et al. (2017) and we study the radial abundance gradients along the Galactic thin disc and its dependence upon several parameters: i) the timescale for the formation of the thin disc, increasing with Galactic radius according to the inside-out scenario (Matteucci & Francois 1989; Chiappini et al. 2001); ii) the SFE of the thin disc (Colavitti et al. 2009); iii) the radial gas flows, with a variable gas speed (Spitoni & Matteucci 2011).

In Table 4.1, we summarize the input parameters of the chemical evolution models. In the first column, we write the name of the model. In the second column, there is the SFE of the thin disc at different radii (4-6-8-10-12-14-16 kpc from the Galactic center). Finally, in the last column, we indicate the presence or the absence of radial gas flows. In each model, we adopt Kroupa et al. (1993) IMF and the inside-out law for the timescale of mass accretion in the thin disc, as expressed by Eq. (4.2). 2IM A is the two-infall model with inside-out scenario for the Galactic thin disc. Similarly, 1IM A is the

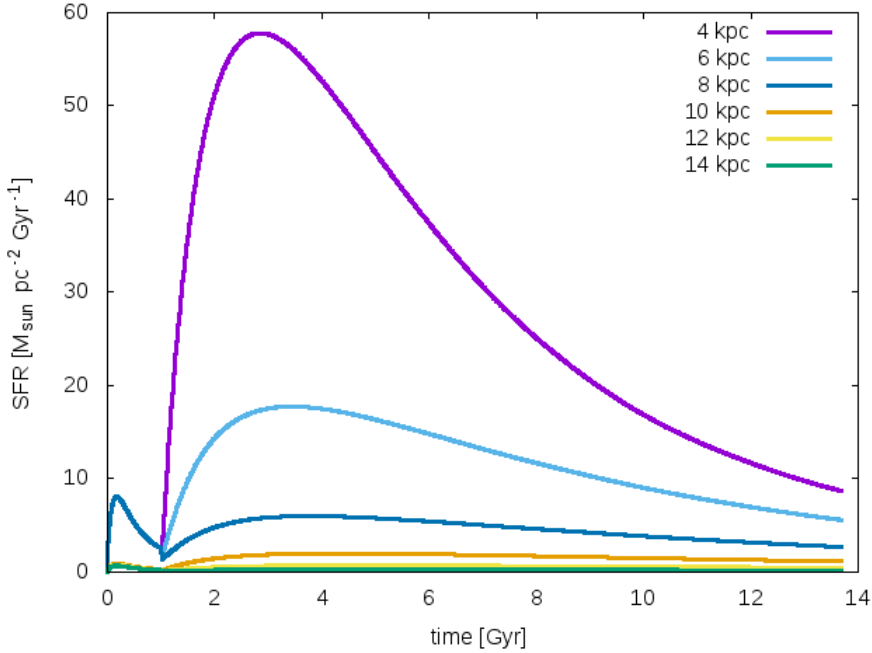


Figure 4.2: Time evolution of the SFR, as predicted by the model 2IM A at various Galactocentric distances.

one-infall model for the thin disc with inside-out scenario. 1IM B is the one-infall model for the Galactic thin disc with inside-out and also a variable SFE. 1IM C is the one-infall model for the Galactic thin disc with inside-out and also the implementation of radial gas flows. 1IM D is the one-infall model for the Galactic disc with inside-out and both a variable SFE and radial gas flows.

Before discussing the abundance patterns and gradients for these models, in Fig. 4.2 we show the time evolution of the SFR as predicted by the 2IM A at various Galactocentric distance: 4, 6, 8, 10, 12, 14 kpc. The SFR during

CHAPTER 4. ABUNDANCE GRADIENTS ALONG THE GALACTIC DISC

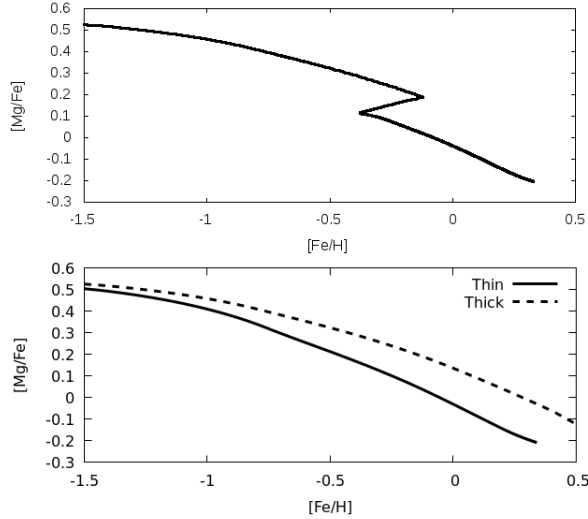


Figure 4.3: Predicted abundance patterns of $[Mg/Fe]$ vs. $[Fe/H]$ in the solar neighbourhood for the two scenarios, the two-infall (upper panel) and the parallel (lower panel).

the thick disc phase is the same for every Galactocentric distance up to 8 kpc, because the assumed thick disc mass density in this model is constant up to 8 kpc. However, for $R > 8$ kpc the thick disc mass density is assumed to go with the inverse of the distance and this is reflected into the SFR which is damped at large Galactocentric distances. We note that there is no real gap between the thick and thin disc phases due to the fact that there is no assumed threshold for the star formation, but still there is a quenching of star formation between the two phases. In the thin disc phase, the SFR is much higher at smaller Galactocentric distances since the total surface mass density is higher (see Eq. (4.2)).

In the following, we show the results for the abundance patterns ($[Mg/Fe]$

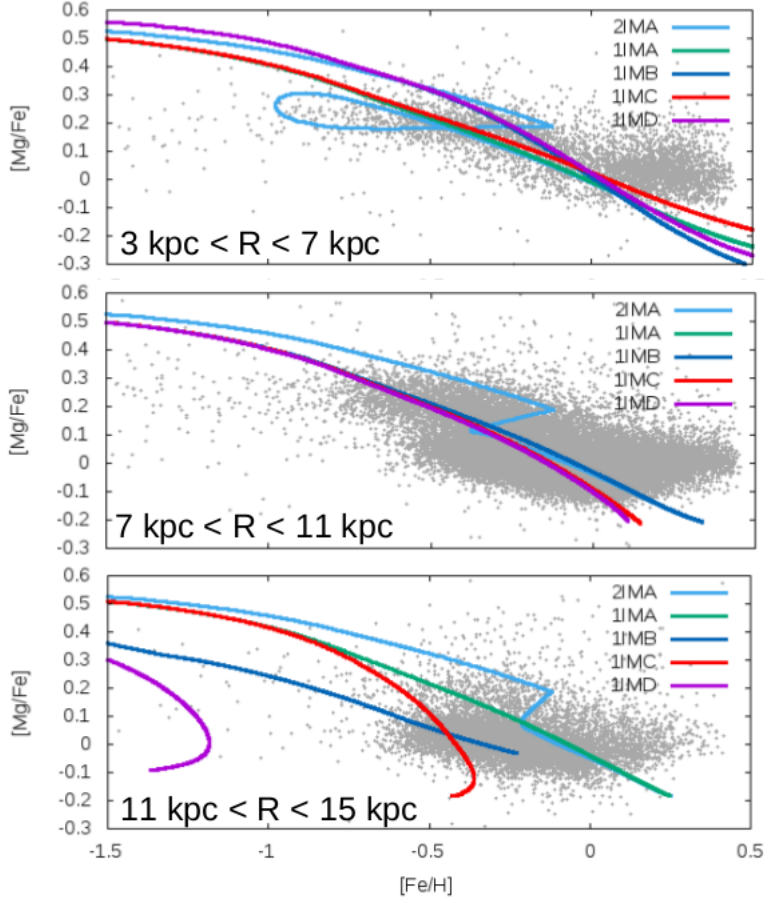


Figure 4.4: Observed and predicted abundance patterns of $[Mg/Fe]$ vs. $[Fe/H]$. The data are from Hayden et al. (2015) and are divided as follows: 3-7 kpc (upper panel), 7-11 kpc (middle panel), 11-15 kpc (lower panel). The predictions are from model 2IM A (light-blue line), 1IM A (green line), 1IM B (blue line), 1IM C (red line) and 1IM D (magenta line) computed at different Galactocentric distances: 4 kpc (upper panel), 8 kpc (middle panel), 14 kpc (lower panel).

CHAPTER 4. ABUNDANCE GRADIENTS ALONG THE GALACTIC DISC

vs. $[\text{Fe}/\text{H}]$) at various Galactocentric distances, for the present-day gradients and for the time evolution of gradients.

4.4.1 ABUNDANCE PATTERNS

Our starting point is represented by the study of Grisoni et al. (2017), which explored the two different scenarios for the Galactic thick and thin discs in the solar neighbourhood: the two-infall and the parallel one. In Fig. 4.3, we report the predictions of the two different theoretical approaches, i.e. the two-infall and the parallel models. In the case of the two-infall model (left panel), we predict an overabundance of Mg relative to Fe almost constant until $[\text{Fe}/\text{H}] < -1.5$ dex and then for $[\text{Fe}/\text{H}] \sim -1.5$ dex the trend shows a decrease due to the delayed explosion of Type Ia SNe. This behaviour of the abundance patterns of α -elements such as Mg is well-interpreted in terms of the time-delay model due to the delay of iron ejection from Type Ia SNe relative to the faster production of α -elements by core-collapse SNe (see Matteucci 2001; 2012). Then, there is a gap, which marks the transition between the thick and thin disc phases, and then the thin disc phase starts. On the other hand, in the case of the parallel model (right panel), we have two distinct evolutionary paths for the thick and thin discs, with the thick disc being more α -enhanced due to the faster timescale of formation (see Grisoni et al. 2017 for further discussion on the two approaches; Grand et al. 2018 for an interpretation of the two sequences in the $[\alpha/\text{Fe}]$ vs. $[\text{Fe}/\text{H}]$ plane in terms of cosmological simulations).

Now, we focus on how the tracks in the abundance patterns vary with the Galactocentric distance and we compare our model predictions with APOGEE data (Hayden et al. 2015). In Fig. 4.4, we show the abundance patterns of $[\text{Mg}/\text{Fe}]$ vs. $[\text{Fe}/\text{H}]$ at different radii in the case of the models of Table 4.1. First, we discuss the predictions of the two-infall model 2IM

A at various Galactocentric distances. We note that the various tracks are similar in the thick disc phase, because we do not assume an inside-out formation for the thick disc (see also Haywood et al. 2018). Then, there is a dilution which is due to the second infall episode, stronger in the inner regions than in the outer ones. In the thin disc phase, we can see that there is a slight difference between the various tracks due to the inside-out scenario for the thin disc, but the effect is not very noticeable. Similarly, for the 1IM A for the Galactic thin disc with only inside-out, the various tracks at different radii are very similar and there is not so much difference between them. On the other hand, in the case of the 1IM B with variable SFE, the tracks are different, as the variable SFE increases the spread among them and the agreement with the data is good, in particular for the outer radii. Similarly, Spitoni et al. (2015) found that a variable SFE can reproduce the spread in the $[\alpha/\text{Fe}]$ vs. $[\text{Fe}/\text{H}]$ plot. Then, we show the results for the 1IM C with radial gas flows. Also in this case, we have a much larger spread among the various tracks due to the presence of radial gas flows, even if the effect is different with respect to the previous case. In fact, in the case of radial gas flows, the various tracks show a similar behaviour at low metallicities, then radial gas flows become relevant for larger metallicities and the spread between the tracks appears; in fact, radial gas flows become more effective with time (and thus, metallicity), at variance with the case with variable SFE, where the star formation process is more effective at earlier times, as can be seen in the star formation history. Finally, we discuss the results for the 1IM D with both variable SFE and radial gas flows. In this case, the spread among the various tracks is present both at low and high metallicities, due to the fact that we have combined the two effects: on one hand, the variable SFE, which acts at lower metallicities, and on the other, the radial gas flows, which act at higher metallicities. We can see

CHAPTER 4. ABUNDANCE GRADIENTS ALONG THE GALACTIC DISC

that the combined effects are too strong, since the law for the variable SFE and the radial gas flows have been fine-tuned separately to best fit the data. Other combinations of the radial gas flows and variable efficiency of star formation, including the ones of Spitoni et al. (2015) (with constant radial gas flows and variable efficiency), have been tested and they produce results in between model 1IM C and 1IM D.

So, concluding, the best model to reproduce the APOGEE data is the model with a variable SFE, which can recover the spread among the various tracks and can provide a good match with observations.

We note that there is a clear discrepancy between all model predictions and observations at solar and super-solar metallicities. In fact, none of the models can reproduce $[\text{Mg}/\text{Fe}]$ at high $[\text{Fe}/\text{H}]$. The observations indicate that $[\text{Mg}/\text{Fe}]$ is essentially flat for $[\text{Fe}/\text{H}] > 0$, while all models predict a decline. The disagreement between model and observations is probably related to the choice of the Mg stellar yields and/or to our poor understanding of the complete processes involved in the nucleosynthesis of Mg. For example, Romano et al. (2010) suggested the need for either a revision of current SNII and HN yields for solar and/or super-solar metallicity stars, or larger contributions to Mg productions from SNIa, or significant Mg synthesis in low and intermediate mass stars, or a combination of all these factors to reproduce the behaviour of Mg. This has been extensively discussed in Magrini et al. (2017), where the differences between α -elements are presented. In Grisoni et al. (2017), we also discussed the nature of the metal-rich high-alpha stars (MRHA) of Mikolaitis et al. (2017), which still have to be well-understood in terms of Galactic chemical evolution models. We concluded that in the parallel approach, the MRHA stars can be interpreted as metal-rich thick disc stars, whereas in the two-infall approach they can only be explained by invoking radial migration from the inner disc. Radial

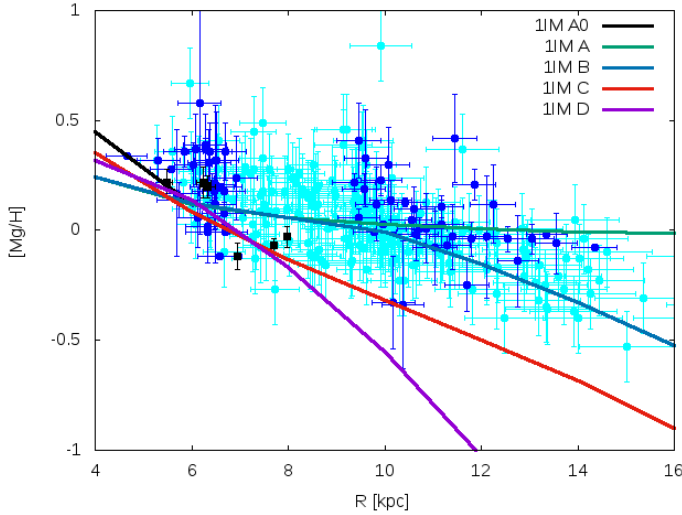


Figure 4.5: Observed and predicted radial abundance gradient for magnesium from Cepheids and young open clusters. The data are from Luck & Lambert 2011 (light-blue dots) and Genovali et al. 2015 (blue dots) for Cepheids, and from Magrini et al. 2017 (black squares) for young open clusters. The predictions are from model 1IM A (green line), 1IM B (blue line), 1IM C (red line) and 1IM D (magenta line), and also 1IM A0 which is the same as 1IM A but with a more extreme law for the inside-out, see text (black line).

migration in Galactic discs is the subject of many investigations and it has been included in several chemical evolution models and simulations (Schönrich & Binney 2009; Minchev et al. 2013; Kubryk et al. 2015a,b; Spitoni et al. 2015; Grand et al. 2015).

4.4.2 PRESENT-DAY GRADIENTS

Here, we consider the present-day abundance gradients.

In Fig. 4.5, we show the observed and predicted radial abundance gradient for

CHAPTER 4. ABUNDANCE GRADIENTS ALONG THE GALACTIC DISC

Mg from Cepheids and OCs. Cepheids are an essentially young populations, whereas OCs can have different ages and so not all OCs are tracers of the present time gradient; thus, here we consider only the young OCs of Magrini et al. (2017), with ages less than 1 Gyr. The predictions are from the one-infall model for the Galactic thin disc in the four different cases summarized in Table 4.1: 1IM A with only inside-out (light-blue line), 1IM B with variable SFE (blue line), 1IM C with radial flows (red line) and 1IM D (magenta line). We show also the model 1IM A0 (black line), which is the same as 1IM A but with a more extreme law for the inside-out: in particular, we assume a timescale of 0.1 Gyr at 4 kpc and 50 Gyr at 16 kpc. However, we can see that the models with only inside-out scenario predict a too flat gradient; the more extreme case might steepen the gradient in the inner disc, but the results do not change in the outer disc, where the two models basically overlap. To steepen the gradients we need more ingredients such as a variable SFE or radial gas flows, and by combining the two ingredients we get an even steeper gradient. As we have noted in the case of abundance patterns at different Galactocentric distances, only inside-out does not seem to be sufficient to explain entirely the observations.

In Fig. 4.6, we show the observed and predicted radial abundance gradient for oxygen from HII regions and PNe. Only young PNe can be considered together with HII regions, whereas older PNe are not tracers of the present time radial O/H gradient; thus, here we consider only YPPNe, i.e. PNe whose progenitor stars are younger than 1 Gyr (Stanghellini et al. 2018). The predictions are from the one-infall model for the Galactic thin disc in the four different cases summarized in Table 4.1, but compared now with data from HII regions and young PNe. Also in this case and even more evidently, the model with only inside-out is not sufficient to explain the steep abundance gradient: we need a variable SFE or radial flows to explain the

observational data. Therefore, a variable SFE or radial flows are important ingredients for obtaining a steeper gradient (see also Spitoni & Matteucci 2011).

These conclusions are in agreement with the comparison with APOGEE data for abundance ratios, for which we could not recover the spread with only inside-out, but we had to add the variable SFE and radial flows to better fit the observations; we note that the former looks consistent with the Mg gradient (Fig. 4.5), while the latter looks consistent with the O gradient (Fig. 4.6).

In this context, radial migration can also have an effect, as already discussed at the end of the previous section. For example, Loebman et al. (2016) claimed that the results of radial migration can be important. If migration is important in well defined parts of the Galaxy, as for instance the outer disc, it can change the shape of the gradient. In particular, radial migration should flatten the gradient, but it has been shown that the effect may not be large for stars in the Milky Way (Di Matteo et al. 2013; Kubryk et al. 2013; Bovy et al. 2014).

4.4.3 TIME EVOLUTION OF THE GRADIENTS

We focus here on the time evolution of the abundance gradients and show how abundance gradients vary with time in the various scenarios and we compare our model predictions with recent observational data on the time evolution of the radial metallicity gradients (Anders et al. 2017; Stanghellini & Haywood 2018).

In Fig. 4.7, we show the time evolution of the radial abundance gradient for Mg. The predictions are from models 2IM A, 1IM A, 1IM B, 1IM C and 1IM D at different times (2 Gyr, 7 Gyr and 13.6 Gyr). First, we discuss the predictions of the 2IM A. We can see that the two-infall model predicts

CHAPTER 4. ABUNDANCE GRADIENTS ALONG THE GALACTIC DISC

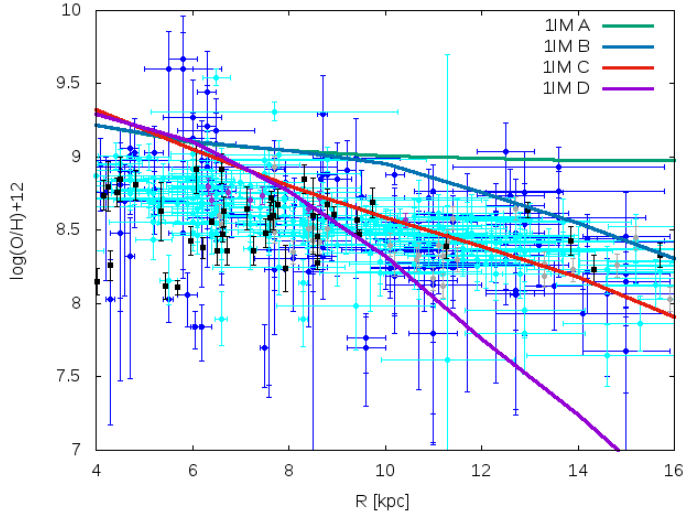


Figure 4.6: Observed and predicted radial abundance gradient for oxygen from HII regions and young planetary nebulae. The data are from Deharveng et al. 2000 (gray dots), Esteban et al. 2005 (violet dots), Rudolph et al. 2006 (blue dots), Balser et al. 2015 (light-blue dots) for HII regions, and from Stanghellini & Haywood 2018 (black squares) for young PNe. The predictions are from model 1IM A (green line), 1IM B (blue line), 1IM C (red line) and 1IM D (magenta line).

a gradient inversion at early times: the gradient has a positive slope (at 2 Gyr), and then it flattens and reaches a slightly negative slope (at 13.6 Gyr). This gradient inversion was observationally claimed by Cresci et al. (2010), who have found an inversion of the O gradient at redshift $z=3$ in some Lyman-break galaxies. They showed that the O abundance decreases going toward the Galactic center, thus producing a positive gradient. This inversion was already noted theoretically by Chiappini et al. (2001) and studied by Mott et al. (2013) in terms of the two-infall model. This is a

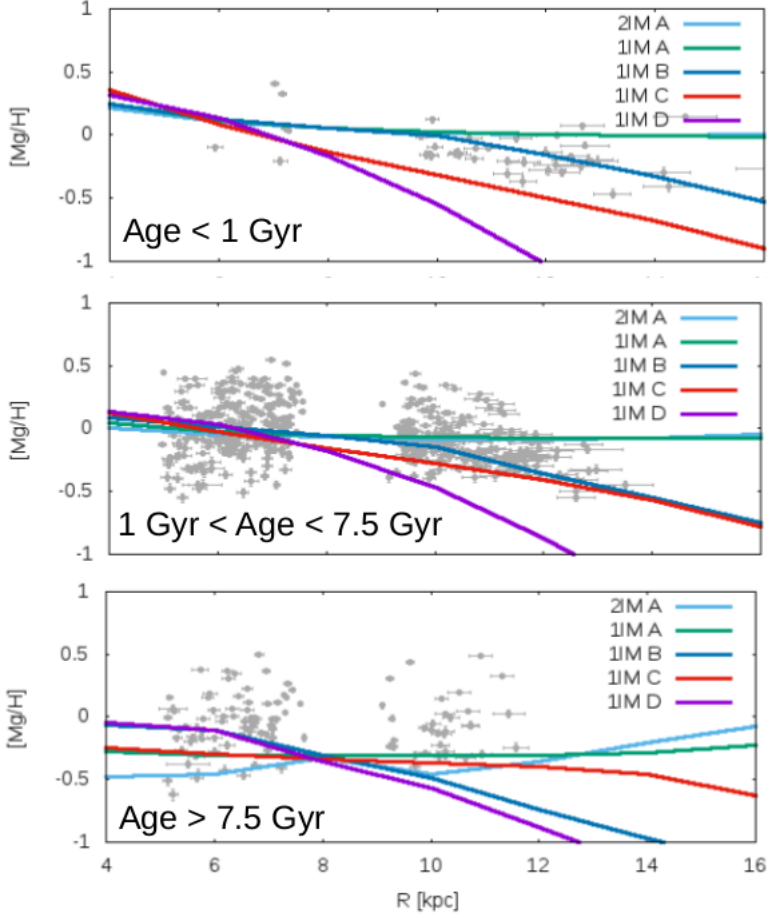


Figure 4.7: Time evolution of the radial abundance gradient for magnesium. The data are from Anders et al. (2017) and are divided in age bins as follows: younger than 1 Gyr (upper panel), between 1 and 7.5 Gyr (middle panel), older than 7.5 Gyr (lower panel). The predictions are from model 2IM A (light-blue line), 1IM A (green line), 1IM B (blue line), 1IM C (red line) and 1IM D (magenta line) computed at the various times.

CHAPTER 4. ABUNDANCE GRADIENTS ALONG THE GALACTIC DISC

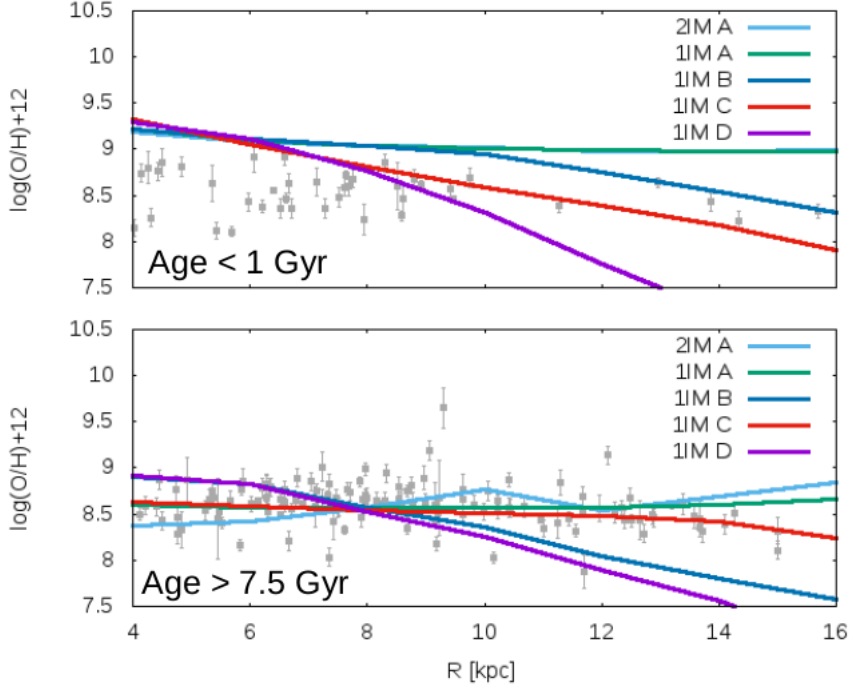


Figure 4.8: Time evolution of the radial abundance gradient for oxygen. The data are from Stanghellini & Haywood (2018) and are divided in age bins as follows: younger than 1 Gyr (upper panel) and older than 7.5 Gyr (lower panel). The predictions are from model 2IM A (light-blue line), 1IM A (green line), 1IM B (blue line), 1IM C (red line) and 1IM D (magenta line) computed at the various times.

characteristic feature of the two-infall model, with its second infall episode of primordial gas which dilutes the gas in the inner regions in spite of the chemical enrichment. Then, we show the predictions of the 1IM A. At variance with the previous case, in the one-infall approach we have no gradient inversion due to the fact that we have no second infall episode of primordial gas which provokes the dilution. The slope of the gradient slightly steepens with time, but the effects is not noticeable, since in the 1IM A we assume only inside-out. Then, we discuss the predictions of the 1IM B with inside-out and also variable SFE. In this case, the time evolution of the gradient is different than in the previous case and the gradient flattens in time. This result is in agreement with other studies which predict a flattening of the gradient with time (Prantzos & Boissier 2000; Mollá & Díaz 2005; Vincenzo & Kobayashi 2018; Minchev et al. 2018). Then, we show the predictions of 1IM C with inside-out and also radial gas flows. The models with radial gas flows predict that the gradient steepens noticeably in time as was found by Mott et al. (2013), but then we have no gradient inversion because it is a one-infall model and not a two-infall one. Finally, we discuss the predictions of the 1IM D with inside-out and also both the variable SFE and radial gas flows. We can see that the gradient starts steep due to the variable SFE at different distances and then it becomes even steeper in time due to the effect of radial gas flows, which becomes dominant at later time. Then, in Fig. 4.8, we compare our model predictions also with PNe data from Stanghellini & Haywood (2018), which show that the OPPNe oxygen gradient is shallower than that derived from YPPNe. Also in this case, the predictions are from models 2IM A, 1IM A, 1IM B, 1IM C and 1IM D at the different times.

Concluding, the model 1IMB with the variable SFE still provides a good agreement with the observational data, in particular at recent times, but

CHAPTER 4. ABUNDANCE GRADIENTS ALONG THE GALACTIC DISC

it predicts a steeper behaviour at earlier times which is not present in the data. To recover a flatter gradient at earlier times, we should rather consider models 1IMA and 1IMC, whereas with the two-infall model 2IMA we can even get an evident gradient inversion, as we have discussed previously. The difference between model predictions is due to the fact that the gas chemical evolution is very sensitive to the prescriptions of the physical processes that lead to the enrichment of inner and outer discs, and the flattening or steepening of gradients in time depends on the interplay between infall rate and star formation rate along the Galactic disc. Different recipes of the star formation process or gas accretion mechanisms can provide very different predictions for the abundance gradients.

4.5 CONCLUSIONS

In this work, we have studied the formation and chemical evolution of the Milky Way discs with particular focus on the abundance patterns at different Galactocentric distances, the present-time abundance gradients along the disc and the time evolution of abundance gradients. We have considered the recently developed chemical evolution models by Grisoni et al. (2017) for the solar neighbourhood, both the two-infall and the one-infall, and we have extended our analysis to the other Galactocentric distances, also implementing radial gas flows in the code for this purpose. In particular, we have examined the processes which mainly influence the formation of abundance gradients: i) the inside-out scenario for the formation of the Galactic thin disc, ii) a variable star formation efficiency, and iii) radial gas flows along the Galactic disc.

Our main conclusions are as follows.

- As regard to the abundance patterns (in particular $[\text{Mg}/\text{Fe}]$ vs. $[\text{Fe}/\text{H}]$)

at different Galactocentric distances, the inside-out scenario for the thin disc is a key element, but provides only a slight difference between the various tracks at different radii and so it is not sufficient to explain the data at various radii. In order to have a more significant spread among the various tracks, we need further ingredients such as a variable star formation efficiency or radial gas flows: the variable star formation efficiency produces a spread at lower metallicities, whereas the radial gas flows become significant at higher ones. The case with a variable star formation efficiency provides a very good agreement with the observational data, in particular for the outer radii. However, we note that none of the models can reproduce $[\text{Mg}/\text{Fe}]$ at high $[\text{Fe}/\text{H}]$, and this can be due to a general problem in our understanding of Mg production (as also pointed out by Romano et al. 2010; Magrini et al. 2017).

- Also concerning the present-day abundance gradients along the Galactic thin disc, the inside-out scenario provides a too flat gradient and cannot explain the observational data, neither of Cepheids, young OCs, young PNe and HII regions which show a steeper gradient. To recover the steeper gradient, we need the variable star formation efficiency or radial gas flows; we note that the former looks consistent with the Mg gradient, while the latter looks consistent with the O gradient.
- On the other hand, for the time evolution of abundance gradients, the model with the variable star formation efficiency provides a good agreement with the observational data at recent times, but it predicts a steeper behaviour at earlier times which is not present in the data. To reproduce a flatter gradient at earlier times, we should rather consider the models with constant star formation efficiency or we would need

CHAPTER 4. ABUNDANCE GRADIENTS ALONG THE GALACTIC DISC

radial migration, more efficient for the older populations. Thus, what we are observing is a gradient flattened by radial migration, and not the original one (see for instance Magrini et al. 2016). With the two-infall model, we can even get an evident gradient inversion at high redshift, when the efficiency of star formation is constant.

- In our scenario, the Galactic thick disc formed on a very short timescale ($\tau_1 = 0.1$ Gyr, see Grisoni et al. 2017), which is assumed to be constant with radius. Therefore, there is no inside-out scenario for the thick disc, in agreement with Haywood et al. (2018).

In summary, we conclude that the inside-out scenario is a key ingredient for the formation of Galactic discs, but cannot be the only one to explain abundance patterns at different Galactocentric distances and abundance gradients. Further ingredients are needed, such as a variable star formation efficiency and radial gas flows; in particular, we note that the former looks consistent with the Mg gradient, while the latter looks consistent with the O gradient. The flattening or steepening of gradients in time is due to the fact that the gas chemical evolution is very sensitive to the prescriptions of the physical processes that lead to the enrichment of inner and outer discs, mainly to the constancy or variability of the star formation efficiency. Therefore, different recipes of the star formation process or gas accretion mechanisms can provide very different predictions for the abundance gradients, as we have shown in this work. Also radial migration could have an effect, although it has been shown that this may not be a large factor for stars in the Milky Way (Di Matteo et al. 2013; Kubryk et al. 2013; Bovy et al. 2014).

CHAPTER 5

Chemical evolution of the Galactic bulge

In this Chapter, I discuss the results on the formation and chemical evolution of the Galactic bulge. The fundamental question that I would like to address in this Chapter can be summarized as follows. How did the Galactic bulge form? What can be the origin of two distinct stellar populations in the bulge? How old are the bulge stars? The Chapter is organized as follows. In Section 5.1, I introduce the context in which this Chapter fits. In Section 5.2, we present the data which have been used to compare with the predictions of our models. In Section 5.3, we describe the models adopted in this work. In Section 5.4, we show the results based on the comparison between data and model predictions. Finally, in Section 5.5, we summarize the main conclusions. The results presented in this Chapter are described in the published paper Matteucci, Grisoni et al. (2019), for which I performed several calculations, as second-author of the paper.

5.1 INTRODUCTION

In the last few years, several spectroscopic surveys: Gaia-ESO (Gilmore et al. 2012), APOGEE (Majewski et al. 2017), Argos (Freeman et al. 2012) and GIBS (Zoccali et al. (2014), as well as photometric (VVVX, which is the extension of the VVV survey, Minniti et al. 2010) surveys and missions (Gaia mission, Perryman et al. 2001) have been developed in order to study the formation and evolution of the Galactic bulge. The picture for the bulge formation which is arising from these data is rather complex, and still has to be well understood in terms of Galactic chemical evolution models.

In particular, Hill et al. (2011) by observing bulge red clump stars concluded that their distribution is doubled-peaked, with one peak at $[\text{Fe}/\text{H}]=-0.30$ dex and the other at $[\text{Fe}/\text{H}]=+0.32$ dex, calling the two populations metal poor (MP) and metal rich (MR), confirmed by Uttenthaler et al. (2012). More recently, Rojas-Arriagada et al. (2017) with Gaia-ESO data and Schultheis et al. (2017) with APOGEE data, concluded that the MDF in the bulge is indeed bimodal. Zoccali et al. (2017) also confirmed the existence of two main stellar populations with the MP one being more centrally concentrated. Bensby et al. (2011; 2013; 2017) by studying microlensed dwarfs and subgiant stars found that the bulge metallicity distribution is multi-modal, with at least four peaks corresponding to different star formation episodes occurred 12, 8, 6 and 3 Gyr ago, thus implying the existence of relatively young stars in the bulge. The existence of young bulge stars has been suggested also by Haywood et al. (2016), implying that these stars belong to the inner disc. On the other hand, Clarkson et al. (2011), Valenti et al. (2013), Renzini et al. (2018) and Nogueras-Lara et al. (2018) concluded that most of the bulge stars are quite old (> 10 Gyr). In Renzini et al. (2018), from color-magnitude and luminosity functions of the MP and MR populations obtained from

HST photometry, it is concluded that both MP and MR populations are similarly old. Bernard et al. (2018) inferred the history of star formation of the bulge from deep color-magnitude diagrams of four low reddening bulge regions and concluded that only 10% of bulge stars are younger than 5 Gyr, but this fraction rises to 20-25% in the metal rich peak.

From the theoretical point of view, several scenarios for the bulge formation have been proposed. Matteucci & Brocato (1990) first suggested that to reproduce the MDF in the bulge, one should assume a strong and short burst of star formation with the bulk of stars formed in the first 0.5 Gyr, plus an IMF more top-heavy than the one in the solar neighbourhood, as for example the IMF of Scalo (1986) derived for local stars. As a consequence of this, they predicted a plateau in the $[\alpha/\text{Fe}]$ ratios in bulge stars longer than in the solar vicinity, with a knee close to $[\text{Fe}/\text{H}]=0.0$ dex. Their prediction was somewhat confirmed by the first data on $[\alpha/\text{Fe}]$ ratios by McWilliam & Rich (1994).

Wyse & Gilmore (1992) considered various possibilities for the bulge formation, including the model of Matteucci & Brocato (1990): i) the bulge formed by accretion of extant stellar systems, which by dynamical friction eventually settled in the center of the Galaxy; ii) the bulge formed by accumulation of gas at the center of the Galaxy and evolved independently of the other components of the Galaxy, with either rapid or slow star formation; iii) the bulge formed by accumulation of metal-enriched gas from the thick or thin disc.

Later on, Ballero et al. (2007) presented an updated version of the model by Matteucci & Brocato (1990) and again concluded that the bulge formed on a very short timescale, of the order of 0.1 Gyr, that the star formation was much more efficient than in the solar vicinity by a factor of ~ 20 , and that the IMF was flatter than the one adopted for the solar neighbourhood.

These conclusions were also supported by the paper of Cescutti & Matteucci (2011), where it was suggested that either a Salpeter or a flatter IMF were required to reproduce the bulge abundance patterns.

Then, Grieco et al. (2012) aimed at explaining the existence of the two main stellar populations observed in the bulge. They concluded that a stellar population forming by means of a classical gravitational gas collapse can be mixed with a younger stellar population created perhaps by the bar evolution.

Several other works have considered that the bulge formed as a result of secular evolution of the inner disc through bar formation and its subsequent buckling into a pseudo-bulge B/P structure (Combes et al. 1990; Norman et al. 1996; Athanassoula 2005; Bekki & Tsujimoto 2011; Shen et al. 2010; Debattista et al. 2017; Buck et al. 2017; Fragkoudi et al. 2018), or a mixed scenario where the secular and spheroidal components coexist (Samland & Gerhard 2003; Tsujimoto & Bekki 2012).

The aim of this work is to study the chemical evolution of the Galactic bulge by means of detailed chemical evolution models in the light of the newest observational data. We will also study the abundance patterns, MDF and age distribution of the Galactic bulge, and compare the observational data with our model predictions in order to constrain the bulge formation and evolution. In particular, we will discuss how the presence of different episodes of star formation, separated by quiescent periods, can produce visible effects on the $[\alpha/\text{Fe}]$ vs. $[\text{Fe}/\text{H}]$ relations, and whether we can build a self-consistent scenario which accounts for the MDF shape, the stellar ages and the $[\alpha/\text{Fe}]$ vs. $[\text{Fe}/\text{H}]$ relations at the same time.

5.2 OBSERVATIONAL DATA

The observational spectroscopic data that we have used as a comparison to our model predictions are from Gaia-ESO survey (Rojas-Arriagada et al. 2017) and APOGEE (Rojas-Arriagada et al. 2019). In Rojas-Arriagada et al. (2017), 2500 red clump stars were observed in 11 bulge fields: their analysis confirmed the existence of two different stellar populations where the MR one is associated with the boxy/peanut bulge, formed as a result of the secular evolution of the inner disc. We compared our models with both the $[\text{Mg}/\text{Fe}]$ vs. $[\text{Fe}/\text{H}]$ and the MDF, found in this work. Rojas-Arriagada et al. (2019) analysed the 14th data release from APOGEE data. We have compared again our models with the $[\text{Mg}/\text{Fe}]$ vs. $[\text{Fe}/\text{H}]$ relation (DR14) which shows a slightly lower $[\text{Mg}/\text{Fe}]$ ratio at low metallicity relative to the Gaia-ESO survey data. This can be a problem of different calibrations in the two sets of data. Their MDF is also slightly different from that of Gaia-ESO survey and the existence of the dip indicating two stellar populations is not so evident (see also discussion about differences in the MDF in Schultheis et al. 2017).

Finally, we adopted the ages derived for the bulge stars by Bernard et al. (2018) and Schultheis et al. (2017) by using the CMD-fitting technique, and individual ages based on the CN abundances. Besides finding that 10% of bulge stars is younger than 5 Gyr, they suggested a fast enrichment rate, in particular $dZ/dt \sim 0.005 \text{ Gyr}^{-1}$ for the interstellar medium in the bulge.

5.3 THE MODELS

In this work, by means of detailed chemical evolution models we aim at modelling the two stellar populations of the Galactic bulge, the metal-poor (MP) and the metal-rich (MR) ones. We consider two possibilities: i) the MP

and MR populations originate from star formation in situ and the MR one forms after a stop in the star formation in the bulge, ii) the MR populations is made of stars originally belonging to the inner disc, whose evolution has been completely disentangled from that of the MP stars.

The chemical evolution model for the Galactic bulge that we consider here is the one developed by Grieco et al. (2012, see also Rojas-Arriagada et al. 2017). On the other hand, the chemical evolution model for the Galactic thin disc that we consider here is the one-infall model of Grisoni et al. (2017) (see also Grisoni et al. 2018; Matteucci et al. 2018).

We start with a model where the bulge forms by fast gas infall. The assumed gas accretion law for the Galactic bulge is given by Eq. (2.12), and we assume a similar functional form for the inner disc (Eq. (3.3), Grisoni et al. 2017, 2018), but with different timescales of formation. The parameter τ corresponds to the timescale for mass accretion in each Galactic component: in particular, for the Galactic bulge it is assumed to be 0.1 Gyr, whereas for the Galactic thin disc is 7 Gyr in the solar vicinity and it changes with the Galactocentric distance according to the inside-out scenario (Chiappini et al. 2001; Grisoni et al. 2018); therefore the timescale corresponding to the inner disc (4 kpc) is ~ 2.7 Gyr.

The SFR is parametrized according to the Schmidt-Kennicutt law (Kennicutt 1998). The adopted IMF is the Salpeter (1955) one by default for the Galactic bulge and the Kroupa et al. (1993) one for the Galactic disc. We also tested the Calamida et al. (2015) IMF for the Galactic bulge; this IMF was specifically suggested for the bulge stars.

Here, we adopt the nucleosynthesis prescriptions of the best model of Romano et al. (2010). However, in one model (Model A*) the yields of Mg from SNe Ia were artificially increased. This was done for reproducing the observed flattening of $[\text{Mg}/\text{Fe}]$ at high metallicity, present in the APOGEE data,

although this effect is probably artificial (see Nandakumar et al. 2018). In particular, we increased by a factor of 10 the Mg produced in Type Ia SNe. Clearly, this hypothesis is artificial and does not follow what nucleosynthesis models for Type Ia SNe suggest. However, it is interesting to see the effect of increasing the Mg in order to explain the data. All the models are described in Table 5.1, where we show the main characteristics of each model: in the first column is the Model name, in column 2 there is the SFR with the indication of whether the star formation has been halted and for how long, in column 3 is the assumed efficiency of star formation, in column 4 the assumed IMF and finally, in column 5 the assumption about Mg from SNeIa is shown. We show also the inner disc model that we computed under the hypothesis that the MR population comes from the inner disc, as well as the multiple burst model.

5.4 RESULTS

Here we show the results for the abundance pattern ($[\text{Mg}/\text{Fe}]$ vs. $[\text{Fe}/\text{H}]$), metallicity distribution function and age distributions as predicted by the various models listed in Table 5.1.

5.4.1 ABUNDANCE PATTERNS AND MDFs

The first model we started with is the same as in Rojas-Arriagada et al. (2017) and in Grieco et al. (2012) for the MP population: in other words, it is a continuous model characterized by a short and intense star formation burst, typical of classical bulges. This model (Model A in Table 5.1) can well reproduce the $[\text{Mg}/\text{Fe}]$ vs. $[\text{Fe}/\text{H}]$ found by the Gaia-ESO survey, but it does not reproduce well the MDF derived from the same data. In Fig. 5.1., we show the $[\text{Mg}/\text{Fe}]$ ratio versus metallicity as well as the MDF predicted by Model A. It is evident that the bimodality observed in the MDF is

Table 5.1: Input parameters for the chemical evolution models. In the first column, we write the name of the models. In the second column, we indicate whether we consider a continue star formation or a stop in the star formation process. In the third column, there is the star formation efficiency (in Gyr^{-1}). Finally, in the last column, there is the IMF. The IMF labelled Kroupa refers to that of Kroupa et al. (1993), the one labelled Calamida refers to the one of Calamida et al. (2015) and finally Salpeter (1955). The label “ Mg_{Ia} normal” indicates the yield of Mg from SNe Ia by Iwamoto et al. (1999), whereas “ Mg_{Ia} increased” is the yield artificially increased, as described in the text.

Model	SFR	ν [Gyr^{-1}]	IMF	Mg_{Ia}
A	continue	25	Salpeter	Mg_{Ia} normal
A*	continue	25	Salpeter	Mg_{Ia} increased
B	stop (50 Myr)	25	Salpeter	Mg_{Ia} normal
C	stop (150 Myr)	25	Salpeter	Mg_{Ia} normal
D	stop (250 Myr)	25	Salpeter	Mg_{Ia} normal
E	stop (350 Myr)	25	Salpeter	Mg_{Ia} normal
F	multiple stops	1–3	Salpeter	Mg_{Ia} normal
G	continue	25	Calamida	Mg_{Ia} increased
H (disc)	continue	1	Kroupa	Mg_{Ia} increased

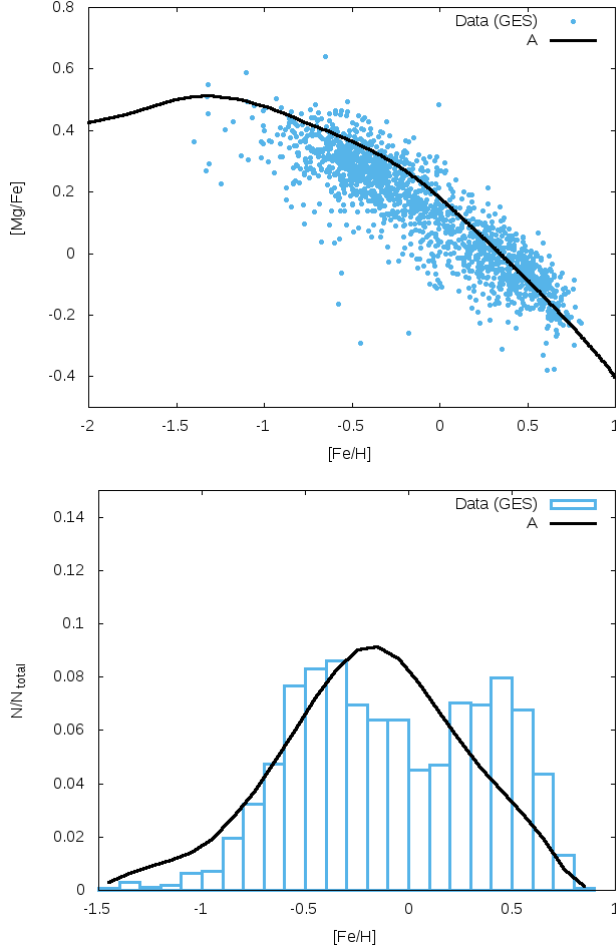


Figure 5.1: *Upper panel:* Predicted $[\text{Mg}/\text{Fe}]$ vs. $[\text{Fe}/\text{H}]$ in the Galactic bulge, in the case of Model A (black continuous line), compared with Gaia-ESO data as in Rojas-Arriagada et al. (2017). *Lower panel:* Predicted MDF in the Galactic bulge for Model A compared with Gaia-ESO data.

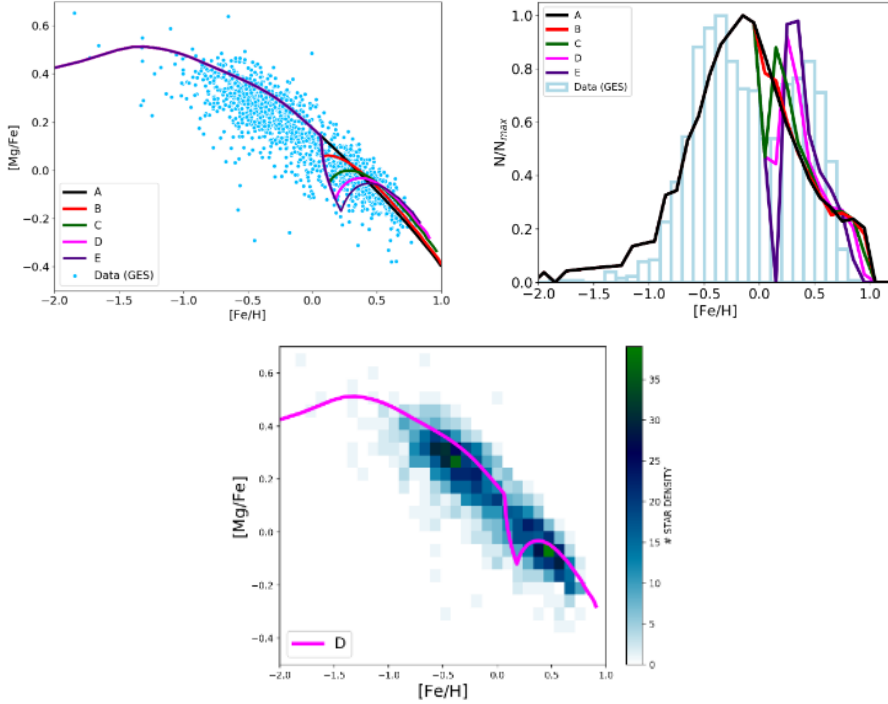


Figure 5.2: *Upper left panel:* Predicted $[\text{Mg}/\text{Fe}]$ vs. $[\text{Fe}/\text{H}]$ in the Galactic bulge, in the case of Models A, B, C, D and E with no-stop and stops in the star formation of 50, 150, 250 and 350 Myr, respectively, compared to Gaia-ESO data. *Upper right panel:* Predicted MDF in the Galactic bulge for Models A, B, C, D and E compared with Gaia-ESO data. As one can see, longer is the stop in star formation and deeper is the dip between the two populations. The model which best reproduces the data is Model D with a stop of 250 Myr. *Lower panel:* a density plot for the Gaia-ESO data compared to the results of Model D.

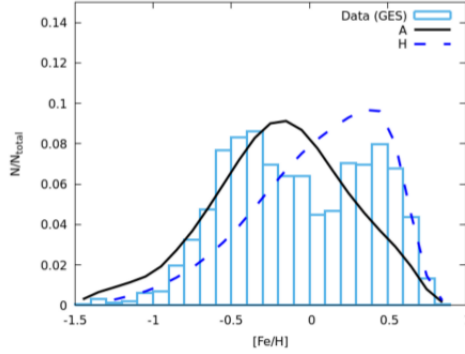


Figure 5.3: Predicted MDF in the Galactic bulge for Models A (black continuous line) and H (inner disc population, blue dashed line) compared with Gaia-ESO data. The two peaks, in this case, should be due to the bulge and inner disc populations, respectively.

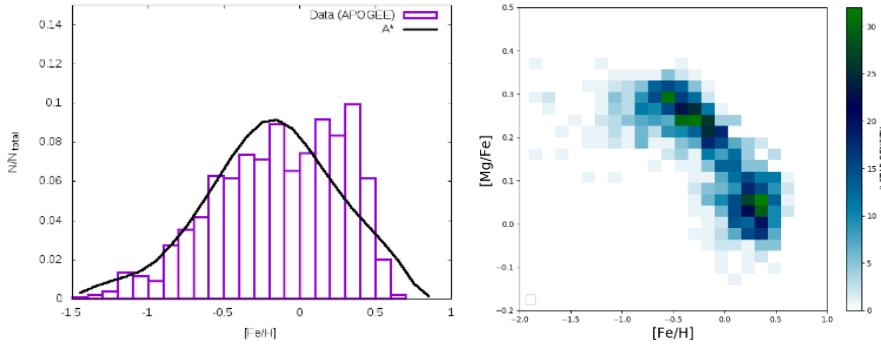


Figure 5.4: *Left panel:* Predicted MDF in the Galactic bulge for Model A* (black continuous line) compared with APOGEE data. *Right panel:* Density plot relative to the APOGEE data for $[\text{Mg}/\text{Fe}]$ vs. $[\text{Fe}/\text{H}]$ in the Galactic bulge.

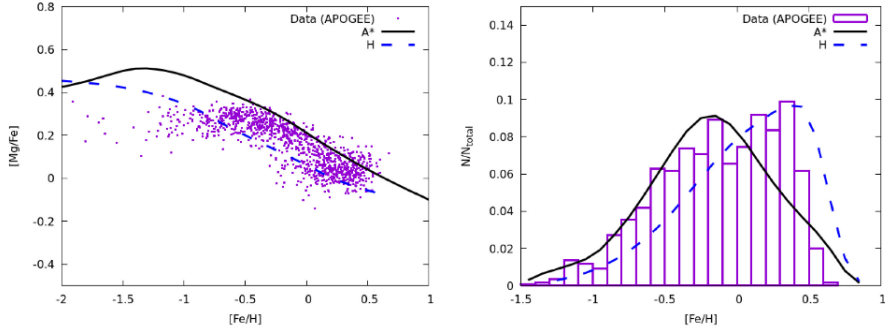


Figure 5.5: *Left panel*: Predicted $[\text{Mg}/\text{Fe}]$ vs. $[\text{Fe}/\text{H}]$ in the Galactic bulge, in the case of Model A* (black continuous line) and Model H (blue dashed line) compared to APOGEE data. *Right panel*: Predicted MDF in the Galactic bulge for Model A* and Model H compared with APOGEE data.

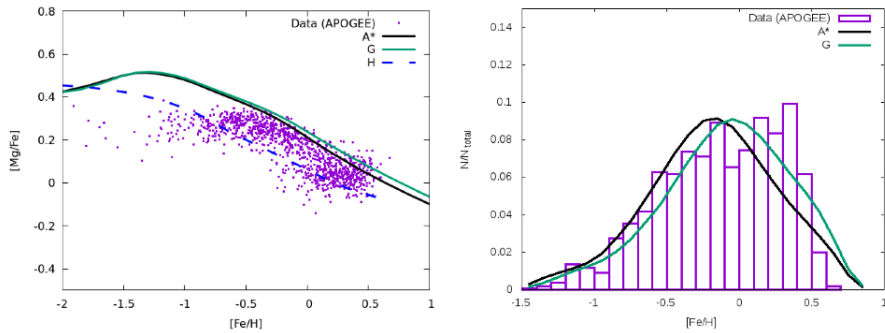


Figure 5.6: *Left panel*: Predicted $[\text{Mg}/\text{Fe}]$ vs. $[\text{Fe}/\text{H}]$ in the Galactic bulge, in the case of Model A* (black continuous line) and Model G (Calamida et al. 2015 IMF, green line almost overlapping the black continuous line) and compared with APOGEE data. *Right panel*: Predicted MDF in the Galactic bulge for Model A* and G compared with APOGEE data.

not reproduced by our Model A, which assumes continuous star formation, therefore we assumed that the star formation stopped during the bulge evolution for a period of time varying from 50 to 350 Myr and we tested the effect that such a halt has on the $[\text{Mg}/\text{Fe}]$ vs. $[\text{Fe}/\text{H}]$ relation and the MDF. These models with a stop in the star formation (Models B, C, D and E) can reproduce the MDF, but produce a hole in the $[\text{Mg}/\text{Fe}]$ vs. $[\text{Fe}/\text{H}]$ relation, not immediately visible in the data. The reason for the occurrence of the hole is that a stop in the star formation determines a stop in the production of Mg, which arises from massive stars, whereas the Fe production continues thanks to SNe Ia which explode, even in absence of star formation, because of their long lifetimes. To test the existence of such a hole, we have performed a density-plot for the Gaia-ESO data, as shown also in Fig. 5.2,. The stellar density plot shows indeed two overdensity regions in correspondance of $[\text{Fe}/\text{H}]=-0.5$ and $+0.5$ dex, respectively, in agreement with the MDF. Therefore, the hypothesis of a stop in the star formation as the origin of the MR and MP populations cannot be ruled out. Among the various models, the one which best reproduces the MDF is Model D with a stop of 250 Myr. However, from the kinematical point of view, the MR population is associated to the Boxy/Peanut X-shaped bulge (Zoccali et al. 2017), while the MP population seems to be distributed isotropically. These facts can support a scenario in which the MR population can originate from the inner disc (e.g. Zoccali et al. 2017) and not simply from a stop in star formation, although Debattista et al. (2017) have shown that old metal poor stars are dynamically hotter by the time the bar forms and therefore form a weak bar, whereas the more metal rich younger stars are kinematically cooler and therefore form a strong bar with a prominent X-shape, a scenario consistent with a stop in the star formation. Because of these suggestions, we have then explored also the possibility that the MR population is made

of stars of different origin, namely inner disc stars.

To test also this hypothesis, in Fig. 5.3, we show the MDF from Gaia-ESO data compared with Models A (for the bulge) and H (for the inner disc). It is worth noting that Model H originates from the thin disc model presented in Grisoni et al. (2018) which reproduces the abundance gradients along the thin disc. The results of Model H can represent the MR population, as shown from the predicted MDF. Model H is devised for the inner thin disc and it assumes an IMF which contains less massive stars than the Salpeter one and is the same as the IMF usually adopted for the solar vicinity (in this case Kroupa et al. 1993). Moreover, Model H assumes a lower star formation efficiency (see Table 5.1) than assumed for the bulge (see Grisoni et al. 2018). We can see from Fig. 5.3 that the disc population can in principle reproduce the second peak in the MDF, and therefore this hypothesis for explaining the MR population appears likely.

In Fig. 5.4, we show recent APOGEE data (Rojas-Arriagada et al. 2019), and in particular the MDF and the density plot of $[\text{Mg}/\text{Fe}]$ versus metallicity. The MDF is compared to the results of our Model A* (Model A with increased Mg yields from SNe Ia). In Fig. 5.5, we show the same $[\text{Mg}/\text{Fe}]$ data as in Fig. 5.4, compared to the predictions of Model A*. What we see from these Figures is that Model A* seems to overproduce Mg at low metallicities, since these new data have lower $[\text{Mg}/\text{Fe}]$ ratios at low metallicities; this effect was not present in the comparison with the Gaia-ESO data, as shown in Fig. 5.1, where Model A was fitting very well the observational points. This discrepancy can be due to different calibrations adopted in data reduction for the two different data samples. On the other hand, the increased Mg from Type Ia SNe produces a flatter $[\text{Mg}/\text{Fe}]$ ratio at high metallicities, in agreement with these data. However, this flattening of the $[\text{Mg}/\text{Fe}]$ ratio at high metallicity is not yet confirmed and we should be careful in drawing

firm conclusions on the yield variation. We are showing this case here only to suggest a possible solution if this trend will be confirmed.

As we can see in Fig. 5.4, these new APOGEE data do not show immediately a clear bimodality in the MDF, as it is instead more evident in Fig. 5.2, middle panel, for Gaia-ESO data. However, the existence of two separate populations in these data is evident from the $[\text{Mg}/\text{Fe}]$ density plot in Fig. 5.4.

Concerning the apparent differences in the MDFs derived from Gaia-ESO and APOGEE data, it should be due to the different spatial regions sampled by the two datasets: in the case of the APOGEE sample, it was selected to contain stars which are close to the plane, with $|z| < 0.5$ kpc. This translates approximately in the stars being located at $|b| < 4^\circ$ in Galactic latitude. Instead, the Gaia-ESO sample is composed of stars located in a more far-from-the-Galactic-plane region, with $-4 > b > -10$. As it has been shown by Gaia-ESO and GIBS data, the bulge MDF becomes progressively more dominated by metal-rich stars when we go closer to the Galactic plane. So, in the case of APOGEE data the dip in between the metal-rich and metal-poor peaks is less evident than in Gaia-ESO MDF, because of the larger proportion of metal-rich stars in the APOGEE data sample. In Fig. 5.5 we show Model A* and Model H (for the disc) predictions compared to the APOGEE data, both for the $[\text{Mg}/\text{Fe}]$ versus metallicity and the MDF. As one can see, in this case the mixture of these two populations provides results in reasonable agreement with both $[\text{Mg}/\text{Fe}]$ and MDF, so we can conclude that this is an acceptable solution. In Fig. 5.6 we show Model A and G; Model G is identical to Model A except for the IMF which is that of Calamida et al. (2015) instead of the one of Salpeter. It is evident that the difference between the predictions for the two IMFs is negligible, both in the $[\text{Mg}/\text{Fe}]$ vs. metallicity relation and the MDF, and we can conclude that

both IMFs are acceptable for describing the bulge stellar populations, with a slight preference for the Salpeter one. Such IMFs require a larger number of massive stars than in the IMFs derived for the solar vicinity, including Kroupa's (2001) IMF.

5.4.2 MULTIPLE STOPS IN THE STAR FORMATION

Bensby et al. (2017), by studying the abundances in microlensed bulge stars, have suggested that there is a multi-modal rather than a bimodal MDF in the bulge, indicating at least four main stellar populations created in starburst episodes occurred 12, 8, 6 and 3 Gyr ago. Although this multi-populations are still to be confirmed, here we have tried to reproduce this situation by allowing several stops in the star formation rate in our standard Model A, called Model F in Table 5.1.

In particular, in the upper left panel of Fig. 5.7 we show the predicted SFR as a function of time for Model F; in this model we have assumed four star formation bursts, with a fixed duration of 250 Myr and separated by long quiescence periods. A longer burst duration is not likely, because in such a case the bulge stars would form all in the first two episodes. The star formation efficiency is lower than assumed in Model A. In fact, by assuming $\nu=25 \text{ Gyr}^{-1}$, as in Model A, most of the bulge stars form inside the first 1 Gyr of evolution, so if the star formation occurred in different episodes, distributed over 12 Gyr, the efficiency of star formation during these episodes should have been much lower ($\nu=1\text{-}3 \text{ Gyr}^{-1}$). In Model F we assumed a star formation efficiency of 1 Gyr^{-1} in the first burst, whereas in the second, third and fourth burst the efficiency is 3 Gyr^{-1} . This choice is rather arbitrary but it allows us to reproduce a situation where an important fraction of young stars is created in the bulge (see next paragraph). In any case, we have tested that the total mass of bulge stars formed in this model corresponds

to that in Model A ($\sim 1.5 \cdot 10^{10} M_{\odot}$). The presence of multiple star bursts is clearly reflected in the MDF, which appears to show with multiple peaks (see the right upper panel of Fig. 5.7). The agreement between the observed MDF (Bensby et al. 2017) and the predictions of model F is reasonably good. Finally, we have also checked the effect of the multiple bursts on the abundance pattern, in particular on $[\text{Mg}/\text{Fe}]$ vs. $[\text{Fe}/\text{H}]$: what we can see here, is that the predicted track shows holes in correspondance of the stops in the star formation, although they are not so deep as those in Models B, C, D, E. This is due to the lower efficiency of star formation adopted in model F. In fact, a lower efficiency means less stars formed in each burst, so when star formation stops and core-collapse SNe stop exploding, SNe Ia continue to produce Fe thus decreasing the Mg/Fe ratio. The decrease in the $[\text{Mg}/\text{Fe}]$ ratio is then lower than in the case where the star formation before the stop has been much higher, with a consequent higher number of SNe Ia produced. In Fig. 5.7 we show also the density plot for the Bensby et al. (2017) stars. This plot shows that our model predictions are generally following the trend of the data but they are lower than the observations. This is due to the rather low assumed star formation efficiency which produces on average lower $[\text{Mg}/\text{Fe}]$ ratios, for a given IMF. The lower predicted $[\text{Mg}/\text{Fe}]$ ratios may suggest that for the bulge a more intense star formation rate should be assumed, in agreement with the previous models, but in such a case most of the stars would form early, thus making the multiburst assumption at variance with the observed abundance ratios.

5.4.3 AGE DISTRIBUTION

The ages of the bulge stars can provide a further constraint on the number of stellar populations, although many uncertainties are still present in the derivation of stellar ages.

CHAPTER 5. CHEMICAL EVOLUTION OF THE GALACTIC BULGE

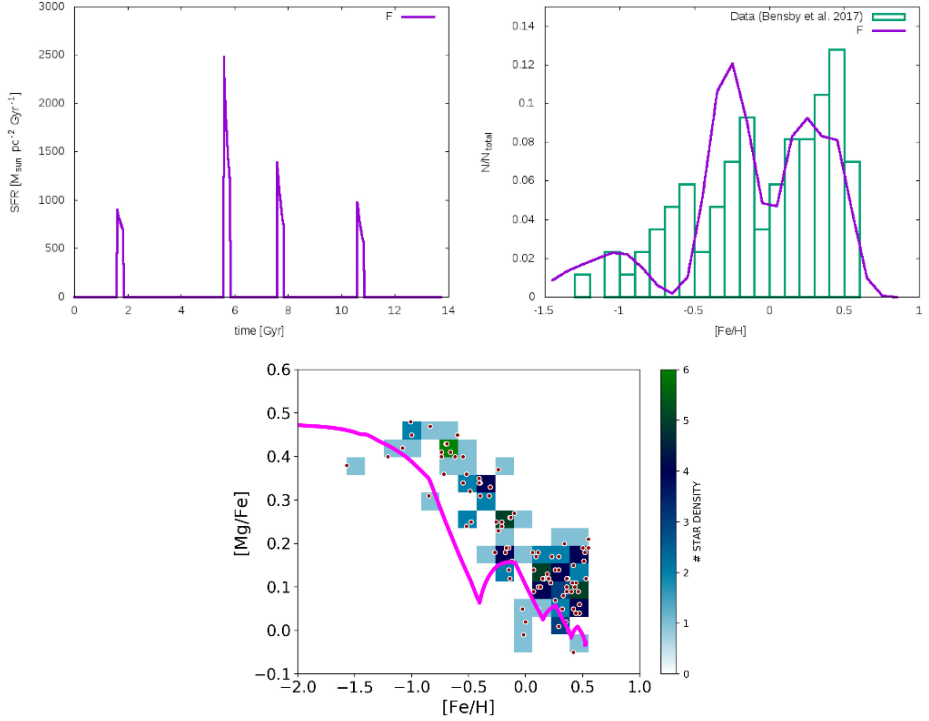


Figure 5.7: *Upper left panel:* SFR as a function of time, predicted by Model F. *Upper right panel:* Predicted and observed MDF. The predictions are from Model F, the data are from Bensby et al. (2017). *Lower middle panel:* Predicted and observed $[\text{Mg}/\text{Fe}]$ vs. $[\text{Fe}/\text{H}]$ in the Galactic bulge, in the case of Model F compared to the data of Bensby et al. (2017). The data are shown as a density plot.

In Fig. 5.8, we show the predicted and observed age distribution in the Galactic bulge. The predictions are from the various models considered here. The model predictions for the bulge from Models A, D and H are presented as they are computed, as well as corrected by taking into account the errors on the ages obtained by Schultheis et al. (2015; 2017) (with the method of the $[C/N]$ ratio) and by considering only stars not older than 12 Gyr, in accordance with that paper. Schultheis et al. (2015) did not apply any age-cut in their sample. However, due to the limitation of the Martig et al. (2016) method, only 74 stars in the Baade Window do have an age determination. The oldest ages they obtained was 12 Gyr. In our case, in order to consider only stars not older than 12 Gyr we had to remove a large fraction of stars oscillating between $\sim 70\%$ (Model A) and $\sim 60\%$ (Model A+H). It is worth noting that we did not shift our model results artificially to lower ages. To include the observational errors ($\sim 25\%$), we followed the approach of Spitoni et al. (2019), as described in their eq. (10). At each Galactic time, we added a random error to the ages of the stellar populations formed at Galactic time t . These random errors are uniformly distributed in the interval described by the average errors estimated at that time. In Fig. 5.8, we can see that data and model agree remarkably well in the case of Model A, showing that the majority of bulge stars, both from a theoretical and observational point of view, are peaked around an age of 11 Gyr. The peak at 11 Gyr is present also for Model D and Model A+H. The reason why the peak is not at 12 Gyr, as it could be expected, is due to the redistribution and smearing of stellar ages after the cut and the convolution with the observational error; in fact, the bin which includes the age of 12 Gyr spans a range between 11.7 and 12.2 Gyr (see green histograms in Fig. 5.8), and therefore is affected by the cut at 12 Gyr (stars between 12 and 12.2 have been excluded). This is the reason why this bin contains less stars

than bins corresponding to immediately younger ages.

In Model A, the predicted number of stars which are younger than 5 Gyr is $\sim 8.7\%$, in agreement with Bernard et al. (2018) who suggest $\sim 10\%$. In Fig. 5.8, we also show the predictions of Model D with a stop in star formation of 250 Myr and therefore with two stellar populations both born in the bulge. As we can see, the difference relative to Model A, with only one population, is negligible and the agreement with the data is still quite good, even if more younger stars are produced due to the stop in the star formation. In Fig. 5.8, we show also the predictions of Model A combined to Model H (for the disc), to test the hypothesis that the MR population can be due to disc stars which formed more slowly than the bulge ones formed in-situ. In this case, the agreement is also good, since the number of young stars (< 5 Gyr) is $\sim 10\%$, in perfect agreement with Bernard et al. (2018). Finally, in Fig. 5.9 we show the predictions of Model F with multiple bursts; here, we show the model predictions after being corrected by the observational errors as quoted by Bensby et al. (2017). This model clearly does not show agreement with the Schultheis et al. (2017) data, so we compared these results with the Bensby et al. (2017) age distribution, from which the suggestion of the multiple bulge populations arose. As one can see in Fig. 5.9, the agreement between our Model F and these data is acceptable when the data are convolved with the errors, and we predict a large fraction of young stars (< 5 Gyr) of $\sim 20\%$. It is worth noting that Bensby et al. (2017) concluded that there are many young stars in the bulge, at variance with other studies, as mentioned in the Introduction. It is not clear the reason of this discrepancy since the method for deriving ages is similar, namely the isochrone fitting in the CMD. In particular, Bensby et al. (2017) derived the stellar ages by using the Bayesian estimation from isochrones, as described in Jørgensen & Lindegren(2005). In this method,

the isochrone fitting is done in the luminosity-temperature plane rather than in the CMD. What arises from these comparisons is that most of the available spectroscopic data on bulge stars suggest that the bulge is formed by a majority of old stars with a minor percentage of truly young stars. Chemical evolution models which well reproduce the $[\alpha/\text{Fe}]$ ratios in bulge stars need to assume a fast and highly efficient star formation rate which naturally leads to a predominantly old bulge, with the fraction of young stars due either to secular evolution from the inner thin disc or to a stop in the star formation during bulge evolution, since both arguments can be supported by kinematical considerations. From the point of view of age distribution, although many uncertainties are still present, the best model appears the one with the MR population made of inner disc stars, although the other cannot be discarded.

5.5 CONCLUSIONS

In this work, we study the formation and chemical evolution of the Galactic bulge with particular focus on the abundance patterns ($[\text{Mg}/\text{Fe}]$ vs. $[\text{Fe}/\text{H}]$), metallicity distribution function and age distribution. We consider detailed chemical evolution models for the Galactic bulge and inner disc, with the aim of shedding light on the formation and evolution of the bulge. In particular, we try to establish if the data can be reproduced by two distinct stellar populations, one metal poor and the other metal rich, and to assess their origin. We explore two main possibilities: i) the two populations have been born in the bulge separated by a period of a stop in the star formation, ii) the MP population was born in the bulge while the MR was formed in the inner disc. We also explore the case of multiple populations born in separate star formation episodes, as suggested by Bensby et al. (2017). In all the studied cases, except this last one, the MP population forms very quickly

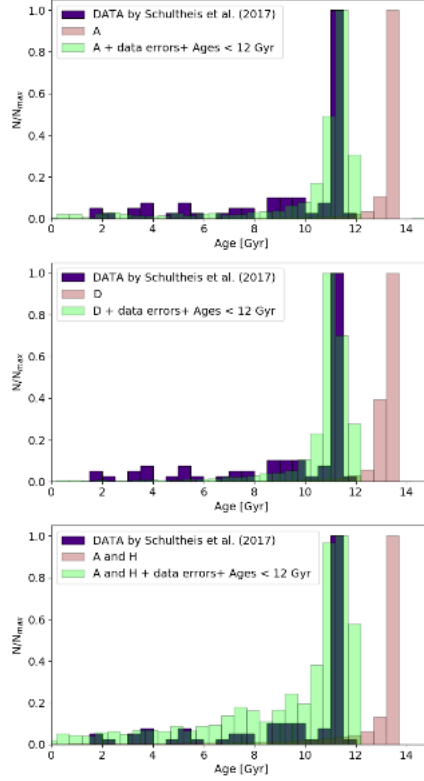


Figure 5.8: Age distribution predicted by the various models, compared to the observational data. *Upper panel* : we show the results of Model A with continuous star formation compared to the data of Schultheis et al. (2017)(deep green distribution): the pink distribution represents the theoretical predictions at a face value, while the light green distribution is the theoretical one after being convolved with the observational errors; *Middle panel*: we show the results of Model D, the colors of the distributions have the same meaning as described for the previous panel; *Lower panel*: we show the results of Model A and model H together, convolved with the observational errors. The colors of the distributions have the same meaning as described for the previous panels.

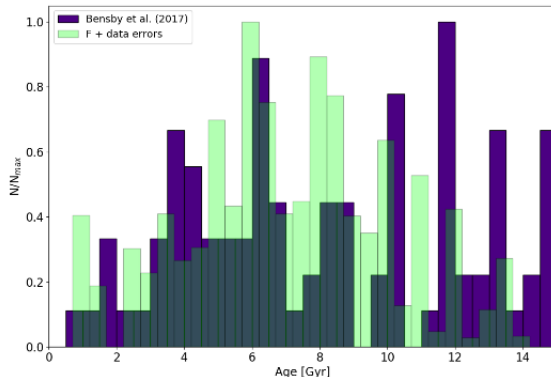


Figure 5.9: Age distribution as predicted by Model F and corrected by the age errors (light green histogram), as described in the text, compared with data of Bensby et al. (2017) (purple histogram).

(less than 500 Myr) and with high star formation efficiency (25 Gyr^{-1}). The same prescriptions are adopted for the MR one if we assume that it is born in the bulge after a halt in the star formation process. On the other hand, in the multiple burst case the efficiency of star formation during different episodes is assumed to be much lower (from 1 to 3 Gyr^{-1}) and the bulge formed on a much longer timescale (several Gyrs). Finally, in the case where MR population is formed by inner disc stars, the efficiency of star formation is low and typical of the thin disc (1 Gyr^{-1}).

After comparing model predictions and observational data we can draw some conclusions, summarized as follows:

- Models with two main stellar populations in the bulge best fit the most recent data from Gaia-ESO and APOGEE.
- In particular, if the two populations have formed as a result of a stop

in the star formation of ~ 250 Myr, occurred at early times, one can reproduce the MDF, the $[\text{Mg}/\text{Fe}]$ ratios and the age distribution of bulge stars. However, this scenario could be inconsistent with stellar kinematics suggesting that the MR stars are belonging to the B/P X-shaped structure of the bulge, whereas the MP stars are distributed isotropically (Zoccali et al. 2017), although other studies (Debattista et al. 2017; Buck et al. 2017) do not exclude the possibility of explaining the X-shape only with stars formed in situ.

- Another possible explanation can be that the metal rich population originates by secular evolution from the inner disc.
- The flattening of the $[\text{Mg}/\text{Fe}]$ ratio at high metallicity in the last APOGEE data could be reproduced by assuming a larger Mg production from SNe Ia. However, this flattening is not present in all the existing bulge data and therefore we cannot draw firm conclusions on this point.
- The assumed Salpeter IMF can well reproduce the data, and the results differ negligibly from those obtained with Calamida et al. (2015) IMF derived for the bulge.
- The results of a multiple burst regime with the bursts occurring from 3 to 12 Gyr ago, as suggested by Bensby et al. (2017), can roughly reproduce their data but is in conflict with all the other data and predict a large fraction of young bulge stars which is not found in the majority of the other studies. In addition, a multiple burst scenario is also inconsistent with the kinematical information.
- Therefore, we conclude that the bulge overall is old and that both the MP and MR populations contain very old stars. The young stars

(10 % with ages < 5 Gyr) belong either to the inner disc stars or they have formed in situ after a stop in star formation no longer than 250 Myr. The bulge formed the majority of its stars in the first 0.5 Gyr of its evolution, in agreement with most of the previous studies (Matteucci & Brocato 1990; Ballero et al. 2007; Cescutti & Matteucci 2011; Grieco et al. 2012).

CHAPTER 6

Galactic lithium evolution

In this Chapter, I present the results on Galactic lithium evolution. The fundamental question that I would like to address here can be summarized as follows. What are the main lithium producers in the Galaxy? How can we explain the ISM lithium decline observed at super-solar metallicities? The Chapter is organized as follows. In Section 6.1, I give a general introduction to Galactic lithium evolution. In Section 6.2, we describe the observational data which have been considered to compare with the predictions of our chemical evolution models. In Section 6.3, we present the models adopted in this work. In Section 6.4, we show our results, that include some predictions to be tested by future observations. Finally, in Section 6.5, we draw our conclusions, based on the comparison between model predictions and available observational data. The results presented in this Chapter are described in the published paper Grisoni et al. (2019).

6.1 INTRODUCTION

Among the open questions in the field of Galactic Archaeology, one of the most puzzling topics is the Galactic lithium evolution. Understanding the evolution of this element, indeed, raises a number of difficult questions, as briefly recalled in the following paragraphs.

Starting from the pioneering work of Spite & Spite (1982), it has been generally acknowledged that most metal-poor ($-2.4 < [\text{Fe}/\text{H}] < -1.4$), warm ($T_{\text{eff}} = 5700\text{-}6800$ K) Galactic halo dwarfs lie on a well-defined plateau, the so-called "Spite plateau", namely, they share roughly the same Li abundance, $A(\text{Li})=2.05\text{-}2.2$ dex (Spite & Spite 1986; Bonifacio & Molaro 1997; Bonifacio et al. 2007). This common abundance, however, is i) lower than that predicted by standard Big Bang nucleosynthesis theory (SBBN) as indicated by the baryon density (see e.g. the Planck results, Coc et al. 2014) and ii) lower than that observed in meteorites (e.g. Lodders et al. 2009) and young T Tauri stars (Bonsack & Greenstein 1960). To make the story a bit more complicated, a huge dispersion in Li abundances is observed for stars at disc metallicities (see Ramirez et al. 2012; Delgado Mena et al. 2015; Guiglion et al. 2016; Fu et al. 2018, among others, for recent work), while observations of extremely metal-poor stars (Sbordone et al. 2010; Melendez et al. 2010; Hansen et al. 2014; Bonifacio et al. 2015) find the Spite plateau to bend down for stars with $[\text{Fe}/\text{H}] < -2.8$ dex. In this work, we do not consider the first problem (the so-called cosmological Li problem). This is quite convincingly addressed in Fu et al. (2015), which explain the discrepancy between the SBBN Li value and the one observed on the plateau, as well as the drop of Li abundances at very low metallicities, as due to stellar mechanisms. We rather concentrate on the second problem, i.e. the Galactic evolution of lithium. As customarily done in the literature,

we assume that the upper envelope of the observations in a $A(\text{Li})$ - $[\text{Fe}/\text{H}]$ diagram faithfully traces the enrichment of Li in time in the Galaxy.

A topic of lively debate is the ISM lithium content decline observed at super-solar metallicities for solar neighbourhood stars. This feature was first pointed out by Delgado Mena et al. (2015), and then confirmed by the AMBRE Project (Guiglion et al. 2016), the Gaia-ESO Survey (Fu et al. 2018), Bensby & Lind (2018), and can be also seen in the recent GALAH DR2 data (Buder et al 2018). The scenarios proposed to explain this feature from the Galactic Chemical Evolution (GCE) point of view can be summarized as follows: i) lower yields of Li from stars at high metallicities, even if no physical reasons for this fact can be found (Prantzos et al. 2017); and ii) the interplay of different populations coming from the inner regions of the Milky Way disc (Guiglion et al. 2019, Minchev et al. 2019). Here, we propose a new explanation for the lithium ISM decline at high-metallicities, based on the importance of novae as producers of lithium.

In fact, novae are important sources of lithium in the Galaxy. In literature, D’Antona & Matteucci (1991) first included novae into a detailed chemical evolution model: they considered as ${}^7\text{Li}$ producers Asymptotic Giant Branch stars (AGB), classical novae and carbon stars, and concluded that novae could be important Li producers especially to explain the steep rise of Li abundance at $[\text{Fe}/\text{H}] > -1.0$ dex. A few years later, Romano et al. (1999) took into account also Li production from Type II SNe and Galactic Cosmic Rays (GCRs), and implemented detailed nova yields coming from 1D hydrodynamic models by Jose’ & Hernanz (1998) in the GCE model. They concluded that the most important ${}^7\text{Li}$ producers were novae and GCRs (see also Romano et al. 2001; 2003). More recently, Matteucci (2010), Izzo et al. (2015) and Cescutti & Molaro (2019) underlined again the importance of novae to explain lithium evolution.

The detections of ${}^7\text{Be}$ (later decaying into ${}^7\text{Li}$) and ${}^7\text{Li}$ in nova ejecta by Tajitsu et al. (2015) and Izzo et al. (2015), respectively, reinforced the idea that novae are important sources of lithium (see also Tajitsu et al. 2016; Molaro et al. 2016; Selvelli et al. 2018). These pieces of observational evidence are extremely important. On a theoretical side, in fact, it is well-known that Li can be produced in stars, either through the "Cameron-Fowler conveyor" (Cameron & Fowler 1971), acting in intermediate-mass stars on the AGB (Sackmann & Boothroyd 1992), or through the cool bottom process combined to some extra deep mixing in low-mass stars climbing the red giant branch (RGB; Sackmann & Boothroyd 1999), or during thermonuclear runaways in nova outbursts (e.g. Starrfield et al. 1978), or through the ν -process (first hypothesised by Domogatskii et al. 1978) in the He-shell of core-collapse SNe. Moreover, a fraction (up to 20-30%) of the meteoritic Li comes from spallation processes triggered by the energetic nuclei of GCRs in the ISM (Reeves et al. 1970; Meneguzzi et al. 1971; Lemoine et al. 1998; Romano et al. 2001; Prantzos 2012). The observational evidence for Li production, however, remains elusive. While it is known that a (small) fraction of RGB and AGB stars are Li-rich (e.g. Kirby et al. 2016, and references therein), the Li production from these stars can be hardly quantified, mostly because of the severe uncertainties on their mass loss rates (see, e.g., Romano et al. 2001; Travaglio et al. 2001, and discussions therein). As regards core-collapse SNe, to the best of our knowledge Li has never been found in their spectra. Thus, the detection of huge amounts of Li in the ejecta of classical novae (in excess of 1D theoretical model calculations) offer the only firm solution to the Galactic lithium problem, and point to novae as the main sources of Li in the Galaxy (Izzo et al. 2015, and discussion therein; see also Cescutti & Molaro 2019).

The aim of this work is to study the chemical evolution of lithium by means

of detailed chemical evolution models in the light of the newest observational data. In particular, we will focus on the decrease of lithium at high metallicities, which is still a topic of lively debate. Here, we test the hypothesis that the fraction of binary systems giving rise to novae is lower at higher metallicities, as suggested by the studies of Gao et al. (2014, 2017) and Yuan et al. (2015). A similar assumption of a metallicity-dependent occurrence probability has been tested by Simonetti et al. (2018) with respect to neutron star mergers.

6.2 OBSERVATIONAL DATA

In this work, to study the Galactic lithium evolution we consider different datasets from literature. In particular, for the Galactic halo we consider the data of Charbonnel & Primas (2005) and Sbordone et al. (2010).

Charbonnel & Primas (2005) revised a large collection of Li measurements for halo stars from the literature, paying particular attention to the quality of the data and exploring in detail the temperature scale issue. NLTE corrections were applied to the Li abundances. Li determinations for stars in their "clean sample" (see Charbonnel & Primas 2005, for details) are consistent with no dispersion on the plateau. We enlarge this dataset with VLT-UVES Li abundances for 28 halo dwarfs in the metallicity range $-3.5 < [\text{Fe}/\text{H}] < -2.5$ by Sbordone et al. (2010), that are measured by means of 3D hydrodynamical spectral synthesis including NLTE. A bending of the Spite plateau below $[\text{Fe}/\text{H}] \sim -3$ is clearly present in the data of Sbordone et al. (2010).

For the discs, we adopt the recent spectroscopic data from the AMBRE Project (Guiglion et al. 2016) and Gaia-ESO Survey (Fu et al. 2018), where a distinction is made between thick and thin disc stars, basing on chemical criteria. The AMBRE catalogue consists of Li abundances for 7300 stars,

homogeneously derived from high-resolution spectra in the ESO archive with an automatic method (see Guiglion et al. 2016 for a description of the method and of the data validation). Overall, the Li abundance in the local ISM is found to increase from $[\text{Fe}/\text{H}] = -1$ to 0 dex, while it clearly decreases in the super-solar metallicity regime. The Li content of thin-disc stars displays a much steeper increase with $[\text{Fe}/\text{H}]$ than that of thick-disc stars, that is found to increase only slightly with time (metallicity). These results are confirmed by the analysis of Fu et al. (2018), which discuss Li measurements for main-sequence field stars from the Gaia-ESO iDR4 catalogue pointing out the higher level of Li enrichment in thin-disc stars, with respect to the thick-disc population. These authors also mention the possibility that the decrease of Li abundance at super-solar metallicities can be due to a reduced nova rate at high $[\text{Fe}/\text{H}]$, coupled to Li depletion -rather than production- in AGB stars (on the latter point, see also Romano et al. 2001), a possibility that we fully address here with our GCE models. For the meteoritic value, we use the determination by Lodders et al. (2009). For the Galactic bulge we adopt the data of Gonzalez et al. (2009) and Bensby et al. (2011). However, the 13 stars with measured Li abundances in the sample of Gonzalez et al. (2009) are all RGB/AGB stars in which the initial atmospheric Li content has been altered, so they can not be used to safely constrain our evolutionary models for the bulge. The sample analysed in Bensby et al. (2011), consisting of 26 microlensed dwarf and subgiant stars, offers, in principle, a better hope. 1D, NLTE Li abundances (based on MARCS models) could be derived, however, only for 5 objects. Out of these, only 2 have $T_{\text{eff}} > 5900$ K, thus further reducing the number of stars that can be taken as reliable tracers of bulge Li enrichment (see Bensby et al. 2011, and references therein). We discuss our predictions about the evolution of Li in the Galactic bulge in Section 4; we caution that these still

wait for a proper dataset in order to be confirmed or disproved.

6.3 MODELS

In this work, we adopt the following chemical evolution models for the Galactic halo, discs and bulge.

- Two-infall model (Chiappini et al. 1997 and Romano et al. 2010). It assumes that the Milky Way forms by means of two major gas infall episodes: the first infall episode gave rise to the halo-thick disc, whereas during the second one, which is slower and delayed with respect to the first one, the thin disc forms.
- Parallel model (Grisoni et al. 2017, 2018). It assumes that the thick and the thin disc stars formed out of two separate infall episodes in two distinct evolutionary phases, which evolve independently. This model was tested in Grisoni et al. (2017) for the solar neighbourhood, and then extended to the other Galactocentric distances in Grisoni et al. (2018).
- For the Galactic bulge, we consider the model by Matteucci et al. (2019) which assumes a fast formation on a short timescale and with high star formation efficiency ($\nu=25 \text{ Gyr}^{-1}$, see Table 6.1).

6.3.1 MODEL EQUATIONS

The time evolution of G_i , which is the mass fraction of the element i in the gas, is described by Eq. (2.8).

The SFR is given by the Schmidt-Kennicutt law (Kennicutt 1998a). The parameter ν corresponds to the star formation efficiency, which is fixed in order to reproduce the SFR at present time. For the IMF, we use the

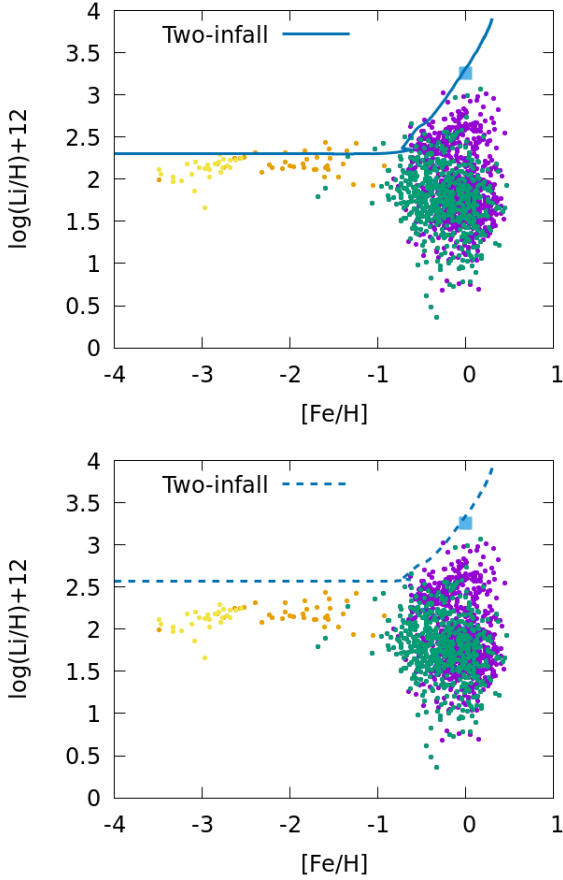


Figure 6.1: *Left panel:* Observed and predicted lithium abundance as a function of metallicity in the solar neighbourhood. The predictions are from the two-infall model (blue line). The data are from Charbonnel & Primas (2005) (orange dots), Sbordone et al. (2010) (yellow dots) and from Gaia-ESO Survey (Fu et al. 2018) for the thick disc (green dots) and thin disc (purple dots). The meteoritic value is the one by Lodders et al. (2009) (light-blue square). *Right panel:* Same as the left panel, when a high-primordial Li abundance is adopted.

Table 6.1: Input parameters for the best chemical evolution models. In the first column, there is the name of the model. In the second column, we show the adopted initial mass function. In the third column, there is the star formation efficiency (ν). In the fourth column, we give the timescales for mass accretion (τ).

Model	IMF	ν [Gyr ⁻¹]	τ [Gyr]
Two-infall	Kroupa et al. (1993)	2 (halo-thick) 1 (thin disc)	1 (halo-thick) 7 (thin disc)
Thick disc	Kroupa et al. (1993)	2	0.5
Thin disc	Kroupa et al. (1993)	1	7
Bulge	Salpeter (1955)	25	0.1

Kroupa et al. (1993) one for the halo, thick and thin discs, and the Salpeter (1955) one for the bulge.

We account for detailed nucleosynthesis from low and intermediate mass stars, super-AGB stars, Type Ia SNe (which originate from white dwarfs in binary systems) and Type Ib, Ic, II SNe (which originate from core-collapse massive stars).

In this work, we focus also on the contribution of novae, which are important lithium producers. Novae are binary systems of a white dwarf (WD) and a low mass main sequence star. The novae rate is computed by assuming that it is proportional to the formation rate of CO WDs (see Matteucci 2012,

Spitoni et al. 2018). In particular:

$$R_{\text{nova}}(t) = \alpha \int_{0.8}^8 \text{SFR}(t - \tau_{m2} - \Delta t) \phi(m) dm, \quad (6.1)$$

where α is the fraction of WDs in binary systems giving rise to novae, τ_m is the lifetime of WD progenitors of mass m , $\Delta t = 1$ Gyr is a suitable average cooling time (see Romano et al 1999, and references therein) and ϕ is the stellar IMF. Following Bath & Shaviv (1978), each nova is supposed to suffer 10^4 eruptions during its life. For the sake of simplicity, we consider all the outbursts to happen at the same time, i.e. at the time of the formation of the nova system (this means no time delay between successive outbursts, but see Cescutti & Molaro 2019).

In the case of the classical two-infall model (Chiappini et al. 1997, Romano et al. 2010), the gas infall law is given by Eq. (2.10). The parameters τ_{01} and τ_2 are the timescales of gas accretion for the halo-thick and thin discs, respectively. The timescales of gas accretion are free parameters in the model, and they have been tuned in order to fit the observed metallicity distribution function in the solar vicinity (see Table 6.1). The coefficients $A_{01}(r)$ and $B(r)$ in Eq. (2.10) are chosen in order to reproduce the total surface mass density at present time in the solar neighbourhood, and we follow the prescriptions of Romano et al. (2000).

On the other hand, in the case of the parallel model, since we assume two separate infall episodes, the gas infall law is given by Eq. (3.2) and Eq. (3.3) for the thick and thin discs, respectively. Here, we follow the prescriptions of Grisoni et al. (2017; 2018), Matteucci et al. (2018).

6.3.2 NUCLEOSYNTHESIS PRESCRIPTIONS

Here, we adopt the following Li nucleosynthesis sources and prescriptions.

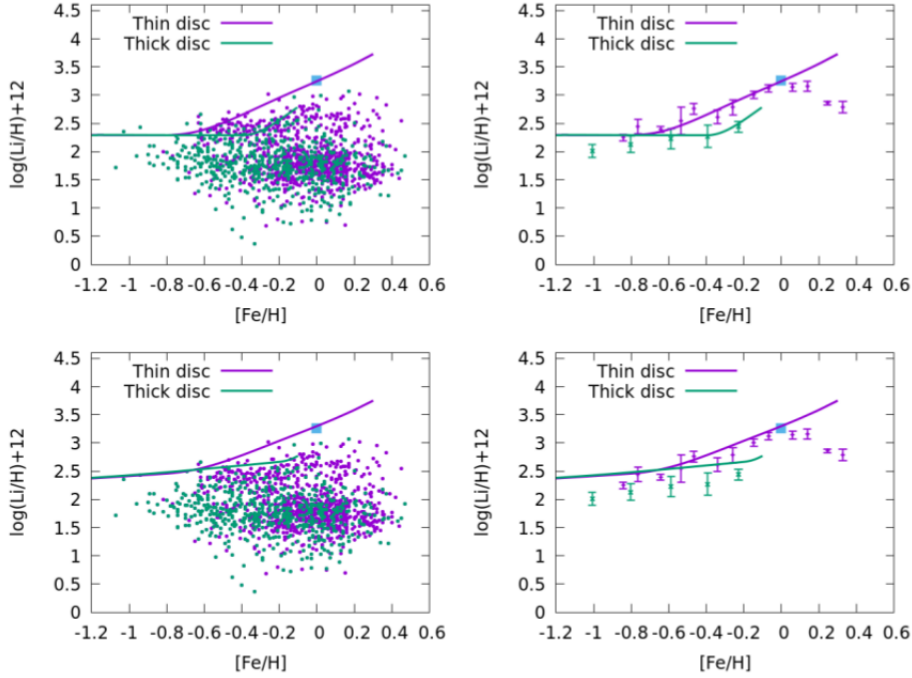


Figure 6.2: *Left-hand upper panel:* Observed and predicted lithium abundance as a function of metallicity for thick- and thin-disc stars in the solar neighbourhood. The predictions are from the parallel model for the thick (green line) and thin disc (purple line). The data are from Gaia-ESO Survey (Fu et al. 2018) for the thick disc stars (green dots) and thin disc stars (purple dots). The meteoritic value is the one by Lodders et al. (2009) (light-blue square). *Right-hand upper panel:* same as the left panel, but with AMBRE data (Guiglion et al. 2016) for the thick disc stars (green dots) and thin disc stars (purple dots). *Lower panels:* same as the corresponding upper panels, but when the contribution from massive stars is taken into account.

- Ventura et al. (2013 + private communication) for LIMS (1-6 MSun) and super-AGB (6-8 MSun);
- Nomoto et al. (2013) for core-collapse SNe. This contribution is very uncertain and, moreover, it turns out to be a minor one; therefore, it is suppressed in our best models;
- The Li ejected during one nova outburst (the total number of outbursts in a nova life is 10^4) is assumed to be in the range given by Izzo et al. (2015), where it was measured that $M_{Li}=0.3-4.8 \cdot 10^{-10} M_{\odot}$ in the ejecta of nova V1369 Cen.
- GCR as in Smiljanic et al. (2009), where it was derived the relation for ${}^9\text{Be}$:

$$\log(\text{Be}/\text{H})=-10.38+1.24[\text{Fe}/\text{H}]. \quad (6.2)$$

Then assuming a scaling ratio of ${}^7\text{Li}/{}^9\text{Be}\sim 7.6$ (see Molaro et al. 1997), it is possible to get the relation also for ${}^7\text{Li}$ (see also Cescutti & Molaro 2019):

$$\log(\text{Li}/\text{H})=-9.50+1.24[\text{Fe}/\text{H}]. \quad (6.3)$$

6.4 RESULTS

In this section, we show the results based on the comparison between model predictions and observations for the various Galactic components: halo, thick and thin discs, and bulge. In Table 6.1, the input parameters of the different models are listed. In the first column, there is the name of the model. Then, we indicate the adopted IMF, the star formation efficiency (ν) and the timescale of formation (τ) of the Galactic components.

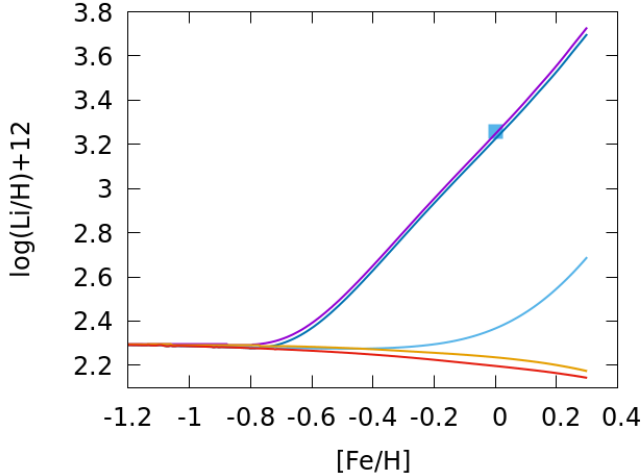


Figure 6.3: Predicted lithium abundance as a function of metallicity for the thin disc, where the various lithium sources are isolated. The predictions are from the parallel model for the thin disc with all the sources (purple line), only novae (blue line), only GCR (light blue line), only AGB (orange line) and only astration (red line). The meteoritic value is the one by Lodders et al. (2009) (light-blue square).

6.4.1 THE GALACTIC HALO

In Fig. 6.1, we show the observed and predicted lithium abundance as a function of $[\text{Fe}/\text{H}]$ as index of metallicity for solar neighbourhood stars. We consider the data from Charbonnel & Primas (2005) (orange dots), Sbordone et al. (2010) (yellow dots) and from Gaia-ESO Survey (Fu et al. 2018) for the thick disc (green dots) and thin disc (purple dots). The predictions are from the two-infall model, when a primordial lithium abundance of $A(\text{Li}) \sim 2.3$ (left panel) or $A(\text{Li}) \sim 2.6$ (right panel) is adopted, respectively. By assuming a primordial Li abundance of $A(\text{Li}) \sim 2.3$, and Li production

from LIMS, super-AGB stars, novae and GCRs as described in Sect. 3.2, we can reproduce the upper envelope of the observational data, as well as the meteoritic value (that is immune from destruction processes) with our model. Still, we must invoke some internal destruction mechanism(s) in the most metal-poor stars to explain the bending of Li abundance at the low metallicity end. If we consider a primordial Li abundance of $A(\text{Li}) \sim 2.6$ as suggested by SBBN and the measurements of Planck and WMAP, instead, the predicted plateau requires the activation of Li destruction channels in all metal-poor halo dwarfs to be made consistent with the data (see Fu et al. 2015).

Because of Li depletion acting in subsequent generations of stars during the whole Galactic evolution, the rise from the plateau requires the same contributors to the Li synthesis, independently of the assumed primordial value of $A(\text{Li})$ (see the discussion in Romano et al. 2003). In particular, the rise from the primordial value is always explained as due to the fundamental contribution of long-lived stellar sources (Romano et al. 1999, 2001). Thus, from now on we do not focus anymore on the discrepancy between the primordial Li values, but concentrate on the Galactic Li evolution. In particular, we set the primordial Li abundance to $A(\text{Li}) \sim 2.3$ and focus on the different Li producers, remembering that the conclusions on the Galactic lithium evolution will not be affected by our particular choice of the primordial Li abundance.

A characteristic feature of the two-infall model that we can appreciate in Fig. 6.1 is the back and forth loop at $[\text{Fe}/\text{H}] \sim -0.8$ dex. This is related to the transition between the halo-thick disc and the thin disc phases. When the formation of the inner halo and thick disc is terminated, in fact, the star formation stops. A new episode of gas infall starts at this point, which provides large amounts of fresh, unprocessed gas. As a consequence, the

metallicity of the ISM first suddenly decreases, then, as soon as the star formation is reactivated, it increases again. This happens about 1 Gyr after the beginning of the Galaxy formation, that is also the time at which novae start to contribute to the Galactic Li enrichment in our model. Therefore, a rapid increase of the ISM Li abundance is predicted to start with the formation of the thin disc component.

In the thin disc phase, there is the rise which is mainly due to novae (Romano et al. 1999, 2001; Izzo et al. 2015; Cescutti & Molaro 2019). In this way, the meteoritic value (Lodders et al. 2009) can be reached. We notice that after the meteoritic value is reached, the model predictions still rise at variance with the observations that show a decline (Gaia-ESO data of Fu et al. 2018, but the decline is evident also in the data of Guiglion et al. 2016, Buder et al. 2018, Bensby & Lind 2018). To better study what happens in the Galactic discs, we apply the parallel approach of Grisoni et al. (2017; 2018) (see next section).

6.4.2 THE GALACTIC DISC(S)

In Fig. 6.2, we show the predicted and observed lithium abundance as a function of metallicity for the thick and thin discs. The predictions are from the parallel model (Grisoni et al. 2017, 2018). This model was tuned to reproduce the $[\text{Mg}/\text{Fe}]$ vs. $[\text{Fe}/\text{H}]$ for the thick and thin disc stars observed by AMBRE (Mikolaitis et al. 2017). In fact, in the $[\text{Mg}/\text{Fe}]$ vs. $[\text{Fe}/\text{H}]$ diagram it is possible to see two distinct sequences corresponding to the thick and thin disc stars, with the thick disc being α -enhanced due to a shorter timescale of formation and higher star formation efficiency with respect to the thin disc. These two sequences corresponding to thick and thin discs stars have been observed also by other surveys, such as APOGEE (Hayden et al. 2015) and Gaia-ESO Survey (Rojas-Arriagada et al. 2017).

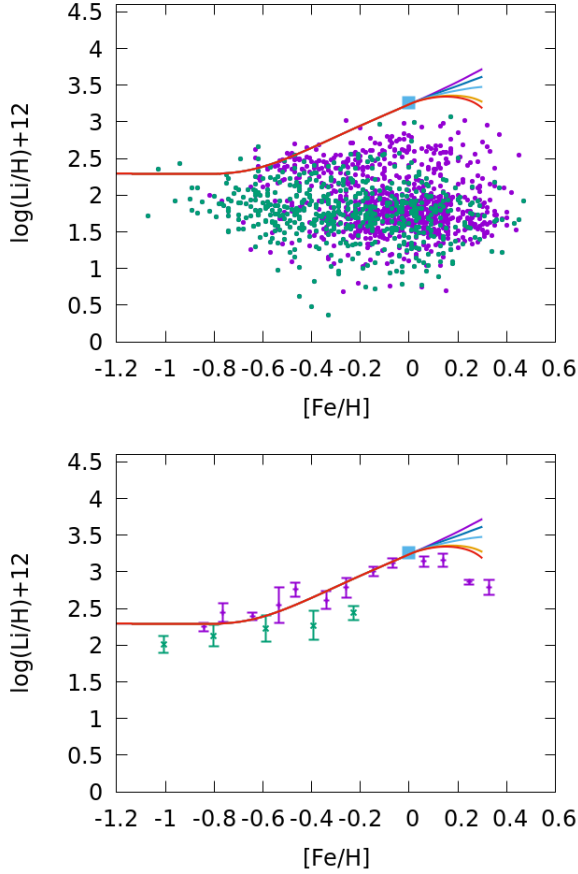


Figure 6.4: *Left panel*: Observed and predicted lithium abundance as a function of metallicity for the thin disc in the case with variable fraction of binary systems giving rise to novae. The predictions are from the parallel model for the thin disc with constant α (purple line) and with different variable α laws. The data are from Gaia-ESO Survey (Fu et al. 2018) for the thick disc stars (green dots) and thin disc stars (purple dots). The meteoritic value is the one by Lodders et al. (2009) (light-blue square). *Right panel*: same as the left panel, but with AMBRE data (Guiglion et al. 2016) for the thick disc stars (green dots) and thin disc stars (purple dots).

A dichotomy between thick and thin discs is observed also in the $A(\text{Li})$ vs. $[\text{Fe}/\text{H}]$ plane, as clearly shown by the data of Fu et al. (2018) and Guiglion et al. (2016) (Fig. 6.2, left-hand and right-hand panels, respectively) and has been studied by Prantzos et al. (2017) and Cescutti & Molaro (2019) by means of chemical evolution models.

Here, we consider the models of Grisoni et al. (2017, 2018) to explore this dichotomy between the thick and thin discs. In Fig. 6.2, we show our results. Since the evolution of the thin disc happens on relatively long timescales, novae can contribute to lithium enrichment in this Galactic component much more than they do in the thick disc, that is evolving at a quicker pace (see Table 6.1). With these models, we can reproduce the plateau at low metallicities, as well as the subsequent rise. In the lower panels of Fig. 6.2, we show the case when the contribution from massive stars is taken into account, while this contribution is suppressed in the model predictions displayed in the upper panels. We can see that for the thin disc the results remain almost unchanged, because of the overwhelming production from novae and GCRs. For the thick disc, instead, we get a mild enhancement since in this case we have a faster evolution and, hence, basically no contribution to Li enrichment from novae, but a higher number of contributing massive stars. In the following, when talking about the thin disc we will not take into account the contribution by massive stars since the results for this Galactic component remain almost unchanged (see also model B of Prantzos et al. 2012, as well as Cescutti & Molaro 2019 that do not take into account the contribution from massive stars in their models). In Fig. 6.3, we show the different contributions from the different lithium sources: all sources, novae, GCR and AGB/super-AGB. The figure is similar to Fig. 1 of Cescutti & Molaro (2019), and also in our case we can see that the main contribution comes from novae which are the main responsible for

the rise at $[\text{Fe}/\text{H}] \sim -0.6$ dex. In the following, we summarize the contribution from the various sources to the meteoritic lithium content. About 10% of the meteoritic ${}^7\text{Li}$ comes from primordial nucleosynthesis, after taking into account all factors affecting the evolution (and therefore also astration). Then, 16% is due to GCR. Therefore, more than 70% comes from stellar sources (in agreement with Prantzos 2012). In particular, novae represent our main source of lithium. Overall, from the analysis of the various lithium producers, we confirm that novae are a fundamental source of lithium in the Galaxy, in agreement with other previous studies (Romano et al. 1999, 2001, 2003; Matteucci 2010). In particular, they are the most important one (Izzo et al. 2015 and then also Cescutti & Molaro 2019).

The models discussed up to now can reproduce the plateau at low metallicity, as well as the rise at disc metallicities. However, they cannot reproduce the decrease at super-solar metallicities which, as recalled in the Introduction, has been claimed by recent observations, such as Gaia-ESO (Fu et al. 2018) and AMBRE (Guiglion et al. 2016). To reproduce this decrease, we assume that the fraction of binary systems giving rise to novae is no more constant, but it decreases at high metallicities, as suggested by the studies of Gao et al. (2014, 2017) and Yuan et al. (2015).

In Fig. 6.4, we show the predicted and observed lithium abundance as a function of metallicity, under different laws for the fraction of binary systems giving rise to novae, namely α , see Eq. (6.1). In the case with constant α , we considered $M_{\text{Li}} = 4.8 \cdot 10^{-10} M_{\odot}$ (maximum value from Izzo et al. 2015) and $\alpha = 0.017$ to reproduce the present time novae rate ($R_{\text{novae}} \sim 20 - 30 \text{ yr}^{-1}$; see also Izzo et al. 2015). Then, we consider variable α laws. In particular, we take for the mass produced by each nova $M_{\text{Li}} = 0.8 \cdot 10^{-10} M_{\odot}$ (also in the range measured by Izzo et al. 2015) and we assume that:

$$\alpha = \begin{cases} 0.1, & \text{if } [\text{Fe}/\text{H}] \leq 0 \\ 0.1 - \beta[\text{Fe}/\text{H}], & \text{if } [\text{Fe}/\text{H}] > 0 \end{cases} \quad (6.4)$$

where $\alpha(>0)$ is constant up to $[\text{Fe}/\text{H}]=0$ and then decreases linearly with metallicity. We test different β values ($\beta=0.1, 0.2, 0.3, 0.33$) and therefore different laws, as it can be seen in the figure. With this assumption, we get the plateau, the rise, and then also the bending which is due to the lower fraction of binary systems at the higher metallicities according to Eq. (6.4). We stress that, given the uncertainties involved in this kind of calculations, our results are qualitative, rather than quantitative. A better understanding of the formation and evolution of the nova systems is needed before we can work out a more refined model.

Other possible explanations that have been proposed for the decrease at high metallicities are: i) lower yields of Li from single stars at high metallicity (Prantzos et al. 2017), even if no physical justification for this fact can be found, and ii) the effect of radial migration of stars reflecting different evolutionary paths from the inner thin disc regions (Guiglion et al. 2019). Some uncertainties might be introduced by the Li depletion in the super-solar metallicity stars. Li depletion during the stellar evolution is the link between the ISM Li abundance and the current Li abundance measured in dwarf stars. It is expected to be small in principle. The two processes that are responsible for reducing the surface chemical abundances are microscopic diffusion and nuclear burning. The first mechanism takes the surface element to the base of the surface convective zone in a long timescale and is weakened with strong mixing. Fu et al (2018) show that main sequence diffusion in a 7-10 Gyr time reduces the surface Li abundance of a low mass solar metallicity star for $\lesssim 0.2$ dex. The latter process, with the reaction ${}^7\text{Li}(p, \gamma){}^4\text{He} + {}^4\text{He}$, burns

Li in the surface convective zone. Metal-poor and solar-metallicity main sequence stars ($M \gtrsim 0.7M_{\odot}$) have a very thin surface convective zone, even the bottom of the convective zone is not hot enough to burn Li efficiently. In contrast, super-solar metallicity stars have a relatively extended surface convective zone even during the main sequence and will eventually burn some Li. Unfortunately, standard stellar models are not applicable for Li evolution at super-solar metallicity though safe for the more metal-poor stars and most of the other elements. Standard stellar models homogenize the convective zone and treat it as a single radiative zone, thus the surface Li is erased almost immediately because of the high temperature at the base of the deep convective zone. In reality, the time scale of the nuclear reactions is comparable to the mixing time scale, Li burns in a mild temperature gradient during the convection. To quantitatively model Li evolution at this metallicity, new stellar models with the so-called "diffusive convection" is needed. Before the recent large Galactic surveys we discussed before, super-solar metallicity stars are rarely studied in the literature. Now it is the golden time to call for stellar models optimized for super-metallicity, and the new stellar modeling results will help to examine the nova rate law we use (Eq. (6.4)) in the Galactic chemical evolution models.

6.4.3 THE GALACTIC BULGE

Finally, we show also the results in the case of the Galactic bulge. The model for the Galactic bulge used here is the one by Matteucci et al. (2019), which assumes a fast formation on a short timescale and with high star formation efficiency ($\tau=0.1 \text{ Gyr}^{-1}$ and $\nu=25 \text{ Gyr}^{-1}$), and a flatter IMF with respect to the solar-vicinity, i.e. a Salpeter (1955) IMF instead of the Kroupa et al. (1993) one (see Table 6.1). This model reproduces the $[\text{Mg}/\text{Fe}]$ vs. $[\text{Fe}/\text{H}]$ relation, as well as the MDF of the bulge stars observed

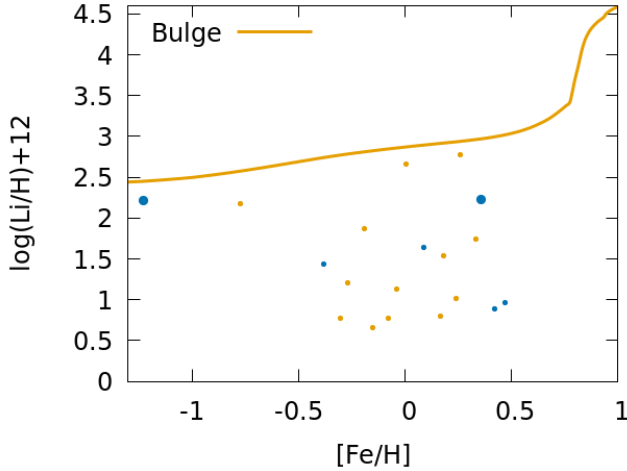


Figure 6.5: Observed and predicted lithium abundance as a function of metallicity in the Galactic bulge. The predictions are from the model of the Galactic bulge of Matteucci et al. (2019). The data of bulge stars are from Gonzalez et al. (2009) (orange dots) and Bensby et al. (2011) (blue dots, with the two bigger dots corresponding to the two stars which have $T_{eff} > 5900$ K).

by Gaia-ESO (Rojas-Arriagada et al. 2017) and APOGEE (Rojas-Arriagada et al. 2019), and it refers to the real bulge stars, i.e. the so-called "classical" bulge. In fact, in the Galactic bulge, there is the possibility of a different stellar population originating via secular evolution from the inner disc and cohabiting with the bulge stars formed in situ, although firm conclusions are still not reached. Here, we take into account only the classical bulge population, which should be the dominant one.

In Fig. 6.5, we show the predicted $A(\text{Li})$ vs. $[\text{Fe}/\text{H}]$ relation in the bulge in comparison to observations of bulge stars. In particular, we adopt the

data of Gonzalez et al. (2009) (orange dots) and Bensby et al. (2011) (blue dots, with the two bigger dots corresponding to the two stars which have $T_{eff} > 5900$ K). As regards to the model predictions, the Galactic bulge has evolved much faster than the disc and the contribution of novae appears at very high $[Fe/H]$, according to the time-delay model (Matteucci 2012). In agreement with previous studies (Matteucci et al. 1999, Romano et al. 1999), we predict that the present time Li abundance in the bulge is much higher than in the solar vicinity.

We can see that up to now the agreement between the classical bulge model and the bulge data is rather good, but more data will be necessary to draw firm conclusions about the evolution of lithium in the Galactic bulge.

6.5 CONCLUSIONS

In this work, we have studied the evolution of lithium in the Milky Way halo, discs and bulge. In particular, we have focused on the puzzling decrease of lithium at high metallicity. We considered the most recent observational data from Galactic stellar surveys and we compared the observations with our detailed chemical evolution models. The adopted models have been already tested on the evolution of the α -elements and Fe in the thick and thin discs (Grisoni et al. 2017, 2018), as well as the bulge (Matteucci et al. 2019).

Our main results can be summarized as follows.

- We confirm that novae are important sources of lithium, as pointed out by previous studies (D’Antona & Matteucci 1991; Romano et al. 1999, 2001, 2003; Matteucci 2010; Izzo et al. 2015). In particular, they are the most important source, in agreement with the recent results by Izzo et al. (2015, see their figure 5) and then also Cescutti

& Molaro (2019). These conclusions are supported by the Be and Li line identifications in nova ejecta by Tajitsu et al. (2015) and Izzo et al. (2015), respectively, that reinforced the idea that novae can be important sources of lithium.

- Concerning the decrease of Li at high metallicities in the thin disc, we propose a novel explanation. In particular, we show that this can be due to a lower fraction of binary systems giving rise to novae at high metallicities. This assumption of a metallicity dependent occurrence probability for this kind of systems is supported observationally by the studies of Gao et al. (2014, 2017) and Yuan et al. (2015), and it can be crucial to explain the decrease of lithium at high metallicities. Other alternative explanations that have been proposed in the literature to explain this feature by means of chemical evolution models are: i) lower yields of Li from stars at high metallicities, even if no physical reasons for this fact can be found (Prantzos et al. 2017); and ii) stellar migration of stars coming from the inner regions of the Milky Way disc (Guiglion et al. 2019).
- We also considered the lithium evolution in the Galactic bulge. In particular, we consider a model for the "classical" bulge as in Matteucci et al. (2019) with very high SFR compared to the other components, and we showed that the Galactic bulge has evolved much faster than the disc and the contribution of novae appears at very high $[\text{Fe}/\text{H}]$, according to the time-delay model (Matteucci 2012). In agreement with previous studies (Matteucci et al. 1999, Romano et al. 1999), we predict that the present time Li abundance in the bulge is much higher than in the solar vicinity. However, we still need further data to draw firm conclusions about lithium evolution in this Galactic component.

CHAPTER 7

Neutron capture elements

In this Chapter, I present the results on neutron capture elements, in particular Zr, La, Ce and Eu. The fundamental question that I would like to address here is: can we constrain the evolution of the Milky Way discs and bulge also looking at the abundance patterns of neutron capture elements? This Chapter is organized as follows. In Section 7.1, I give a general introduction about neutron capture elements. In Section 7.2, I describe the observational data which have been considered to compare with the predictions of our chemical evolution models. In Section 7.3, I present the models adopted in this work. In Section 7.4, I show our results, based on the comparison between observational data and model predictions. Finally, in Section 7.5, I draw the conclusions of this work. The results presented in this Chapter are described in the paper Grisoni et al. (2020).

7.1 INTRODUCTION

Another open question in Galactic Archaeology that still need to be answered by means of detailed theoretical models regards the chemical evolution of neutron capture elements.

Neutron capture reactions were proposed by Burbidge et al. (1957) and Cameron (1957) to explain the origin of elements beyond Fe. In fact, chemical elements heavier than Fe cannot be produced by exoenergetic fusion reactions in stars. Instead, they must be the result of neutron capture on Fe-peak nuclei. The neutron capture process can be rapid (r-process) or slow (s-process) with respect to the β -decay timescale. Correspondingly, these elements are called r- and s-process elements, according to which of these processes has contributed the most to the production at solar metallicity. For the s-process elements, the main production sites are suggested to be low-mass AGB stars in the mass range $1.5\text{--}3.0 M_{\odot}$ (Cristallo et al. 2009, 2011; Karakas 2010). AGB stars can produce all the neutron capture elements up to Pb and Bi; in this case, the main source of neutrons is the reaction $^{13}\text{C}(\alpha, n)^{16}\text{O}$. Massive stars can also produce neutron capture elements via s-process, but in this case the neutron flux is weaker and it comes from the reaction $^{22}\text{Ne}(\alpha, n)^{25}\text{Mg}$; this is called "weak s-process", and generally the weaker neutron flux does not allow to build up very heavy elements, but only elements up to the magic number 50, such as Sr, Y and Zr.

For the r-process elements, an extremely neutron-rich environment is required and in literature several production sites have been proposed. The recent detection of the gravitational wave transient GW170817 (Abbott et al. 2017) strongly supported neutron star mergers as production sites for r-process elements, but they might not be the only source of r-process elements (Côté et al. 2019, Simonetti et al. 2019 and Bonetti et al. 2019).

In literature, the first production sites proposed were core-collapse SNe (CC SNe) or electron-capture SNe (EC SNe) (Truran 1981; Cowan et al. 1991). However, Arcones et al. (2007) concluded that they do not have enough entropy and neutron fraction to have an efficient r-process activation. Thus, other production sites were suggested, such as neutron star mergers (NSM) (Rosswog et al. 1999) and magneto-rotationally driven SNe (MRD SNe) (Winteler et al. 2012; Nishimura et al. 2015).

From the point of view of Galactic chemical evolution models, Matteucci et al. (2014) have explored the Eu production from NSM versus CC SNe. They concluded that NSM may be responsible for the r-process enrichment in the Galactic halo whether totally or just in part, in a mixed scenario with both SN II and NSMs, giving a very short timescale for the merging after the formation of the neutron star binary (but see for example Schönrich & Weinberg 2019, which have allowed for a 2-phase ISM in order to solve this problem). Other studies have stated the importance of NSM in GCE models, but still NSM may not be the only source (Côté et al. 2019, Simonetti et al. 2019 and Bonetti et al. 2019). Similar studies with GCE have investigated the scenario with MRD SNe (Cescutti & Chiappini 2014) or the one with EC SNe (Cescutti et al. 2013). As regards to the s-process enrichment from GCE models, detailed studies were performed by Cescutti et al. (2006), Cescutti et al. (2013), Cescutti & Chiappini (2014) and Cescutti et al. (2015), and they outlined the importance of s-process driven by rotation in massive stars. In these works, the nucleosynthesis prescriptions of Frischnecht et al. (2012, 2016) were used. Moreover, Prantzos et al. (2018) took into account the nucleosynthesis prescriptions of Limongi & Chieffi (2018) (see Rizzuti et al. 2019 for a comparison between the yields of Frischnecht et al. 2016 and Limongi & Chieffi 2018 in GCE models). Besides classical GCE models, there have been also several works that have used hydrodynamical simulations to

study the r-process enrichment (see for example, Shen et al. 2015, van de Voort et al. 2015, and more recently Haynes & Kobayashi 2019).

From the observational point of view, many studies have recently presented the abundance patterns of neutron capture elements in the different Galactic components, i.e. the Galactic halo, thick and thin discs, and bulge (Delgado-Mena et al. 2017, Forsberg et al. 2019). In particular, these studies show that in the $[\text{Eu}/\text{Fe}]$ vs. $[\text{Fe}/\text{H}]$ diagram, it is possible to see two distinct sequences, corresponding to the thick and thin discs stars (similarly to the $[\alpha/\text{Fe}]$ vs. $[\text{Fe}/\text{H}]$, see Hayden et al. 2015), at variance with other abundance patterns where the different populations are mixed (e.g. in the case of Zr, La and Ce). By studying the abundance patterns of different populations of stars at different metallicities, it is possible to understand which processes played a major role in the production of these elements at a given moment of the history of formation and evolution our Galaxy, and Galactic chemical evolution models can shed light on that.

The aim of this work is to study the chemical evolution of neutron capture elements (in particular, Zr, La, Ce and Eu) by means of detailed chemical evolution models in the light of recent observational data from Forsberg et al. (2019). In particular, we consider the reference model of Grisoni et al. (2017) (see also Grisoni et al. 2018, 2019) for the Galactic thick and thin discs and the one of Matteucci et al. (2019) for the Galactic bulge; these models have been tested in order to reproduce the $[\alpha/\text{Fe}]$ vs. $[\text{Fe}/\text{H}]$ diagrams and MDFs, and now we apply them to study the chemical evolution of neutron capture elements in order to shed light on the recent data by Forsberg et al. (2019).

7.2 OBSERVATIONAL DATA

In this work, we use the data of Forsberg et al. (2019), where the chemical abundances of Zr, La, Ce, and Eu have been determined in 45 bulge giants

and 291 local disc giants from high-resolution optical spectra. The bulge spectra are obtained with the spectrometer FLAMES/UVES mounted on the VLT, Chile, with a resolution of $R \sim 47000$. Five bulge fields are investigated, namely SW, B3, BW, B6, and BL after the naming scheme in [Lecureur et al. \(2007\)](#). The majority of the bulge stars are from the programs 71.B-0617, 73.B-0074 (PI: [Renzini](#)), observed in the years 2001-2003. This sample has been used in many works determining several abundances ([Lecureur et al. 2007](#); [Zoccali et al. 2006, 2008](#); [Barbuy et al. 2013, 2015](#); [van der Swaelmen et al. 2016](#); [da Silveira et al. 2018](#)).

The bulk of the disc spectra in [Forsberg et al. \(2019\)](#) are obtained with the spectrometer FIES ([Telting et al. 2014](#)) at the Nordic Optical Telescope (NOT), La Palma (150 stars). Additional spectra were downloaded from the FIES archive (18 stars), added from [Thygesen et al. \(2012\)](#) (41 stars) and downloaded from the PolarBase data base ([Petit et al. 2014](#)) (19 stars). The PolarBase spectra are obtained with NARVAL and ESPaDOnS. The resolution of the disc spectra are $R \sim 67000$ (FIES) and $R \sim 65000$ (PolarBase). The disc sample has been separated into thick and thin disc components by using both chemistry and kinematics ([Lomaeva et al. 2019](#)).

The used wavelength region for abundance determination is restricted to that of the bulge spectra of 5800 Å- 6800 Å. The stellar parameters and abundances have been derived by fitting synthetic spectra using the code Spectroscopy Made Easy (SME, [Valenti & Piskunov 1996](#); [Piskunov & Valenti 2017](#)). The stellar parameters for the same stellar sample is determined in [Jönsson et al. \(2017a,b\)](#). In [da Silveira et al. \(2018\)](#), the comparison of stellar parameters given between [Zoccali et al. \(2006\)](#) and [Lecureur et al. \(2007\)](#), and the parameters derived in [Jönsson et al. \(2017a,b\)](#) is given.

The typical uncertainties on the determined abundances are around 0.08 dex for disc stars and 0.20 dex for bulge stars. For further details on the

Table 7.1: Input parameters for the chemical evolution models used in this work. In the first column, we indicate the name of the model. In the second column, there is the adopted initial mass function. In the third column, we indicate the star formation efficiency (ν). In the fourth column, we give the timescales for mass accretion (τ).

Model	IMF	ν [Gyr ⁻¹]	τ [Gyr]
Thin disc	Scalo (1986)	1.2	7
Thick disc	Scalo (1986)	2	0.1
Bulge	Salpeter (1955)	20	0.1

observational data and the determined abundances, we refer the reader to Forsberg et al. (2019), where there is also a detailed comparison with previous datasets present in the literature for the disc (Mishenina et al. 2013; Battistini & Bensby 2016; Delgado-Mena et al. 2017; Guiglion et al. 2018) and the bulge (Johnson et al. 2012; van der Swaelmen et al. 2016; Duong et al. 2019).

7.3 THE MODELS

In this Section, we present the chemical evolution models used in this work. To follow the evolution of the Galactic thick and thin discs, we adopt the parallel approach (Chiappini 2009; Grisoni et al. 2017,2019; Cescutti & Molaro 2019). In this approach, we consider that the thick and the thin disc formed by means of two distinct infall episodes and evolve separately. The model adopted here was developed for the solar neighborhood in Grisoni et al. (2017), and also tested for the other Galactocentric distances in Grisoni et al. (2018). For the Galactic bulge, we adopt the reference model of Matteucci

et al. (2019), which considers a very short timescale of formation, higher star formation efficiency and flatter initial mass function (IMF) than the solar vicinity. These assumptions are required in order to reproduce the observed MDF of bulge stars, as first suggested by Matteucci & Brocato (1990) and then confirmed also by subsequent theoretical studies (Ballero et al. 2007; Cescutti & Matteucci 2011; Grieco et al. 2012; Cescutti et al. 2018; Matteucci et al. 2019). This corresponds to the so-called "classical bulge", but there can be other stellar populations coming via secular evolution from the inner disc (for a review on the chemodynamical evolution of the bulge, Barbuy et al. 2018 and references therein). The three Galactic components considered in this work thus differ by the different assumed IMF, timescales of gas accretion and efficiencies of star formation (see Table 1 for details). These assumptions have already been tested in previous works in order to reproduce the main observational features, such as the $[\alpha/\text{Fe}]$ vs. $[\text{Fe}/\text{H}]$ diagrams and MDF of disc stars (Grisoni et al. 2017, 2019) and bulge stars (Matteucci et al. 2019).

7.3.1 MODEL EQUATIONS

The fundamental equations that describe the evolution with time of the mass fraction of the element i in the gas G_i are Eq. (2.8).

The SFR is parametrized according to the Schmidt-Kennicutt law (Kennicutt 1998a). The parameter ν is the star formation efficiency, which is fixed in order to reproduce the present time SFR in the considered Galactic components; in particular, for the Galactic bulge ν is very high compared to the ones of the thick and thin discs (see Table 7.1). For the IMF, we adopt the Scalo (1986) IMF for the Galactic thick and thin discs, and the Salpeter (1955) IMF for the Galactic bulge (in fact, the IMF for the bulge should be flatter than the one adopted for the solar neighbourhood, see Matteucci et

al. 2019).

We account for detailed nucleosynthesis prescriptions from low and intermediate mass stars, Type Ia SNe (originating from white dwarfs in binary systems) and Type Ib, Ic and II SNe (originating from core-collapse massive stars). In this work, we consider also the contribution from NSM, which are fundamental europium producers.

The gas accretion rate is given by Eq. (2.12) for the bulge, and Eq. (3.2) and Eq. (3.3) for the thick and thin discs, respectively. The parameter τ represents the timescale for mass accretion in each Galactic component (see Table 7.1). These timescales are free parameters of the model and they are constrained mainly by comparison with the observed metallicity distribution function of long-lived stars in the solar vicinity. The quantity $A(r)$, $B(r)$ and $C(r)$ involved in these equations are parameters fixed by reproducing the total surface mass density at the present time in the considered Galactic component. We follow the prescriptions of Grisoni et al. (2017) for the Galactic discs and Matteucci et al. (2019) for the Galactic bulge.

7.3.2 NUCLEOSYNTHESIS PRESCRIPTIONS

7.3.2.1 YIELDS OF Zr, La AND Ce

Zr, La and Ce are produced by both the r- and s- processes.

The r-process yields are obtained by scaling the Eu yields according to the abundance ratios observed in r-process rich stars (Snedden et al. 2008).

Low-mass AGB stars in the mass range $1.3\text{--}3\text{ M}_{\odot}$ are responsible for most of the s-process, and the corresponding yields are taken from the database FRUITY (FULL-Network Repository of Updated Isotopic Tables & Yields, Cristallo et al. 2009, 2011).

Then, we assume also the s-process contribution from rotating massive stars. This has been first considered by Cescutti et al. (2013), Cescutti

& Chiappini (2014) and Cescutti et al. (2015) by taking into account the nucleosynthesis prescriptions of Frischknecht et al. (2012). Here, we consider the nucleosynthesis prescriptions of Frischknecht et al. (2016) for rotating massive stars.

7.3.2.2 YIELDS OF EU

For Eu, we consider NSM as fundamental production sites, as mentioned in the Introduction. To include the production of Eu from NSM in the Galactic chemical evolution models, we need to define the following quantities (see Matteucci et al. 2014, Cescutti et al. 2015 for further details):

- the fraction of massive stars belonging to double neutron star systems that will eventually merge, or in other words the realization probability of such events (α_{NSM});
- the time delay between the formation of the double neutron star system and the merging (Δt_{NSM});
- the amount of Eu produced during the merging (M_{NSM}^{Eu}).

Concerning NSM yields, we follow the prescriptions of Matteucci et al. (2014) and Cescutti et al. (2015); in particular, we assume a value of $2 \cdot 10^{-6} M_{\odot}$ which is in agreement with the range of yields of Korobkin et al. (2012) who suggest that NSM can produce from 10^{-7} to $10^{-5} M_{\odot}$ of Eu per event.

We assume that a fixed fraction of all the massive stars is a progenitor of NSM and produces r-process material. The progenitors are randomly chosen among the massive stars formed in the stellar mass range $10\text{-}30 M_{\odot}$. The parameter α_{NSM} is taken equal to 0.05, in order to reproduce the present time rate of NSM in the Galaxy as given by Kalogera et al. (2004)

($R_{NSM}=83^{+209}_{-66}\text{Myr}^{-1}$). The recent observations of the rate for the event GW170817 seem to confirm this result (Simonetti et al. 2019, and references therein).

For the time delay due to the coalescence of the two neutron stars, it is fixed and equal to 1 Myr as in Matteucci et al. (2014) and Cescutti et al. (2015) (which is very short, but see Schönrich & Weinberg 2019, Haynes & Kobayashi 2019 for more discussion). It is worth noting also that here it is assumed that all neutron star binaries have the same coalescence time, but a more realistic approach would consider a distribution function of such timescales, in analogy with SNIa for which a distribution for the explosion time is defined (see Simonetti et al. 2019). The aforementioned assumptions on NSM are probably extreme concerning the short and constant merging timescale, but they reproduce very well the $[\text{Eu}/\text{Fe}]$ vs. $[\text{Fe}/\text{H}]$ plot in the solar neighbourhood. On the other hand, both Matteucci et al. (2014) and Cescutti et al. (2015) have demonstrated that they can obtain a good agreement with the data also by assuming CC SNe producing Eu at early times and larger merging timescales.

In the model, Eu is produced also by the main s-process, but this is only the 5% and therefore NSM remain the main source of Eu.

7.3.2.3 YIELDS OF FE

Finally, the iron yields are the ones of Kobayashi et al. (2006) for CC SNe and Iwamoto et al. (1999) for SNIa.

7.4. COMPARISON BETWEEN DATA AND MODEL PREDICTIONS

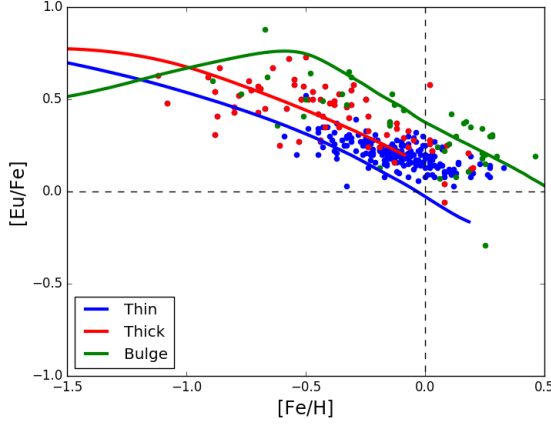


Figure 7.1: Observed and predicted $[\text{Eu}/\text{Fe}]$ vs. $[\text{Fe}/\text{H}]$. The predictions are from the reference models for the Galactic thin disc (blue line), thick disc (red line) and bulge (green line). The data are for the Galactic thin disc stars (blue dots), thick disc stars (red dots) and bulge stars (green dots), and they are taken from Forsberg et al. (2019).

7.4 COMPARISON BETWEEN DATA AND MODEL PREDICTIONS

In this Section, we show our results based on the comparison between model predictions and observations for the various Galactic components: thick disc, thin disc and bulge. In Table 7.1, the input parameters of the different models are listed. In the first column, there is the name of the model. Then, we indicate the adopted IMF, the star formation efficiency (ν) and the timescale of formation (τ) of the Galactic components.

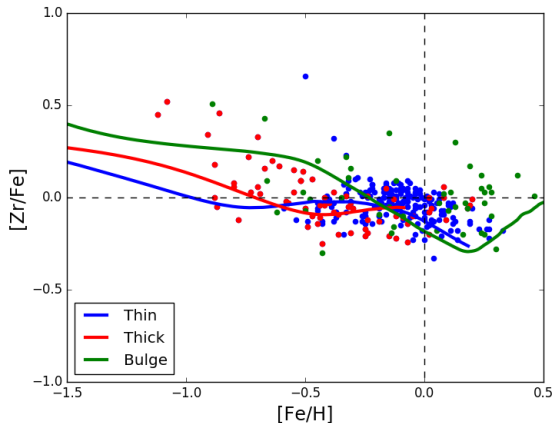


Figure 7.2: Same as Fig. 7.1, but for Zr.

7.4.1 COMPARISON FOR EU

In Fig. 7.1, the observed and predicted $[\text{Eu}/\text{Fe}]$ vs. $[\text{Fe}/\text{H}]$ plot is shown in the range $-1.5 < [\text{Fe}/\text{H}] < 0.5$ dex. The trend shows a plateau at $[\text{Fe}/\text{H}] < -0.6$ dex and then a decrease with metallicity, and we can see that there are three distinct sequences in this diagram, corresponding to the three main Galactic components: thick disc, thin disc and bulge. The bulge is Eu-enhanced with respect to the disc (thick + thin). The bulge abundances are indeed higher than the thin disc, but it is fairly hard to tell if the bulge is higher in abundance than the thick disc due to the larger scatter in the bulge data (Forsberg et al. 2019). As regards to the disc, it clearly shows a dichotomy between the thick and thin disc stars, with the thick disc been Eu-enhanced with respect to the thin disc. The models can nicely reproduce the observations, by assuming different timescales of formation and star

7.4. COMPARISON BETWEEN DATA AND MODEL PREDICTIONS

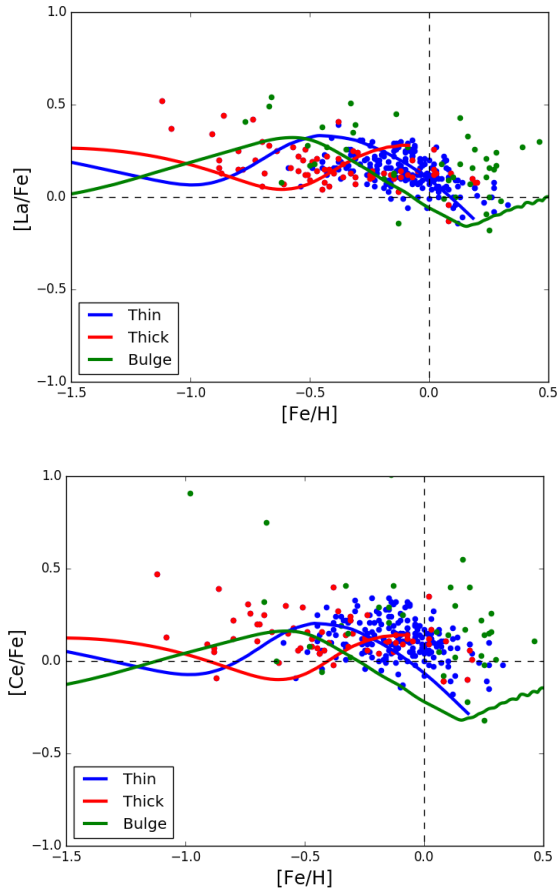


Figure 7.3: Same as Fig. 7.1, but for La and Ce.

formation efficiencies in the three Galactic components. In particular, the bulge has formed on a short timescale of formation and with high star formation efficiency, and the thick disc has a shorter timescale of formation and higher star formation efficiency than the thin disc (see Table 7.1). The adopted input parameters were previously tuned in order to reproduce the observed $[\alpha/\text{Fe}]$ vs. $[\text{Fe}/\text{H}]$ and MDFs for the Galactic thick and thin discs (Grisoni et al. 2017) and for the Galactic bulge (Matteucci et al. 2019). Now, we see that these parameters can nicely fit also the $[\text{Eu}/\text{Fe}]$ vs. $[\text{Fe}/\text{H}]$ relation.

The model for the Galactic thin disc correctly reproduces the solar value, as expected. Regarding the solar value, the observational data seem to be overestimated. In Forsberg et al. (2019), it is indeed noted that the Eu (as well as the La and the Ce) abundances might suffer from systematic errors, causing an overestimation in abundances. Their differential comparison of the disc and bulge components are therefore not affected directly by the overestimation, but should be considered when comparing to our models.

Moreover, we note that the observed $[\text{Eu}/\text{Fe}]$ vs. $[\text{Fe}/\text{H}]$ in the thin disc flattens at high metallicities (see also Delgado-Mena et al. 2017). This could be due to radial migration (Schönrich & Binney 2009; Minchev et al. 2013, 2018; Spitoni et al. 2015) from the inner disc, similarly to what happens in the $[\text{Mg}/\text{Fe}]$ vs. $[\text{Fe}/\text{H}]$ plot (Grisoni et al. 2017). Recently, the importance of radial migration in shaping also the r-process abundance pattern has been investigated by Tsujimoto & Baba (2019).

Concerning the Galactic thick disc, it is characterized by a more intense star formation history than the thin disc. There is a faster evolution, with a stronger efficiency of star formation ($\nu=2 \text{ Gyr}^{-1}$) and shorter timescale of gas infall ($\tau=0.1 \text{ Gyr}$). The chemical evolution of the thick disc lasts for 2 Gyr, but with minimal star formation after approximately 1.2 Gyr. Thus,

7.4. COMPARISON BETWEEN DATA AND MODEL PREDICTIONS

the model predictions for the thick discs stop at $[\text{Fe}/\text{H}] \sim -0.1$ dex. Overall, the predictions for the thick disc lie above the ones for the thin disc, and this is due to the much faster evolution.

A first attempt to reproduce the distinct sequences in the $[\text{Eu}/\text{Fe}]$ vs. $[\text{Fe}/\text{H}]$ plot has been performed in Delgado-Mena et al. (2017) by means of the chemical evolution models of Bisterzo et al. (2017). In that case, the data for the thin disc were nicely reproduced, but the predictions for the thick disc were underestimated with respect to the ones of the thin disc, at variance with the observations. In order to correctly reproduce the observed dichotomy between the thick and thin disc stars, we need to assume that the thick disc formed with a shorter timescale of formation and higher star formation efficiency than the thin disc. Moreover, here we present the predictions of the $[\text{Eu}/\text{Fe}]$ vs. $[\text{Fe}/\text{H}]$ in the Galactic bulge.

Concerning the Galactic bulge, here we consider the model of Matteucci et al. (2019), which assumes an even faster and more efficient evolution ($\nu=20 \text{ Gyr}^{-1}$, $\tau=0.1 \text{ Gyr}$) and a flatter IMF (Salpeter 1955) with respect to the solar vicinity. This model reproduces the $[\alpha/\text{Fe}]$ vs. $[\text{Fe}/\text{H}]$ diagram and MDF of bulge stars, and it corresponds to the so-called "classical bulge". However, in the Galactic bulge there is the possibility of another stellar populations originating via secular evolution from the inner disc and coexisting with the bulge stars formed in situ, but firm conclusions are still not reached at this point. Here, we consider only the classical bulge population, which should be the dominant one. Due to its faster and more efficient formation, the track for the Galactic bulge is Eu-enhanced with respect to the thick and thin discs. However, we notice that the predicted $[\text{Eu}/\text{Fe}]$ at $[\text{Fe}/\text{H}]=-1.5$ dex starts from a lower value than the other Galactic components, but then the track rises and then it decreases with metallicity being Eu-enhanced with respect to the other Galactic components. The knee is thus shifted

towards higher metallicities with respect to the thick and thin discs, and this can be explained in terms of the so-called time-delay model (Matteucci 2012). In fact, the bulge forms on a shorter timescale of formation and with a higher star formation efficiency than the other Galactic components, and therefore its knee is shifted towards higher metallicities.

In summary, by assuming different star formation histories which have already allowed us to reproduce the abundance patterns of the α -elements in the Galactic thick and thin discs (Grisoni et al. 2017) and bulge (Matteucci et al. 2019), we can nicely reproduce the three sequences also in the $[\text{Eu}/\text{Fe}]$ vs. $[\text{Fe}/\text{H}]$ plot.

7.4.2 COMPARISON FOR ZR, LA AND CE

Now, we present the results for the other chemical elements of this study, i.e. Zr, La and Ce.

In Fig. 7.2 and Fig. 7.3, we show the observed and predicted $[\text{X}/\text{Fe}]$ vs. $[\text{Fe}/\text{H}]$ for Zr, La and Ce. As explained in Section 3.2, these chemical elements are produced by both the s- and r- processes, and they show a different abundance pattern than Eu. In particular, the predominant s-process fraction of these elements is produced by long-lived stars (1.5-3.0 M_{\odot}). This fact, coupled with the secondary nature (dependence on metallicity) of s-process elements creates the observed behaviour. Moreover, Zr is a first-peak s-process element, whereas La and Ce are second-peak s-process elements, and indeed the predictions for Zr are slightly different than the ones for La and Ce, which show a more similar behaviour. In these diagrams, the three stellar populations (thin disc, thick disc and bulge) are mixed, and it is more difficult to disentangle the different behaviours. However, we can see that the general behaviour of the observational data for each Galactic component is reproduced by the models, with the thin

disc showing a decrease with increasing $[\text{Fe}/\text{H}]$, at variance with the bulge that shows a slight increase at higher metallicities, whereas the thick disc represents an intermediate case. The different behaviours of the s-process elements in the bulge is due to the time-delay model. In fact, it has a regime of high star formation rate and thus the curve for the thick disc should be shifted towards right in the $[\text{s}/\text{Fe}]$ vs. $[\text{Fe}/\text{H}]$ plot. Also in this diagrams, assuming different timescales of formation and star formation efficiencies can lead to different behaviours in the abundance patterns, even if the different populations are mixed and it is more difficult to disentangle the different patterns at variance with the $[\text{Eu}/\text{Fe}]$ vs. $[\text{Fe}/\text{H}]$ plot where three distinct sequences are evident.

In conclusion, also looking at the abundance patterns of neutron capture elements in the Milky Way discs and bulge can help in constraining the history of formation and evolution of these three Galactic components.

7.5 CONCLUSIONS

In this work, we have studied the chemical evolution of Zr, La, Ce and Eu in the Galactic discs and bulge by means of detailed Galactic chemical evolution models compared with the recent data by Forsberg et al. (2019). The main conclusions of this work can be summarized as follows.

- In the $[\text{Eu}/\text{Fe}]$ vs. $[\text{Fe}/\text{H}]$ plot, we observe and predict three distinct sequences, corresponding to the Galactic thick disc, thin disc and bulge (similarly to what happens in the $[\alpha/\text{Fe}]$ vs. $[\text{Fe}/\text{H}]$ plot, see Grisoni et al. 2017, Matteucci et al. 2019).
- The three sequences in the $[\text{Eu}/\text{Fe}]$ vs. $[\text{Fe}/\text{H}]$ plot are reproduced by assuming three different star formation histories for these Galactic components, with the bulge forming on a shorter timescale of formation

and with higher star formation efficiency than the discs. Moreover, the thick and thin discs show a clear dichotomy, with the thick disc forming faster than the thin one, in agreement with the results of Grisoni et al. (2017).

- The assumed timescales of gas infall and star formation efficiencies have been previously tuned to reproduce the $[\alpha/\text{Fe}]$ vs. $[\text{Fe}/\text{H}]$ plots and the MDFs of the thick and thin discs (Grisoni et al. 2017) and bulge (Matteucci et al. 2019), and they allow us to nicely reproduce also the $[\text{Eu}/\text{Fe}]$ vs. $[\text{Fe}/\text{H}]$ plot.
- On the other hand, we observe and predict a different behaviour for the $[\text{X}/\text{Fe}]$ vs. $[\text{Fe}/\text{H}]$ plots of Zr, La and Ce. This is due to the double nature of these elements, which are produced by either the s- and r- processes. In fact, Zr, La and Ce are mainly produced as s-process elements by low mass stars ($1.5\text{-}3.0 M_{\odot}$) and only partly as r-process. As it is well known, the s-process elements behave as secondary elements. This fact, coupled with the long timescale of their production, produce the increase with metallicity followed by a decline.
- In the $[\text{X}/\text{Fe}]$ vs. $[\text{Fe}/\text{H}]$ plots for Zr, La and Ce, the three stellar populations are mixed and it is more difficult to disentangle them. However, the general behaviour of the observational data also in this case can be reproduced by the models and interpreted in terms of the time-delay model.

In conclusion, in addition to the study of the abundance patterns of α -elements in the Galactic discs and bulge, also looking at the abundance

patterns of neutron capture elements can help in constraining the history of formation and evolution of these three Galactic components.

Final remarks

The aim of this Thesis has been to study the formation and chemical evolution of the Milky Way by means of detailed chemical evolution models in the light of the most recent data from Galactic surveys and missions. First, I focused on modelling the chemical evolution of the Galactic thick and thin discs in the solar neighbourhood. Secondly, I extended my analysis also to the other Galactocentric distances and investigated abundance gradients along the Galactic thin disc. Then, I worked on modelling the chemical evolution of the Galactic bulge. Finally, I applied the models developed to investigate the chemical evolution, from lithium to europium. In the following Sections, I summarize the main results of this Thesis and outline future perspectives of this work.

8.1 SUMMARY AND CONCLUSIONS

CHEMICAL EVOLUTION OF THE THICK AND THIN DISCS

First, I studied the formation and evolution of the Milky Way thick and thin discs on the basis of detailed chemical evolution models to compare with the recent AMBRE [Mg/Fe] vs. [Fe/H] (Mikolaitis et al. 2017).

In particular, I explored two different approaches for modelling Galactic chemical evolution: the two-infall and the parallel approach. In the two-infall scenario, the Galaxy formed by means of two infall episodes: during the first one, the thick disc formed whereas the second one gave rise to the thin disc. On the other hand, the parallel scenario assumes that the various Galactic components started forming at the same time but at different rates.

The best models have been selected after performing several numerical simulations by varying one at the time the most important input parameters. The input parameters of the best models are: $\tau_1=0.1$ Gyr for the timescale of formation of the thick disc and $\tau_2=7$ Gyr for the timescale of formation of the thin disc, $\nu_1=2$ Gyr⁻¹ for the star formation efficiency of the thick disc and $\nu_2=1$ Gyr⁻¹ for the star formation efficiency of the thin disc, $\sigma_{th}=7$ M_⊙pc⁻² for the assumed threshold in the star formation rate, and a Kroupa et al. (1993) IMF.

The main conclusions are as follows.

- As regard to the abundance patterns, I focused on the α -element for which there is a clear distinction between thick and thin disc stars. The two-infall model can reproduce the thick and thin disc stars, but not the MRHA stars; in this scenario, the only way to explain the MRHA stars is by assuming that these stars have migrated from the inner thin disc. On the other hand, the parallel model treats the thick and thin discs as two truly distinct and parallel evolutionary phases

and so there are two distinct tracks in the abundance pattern. With the parallel model, it is possible to reproduce the MRHA stars as the metal rich thick disc stars, since in the parallel approach the thick disc can extend up to high $[\text{Fe}/\text{H}]$, at variance with the two-infall sequential model.

- For the metallicities distribution functions, the two-infall model can reproduce the MDF of the thick and thin disc stars, whereas it cannot reproduce the MRHA stars. On the other hand, with the parallel model the MDF of the thick disc is very broad and includes also the MRHA stars. The MDF represents a fundamental constraint for chemical evolution models because it is strongly dependent on the mechanism of disc formation. In particular, for the best models in the parallel scenario the timescale for the formation of the thick disc is equal to 0.1 Gyr, whereas the timescale for the formation of the thin disc at solar position is much longer and it is equal to 7 Gyr. Both these timescales are dictated by reproducing the MDF of each Galactic component.
- Concerning the solar abundances, the predictions of all models are in reasonable agreement with the observations of Grevesse et al. (2007), but for Mg the canonical yields from massive stars had to increase by a factor 1.2.
- The predicted present-time SFR is $\psi_0 = 2.7 \text{ M}_\odot \text{ pc}^{-2} \text{ Gyr}^{-1}$ (for the two-infall model) and $\psi_0 = 2.4 \text{ M}_\odot \text{ pc}^{-2} \text{ Gyr}^{-1}$ (for the one-infall model of the thin disc), both in good agreement with observations. The predicted present-time SNII rate is 1.4 century^{-1} (for the two-infall model) and 1.2 century^{-1} (for the one-infall model of the thin disc),

whereas the predicted present-time SNIa rate is 0.3 century^{-1} (for the two-infall model) and 0.3 century^{-1} (for the one-infall model of the thin disc), in good agreement with the observations.

- In the two-infall approach, there is a gap in star formation between the thick and thin disc formation of several hundreds of Myr (~ 700 Myr), at variance with the parallel approach where no gap is present.

To summarize, a sequential approach like the one of the two-infall model can reproduce the chemical properties of thick and thin disc stars, but not those of the MRHA stars; in this case, these stars can be explained only by stellar migration from the inner disc. On the other hand, in order to reproduce the chemical properties of the MRHA stars without invoking stellar migration, it is better to consider a parallel scenario where the evolution of the thick and thin discs are separated; in this way, the MRHA stars can be interpreted as metal rich thick disc stars. In particular, the parallel approach can be very useful to follow the evolution of the Galactic thick and thin discs separately, to explore the dichotomy between the two discs in different abundance patterns.

Finally, asteroseismology has become a fundamental tool to constrain chemical evolution models. In Spitoni et al. (2019), we have pointed the importance of a consistent delay in the beginning of the second gas accretion episode as a crucial assumption to reproduce stellar abundances and ages (see also Noguchi 2018). Vincenzo et al. (2019) has interpreted this feature in relation to the chemical evolution of Gaia-Enceladus (or Gaia sausage). Further data from asteroseismology will help in shedding light on this.

ABUNDANCE GRADIENTS ALONG THE GALACTIC DISC

Then, I extended the analysis also to the other Galactocentric distances. I investigated the formation and chemical evolution of the Milky Way discs with particular focus on the abundance patterns at different Galactocentric distances, the present-time abundance gradients along the disc and the time evolution of abundance gradients. I considered the recently developed chemical evolution models by Grisoni et al. (2017) for the solar neighbourhood, both the two-infall and the one-infall, and I extended the analysis to the other Galactocentric distances, also implementing radial gas flows in the code for this purpose. In particular, I examined the processes which mainly influence the formation of abundance gradients: i) the inside-out scenario for the formation of the Galactic thin disc, ii) a variable star formation efficiency, and iii) radial gas flows along the Galactic disc.

The main conclusions are as follows.

- As regard to the abundance patterns (in particular $[\text{Mg}/\text{Fe}]$ vs. $[\text{Fe}/\text{H}]$) at different Galactocentric distances, the inside-out scenario for the thin disc is a key element, but provides only a slight difference between the various tracks at different radii and so it is not sufficient to explain the data at various radii. In order to have a more significant spread among the various tracks, further ingredients are needed, such as a variable star formation efficiency or radial gas flows: the variable star formation efficiency produces a spread at lower metallicities, whereas the radial gas flows become significant at higher ones. The case with a variable star formation efficiency provides a very good agreement with the observational data, in particular for the outer radii. However, none of the models can reproduce $[\text{Mg}/\text{Fe}]$ at high $[\text{Fe}/\text{H}]$, and this can be due to a general problem in our understanding of Mg production (as

also pointed out by Romano et al. 2010; Magrini et al. 2017).

- Also concerning the present-day abundance gradients along the Galactic thin disc, the inside-out scenario provides a too flat gradient and cannot explain the observational data, neither of Cepheids, young OCs, young PNe and HII regions which show a steeper gradient. To recover the steeper gradient, the variable star formation efficiency or radial gas flows are needed; we note that the former looks consistent with the Mg gradient, while the latter looks consistent with the O gradient.
- On the other hand, for the time evolution of abundance gradients, the model with the variable star formation efficiency provides a good agreement with the observational data at recent times, but it predicts a steeper behaviour at earlier times which is not present in the data. To reproduce a flatter gradient at earlier times, we should rather consider the models with constant star formation efficiency or we would need radial migration, more efficient for the older populations. Thus, what we are observing is a gradient flattened by radial migration, and not the original one (see for instance Magrini et al. 2016). With the two-infall model, we can even get an evident gradient inversion at high redshift, when the efficiency of star formation is constant.
- The Galactic thick disc formed on a very short timescale ($\tau_1 = 0.1$ Gyr, see Grisoni et al. 2017), which is assumed to be constant with radius. Therefore, there is no inside-out scenario for the thick disc, in agreement with Haywood et al. (2018).

In summary, we conclude that the inside-out scenario is a key ingredient for the formation of Galactic discs, but cannot be the only one to explain

abundance patterns at different Galactocentric distances and abundance gradients. Further ingredients are needed, such as a variable star formation efficiency and radial gas flows; in particular, we note that the former looks consistent with the Mg gradient, while the latter looks consistent with the O gradient. The flattening or steepening of gradients in time is due to the fact that the gas chemical evolution is very sensitive to the prescriptions of the physical processes that lead to the enrichment of inner and outer discs, mainly to the constancy or variability of the star formation efficiency. Therefore, different recipes of the star formation process or gas accretion mechanisms can provide very different predictions for the abundance gradients, as we have shown in this work. Also radial migration could have an effect, although it has been shown that this may not be a large factor for stars in the Milky Way (Di Matteo et al. 2013; Kubryk et al. 2013; Bovy et al. 2014).

CHEMICAL EVOLUTION OF THE GALACTIC BULGE

Moreover, I investigated the formation and chemical evolution of the Galactic bulge with particular focus on the abundance patterns ($[\text{Mg}/\text{Fe}]$ vs. $[\text{Fe}/\text{H}]$), metallicity distribution function and age distribution. I considered detailed chemical evolution models for the Galactic bulge and inner disc, with the aim of shedding light on the formation and evolution of the bulge. In particular, I try to establish if the data can be reproduced by two distinct stellar populations, one metal poor and the other metal rich, and to assess their origin. I explore two main possibilities: i) the two populations have been born in the bulge separated by a period of a stop in the star formation, ii) the MP population was born in the bulge while the MR was formed in the inner disc. I also explore the case of multiple populations born in separate star formation episodes, as suggested by Bensby et al. (2017). In all the studied cases, except this last one, the MP population forms very

quickly (less than 500 Myr) and with high star formation efficiency (25 Gyr^{-1}). The same prescriptions are adopted for the MR one if we assume that it is born in the bulge after a halt in the star formation process. On the other hand, in the multiple burst case the efficiency of star formation during different episodes is assumed to be much lower (from 1 to 3 Gyr^{-1}) and the bulge formed on a much longer timescale (several Gyrs). Finally, in the case where MR population is formed by inner disc stars, the efficiency of star formation is low and typical of the thin disc (1 Gyr^{-1}).

After comparing model predictions and observational data, the main conclusions can be summarized as follows:

- Models with two main stellar populations in the bulge best fit the most recent data from Gaia-ESO and APOGEE.
- In particular, if the two populations have formed as a result of a stop in the star formation of $\sim 250 \text{ Myr}$, occurred at early times, one can reproduce the MDF, the $[\text{Mg}/\text{Fe}]$ ratios and the age distribution of bulge stars. However, this scenario could be inconsistent with stellar kinematics suggesting that the MR stars are belonging to the B/P X-shaped structure of the bulge, whereas the MP stars are distributed isotropically (Zoccali et al. 2017), although other studies (Debattista et al. 2017; Buck et al. 2017) do not exclude the possibility of explaining the X-shape only with stars formed in situ.
- Another possible explanation can be that the metal rich population originates by secular evolution from the inner disc.
- The flattening of the $[\text{Mg}/\text{Fe}]$ ratio at high metallicity in the last APOGEE data could be reproduced by assuming a larger Mg production from SNe Ia. However, this flattening is not present in all the

existing bulge data and therefore we cannot draw firm conclusions on this point.

- The assumed Salpeter IMF can well reproduce the data, and the results differ negligibly from those obtained with Calamida et al. (2015) IMF derived for the bulge.
- The results of a multiple burst regime with the bursts occurring from 3 to 12 Gyr ago, as suggested by Bensby et al. (2017), can roughly reproduce their data but is in conflict with all the other data and predict a large fraction of young bulge stars which is not found in the majority of the other studies. In addition, a multiple burst scenario is also inconsistent with the kinematical information.
- Therefore, we conclude that the bulge overall is old and that both the MP and MR populations contain very old stars. The young stars (10 % with ages < 5 Gyr) belong either to the inner disc stars or they have formed in situ after a stop in star formation no longer than 250 Myr. The bulge formed the majority of its stars in the first 0.5 Gyr of its evolution, in agreement with most of the previous studies (Matteucci & Brocato 1990; Ballero et al. 2007; Cescutti & Matteucci 2011; Grieco et al. 2012).

GALACTIC LITHIUM EVOLUTION

Once the reference models of the main Galactic components have been developed, I studied the evolution of lithium in the Milky Way halo, discs and bulge. In particular, I focused on the puzzling decrease of lithium at high metallicity. I considered the most recent observational data from Galactic stellar surveys and I compared the observations with detailed chemical

evolution models. The adopted models have been already tested on the evolution of the α -elements and Fe in the thick and thin discs (Grisoni et al. 2017, 2018), as well as the bulge (Matteucci et al. 2019).

The main results can be summarized as follows.

- We confirm that novae are important sources of lithium, as pointed out by previous studies (D’Antona & Matteucci 1991; Romano et al. 1999, 2001, 2003; Matteucci 2010; Izzo et al. 2015). In particular, they are the most important source, in agreement with the recent results by Izzo et al. (2015, see their figure 5) and then also Cescutti & Molaro (2019). These conclusions are supported by the Be and Li line identifications in nova ejecta by Tajitsu et al. (2015) and Izzo et al. (2015), respectively, that reinforced the idea that novae can be important sources of lithium.
- Concerning the decrease of Li at high metallicities in the thin disc, we propose a novel explanation. In particular, we show that this can be due to a lower fraction of binary systems giving rise to novae at high metallicities. This assumption of a metallicity dependent occurrence probability for this kind of systems is supported observationally by the studies of Gao et al. (2014, 2017) and Yuan et al. (2015), and it can be crucial to explain the decrease of lithium at high metallicities. Other alternative explanations that have been proposed in the literature to explain this feature by means of chemical evolution models are: i) lower yields of Li from stars at high metallicities, even if no physical reasons for this fact can be found (Prantzos et al. 2017); and ii) stellar migration of stars coming from the inner regions of the Milky Way disc (Guiglion et al. 2019).

- We also considered the lithium evolution in the Galactic bulge. In particular, we consider a model for the "classical" bulge as in Matteucci et al. (2019) with very high SFR compared to the other components, and we showed that the Galactic bulge has evolved much faster than the disc and the contribution of novae appears at very high $[\text{Fe}/\text{H}]$, according to the time-delay model (Matteucci 2012). In agreement with previous studies (Matteucci et al. 1999, Romano et al. 1999), we predict that the present time Li abundance in the bulge is much higher than in the solar vicinity. However, we still need further data to draw firm conclusions about lithium evolution in this Galactic component.

NEUTRON CAPTURE ELEMENTS

Finally, I studied the chemical evolution of Zr, La, Ce and Eu in the Galactic discs and bulge by means of detailed Galactic chemical evolution models compared with the recent data by Forsberg et al. (2019). The main conclusions of this work can be summarized as follows.

- In the $[\text{Eu}/\text{Fe}]$ vs. $[\text{Fe}/\text{H}]$ plot, we observe and predict three distinct sequences, corresponding to the Galactic thick disc, thin disc and bulge (similarly to what happens in the $[\alpha/\text{Fe}]$ vs. $[\text{Fe}/\text{H}]$ plot, see Grisoni et al. 2017).
- The three sequences in the $[\text{Eu}/\text{Fe}]$ vs. $[\text{Fe}/\text{H}]$ plot are reproduced by assuming three different star formation histories for these Galactic components, with the bulge forming on a shorter timescale of formation and with higher star formation efficiency than the discs. Moreover, the thick and thin discs show a clear dichotomy, with the thick disc forming faster than the thin one, in agreement with the results of Grisoni et al. (2017).

- The assumed timescales of gas infall and star formation efficiencies have been previously tuned to reproduce the $[\alpha/\text{Fe}]$ vs. $[\text{Fe}/\text{H}]$ plots and the MDFs of the thick and thin discs (Grisoni et al. 2017) and bulge (Matteucci et al. 2019), and they allow us to nicely reproduce also the $[\text{Eu}/\text{Fe}]$ vs. $[\text{Fe}/\text{H}]$ plot.
- On the other hand, we observe and predict a different behaviour for the $[\text{X}/\text{Fe}]$ vs. $[\text{Fe}/\text{H}]$ plots of Zr, La and Ce. This is due to the double nature of these elements, which are produced by either the s- and r- processes. In fact, Zr, La and Ce are mainly produced as s-process elements by low mass stars ($1.5\text{--}3.0 M_{\odot}$) and only partly as r-process. As it is well known, the s-process elements behave as secondary elements. This fact, coupled with the long timescale of their production, produce the increase with metallicity followed by a decline.
- In the $[\text{X}/\text{Fe}]$ vs. $[\text{Fe}/\text{H}]$ plots for Zr, La and Ce, the three stellar populations are mixed and it is more difficult to disentangle them. However, the general behaviour of the observational data also in this case can be reproduced by the models and interpreted in terms of the time-delay model.

In conclusion, in addition to the study of the abundance patterns of α -elements in the Galactic discs and bulge, also looking at the abundance patterns of neutron capture elements can help in constraining the history of formation and evolution of these three Galactic components.

8.2 FUTURE PROSPECTS

Still, there are several open questions in the field of Galactic Archaeology that need to be further explored by means of Galactic chemical evolution models. For example, given the reference models developed in this Thesis for the Galactic thick disc, thin disc and bulge, here I propose some future perspectives to my work.

- For the Galactic thick and thin discs, now that we have developed a model which best reproduces the observed metallicity distribution function of thick and thin discs stars and the abundance patterns of α -elements (Grisoni et al. 2017, 2018) as well as the ones of lithium (Grisoni et al. 2019) and neutron-capture elements (Grisoni et al. 2020), we can apply it to follow also the evolution of other chemical elements. For example, recent data have appeared for carbon in the Galactic thick and thin discs (Franchini et al. 2020); in this case, it is of interest to apply the parallel model to study the evolution of carbon in these Galactic components, given the nucleosynthesis prescriptions of the best model of Romano et al. (2019). Also other chemical elements will be interesting to explore, given the separation between the thick and thin discs.
- Also concerning the Galactic bulge, now that we have developed a reference model (Matteucci et al. 2019), we can extend the study also to the other chemical elements. In particular, the recent work by Zasowski et al. (2019) has presented observations for many different chemical elements in the bulge and now it is important to compare with chemical evolution models in order to constrain the production channels of the various chemical elements.

- Regarding the study of lithium, I have investigated the evolution of this element in the Galactic halo, discs and bulge, but recent data have appeared for lithium in the Magellanic Clouds, and this data still need to be interpreted by chemical evolution models.
- More work is going to be done on abundance gradients; starting from the models of Grisoni et al. (2018), we aim at explaining not only the abundance patterns at different Galactocentric distances and abundance gradients along the thin disc, but also other properties, such as stellar, gas and SFR distributions.
- Recently, Bayesian analysis based on Markov Chain Monte Carlo (MCMC) methods has been used to test Galactic chemical evolution models (see for example Côté et al. 2017, Rybizki et al. 2017, Philcox et al. 2018, Frankel et al. 2018, Belfiore et al. 2019). In particular, Spitoni et al. (2020) used a Bayesian framework based on MCMC methods for fitting the two-infall model to the data in the solar neighborhood. The idea is then to extend this study to the other Galactocentric distances and compare with data from APOGEE and Gaia.
- Chemical evolution models are a fundamental tool to reconstruct the history of formation and evolution of our Galaxy. However, it is important to take into account also dynamical effects. The idea is then to combine the models of Grisoni et al. (2018) and Frankel et al. (2018) to perform a chemo-dynamical study of the Milky Way.

In this context, more data for different chemical elements in the different Galactic components will be extremely useful. Ongoing and future surveys will certainly help in shedding light on these and other questions, and the

comparison with theoretical predictions is needed to constrain the history of formation and evolution of our Galaxy.

Bibliography

- Abbott B. P., et al., 2017, PhRvL, 119, 161101
- Adibekyan, V.Z., Sousa, S.G., Santos, N.C., et al. 2012, A&A, 545, A32
- Anders, F., Chiappini, C., Rodrigues, T.S., et al. 2017, A&A, 597, A30
- Andrievsky, S.M., Bersier, D., Kovtyukh, V.V., et al. 2002a, A&A, 384, 140
- Andrievsky, S.M., Kovtyukh, V.V., Luck, R.E., et al. 2002b, A&A, 381, 32
- Andrievsky, S.M., Kovtyukh, V.V., Luck, R.E., et al. 2002c, A&A, 392, 491
- Andrievsky, S.M., Luck, R.E., Martin, P., & Lépine, J.R.D. 2004, A&A, 413, 159
- Arcones A., Janka H.-T., Scheck L., 2007, A&A, 467, 1227
- Argast, D., Samland, M., Gerhard, O.E., Thielemann, F.K. 2000, A&A, 356, 873
- Athanassoula, E. 2005, MNRAS, 358, 1477
- Audouze J., Tinsley B. M., 1976, ARA&A, 14, 43
- Baade W., 1944, ApJ, 100, 137

BIBLIOGRAPHY

- Ballero, S.K., Matteucci, F., Origlia, L., & Rich, R.M. 2007, *A&A*, 467, 123
- Balser, D.S., Wenger, T.V., Anderson, L.D., & Bania, T.M. 2015, *ApJ*, 806, 199
- Barbuy B., et al., 2013, *A&A*, 559, A5
- Barbuy B., et al., 2015, *A&A*, 580, A40
- Barbuy B., Chiappini C., Gerhard O., 2018, *ARA&A*, 56, 223
- Bath, G. T., & Shaviv, G. 1978, *MNRAS*, 183, 515
- Battistini C., Bensby T., 2016, *A&A*, 586, A49
- Bekki, K., & Tsujimoto, T. 2011, *MNRAS*, 416, L60
- Belfiore F., Vincenzo F., Maiolino R., Matteucci F., 2019, *MNRAS*, 487, 456
- Belokurov V., et al., 2006, *ApJL*, 642, L137
- Bensby, T., Adén, D., Meléndez, J., et al. 2011, *A&A*, 533, A134
- Bensby, T., Yee, J. C., Feltzing, S., et al. 2013, *A&A*, 549, A147
- Bensby, T., Feltzing, S., Oey, M.S. 2014, *A&A*, 562, A71
- Bensby, T., Feltzing, S., Gould, A., et al. 2017, *A&A*, 605, A89
- Bensby, T., & Lind, K. 2018, *A&A*, 615, A151
- Benson A. J., Bower R., 2010, *MNRAS*, 405, 1573
- Bernard, E. J., Schultheis, M., Di Matteo, P., et al. 2018, *MNRAS*, 477, 3507

- Bland-Hawthorn J., Gerhard O., 2016, ARA&A, 54, 529
- Bilitewski, T., & Schönrich, R. 2012, MNRAS, 426, 2266
- Bird J. C., Kazantzidis S., Weinberg D. H., Guedes J., Callegari S., Mayer L., Madau P., 2013, ApJ, 773, 43
- Bisterzo S., Travaglio C., Wiescher M., Käppeler F., Gallino R., 2017, ApJ, 835, 97
- Boissier S., 2013, pss6.book, 141, pss6.book
- Boissier S., Prantzos N., 1999, MNRAS, 307, 857
- Bonetti M., Perego A., Dotti M., Cescutti G., 2019, MNRAS, 490, 296
- Bonifacio, P., & Molaro, P. 1997, MNRAS, 285, 847
- Bonifacio, P., Molaro, P., Sivarani, T., et al. 2007, A&A, 462, 851
- Bonifacio, P., Caffau, E., Spite, M., et al. 2015, A&A, 579, A28
- Bonsack, W. K., & Greenstein, J. L. 1960, ApJ, 131, 83
- Bovy, J., & Rix, H.W. 2013, ApJ, 779, 115
- Bovy, J., Nidever, D.L., Rix, H.-W., et al. 2014, ApJ, 790, 127
- Bovy, J. 2015, ApJS, 216, 29
- Brook C. B., Kawata D., Gibson B. K., Freeman K. C., 2004, ApJ, 612, 894
- Brook C., Richard S., Kawata D., Martel H., Gibson B. K., 2007, ApJ, 658, 60

BIBLIOGRAPHY

- Brook C. B., et al., 2012, MNRAS, 426, 690
- Bovy, J. 2017, MNRAS, 470, 1360
- Buck T., Macciò A. V., Obreja A., Dutton A. A., Domínguez-Tenreiro R., Granato G. L., 2017, MNRAS, 468, 3628
- Buck T., Obreja A., Macciò A. V., Minchev I., Dutton A. A., Ostriker J. P., 2020a, MNRAS, 491, 3461
- Buck T., 2020b, MNRAS, 491, 5435
- Buder, S., Asplund, M., Duong, L., et al. 2018, MNRAS, 478, 4513
- Burbidge E. M., Burbidge G. R., Fowler W. A., Hoyle F., 1957, RvMP, 29, 547
- Burstein D., 1979, ApJ, 234, 829
- Calamida, A., Sahu, K. C., Casertano, S., et al. 2015, ApJ, 810, 8
- Calura F., Menci N., 2009, MNRAS, 400, 1347
- Cameron A. G. W., 1957, AJ, 62, 9
- Cameron, A. G. W., & Fowler, W. A. 1971, ApJ, 164, 111
- Cappellaro, E., & Turatto, M. 1997, NATO Advanced Science Institutes (ASI) Series C, 486, 77
- Carollo D., et al., 2007, Natur, 450, 1020
- Carretta E., Gratton R. G., Sneden C., 2000, A&A, 356, 238
- Casagrande, L., Schönrich, R., Asplund, M., et al. 2011, A&A, 530, A138

- Cavichia, O., Mollá, M., Costa, R.D.D., & Maciel, W.J. 2014, MNRAS, 437, 3688
- Cayrel R., et al., 2001, Natur, 409, 691
- Cescutti, G. 2008, A&A, 481, 691
- Cescutti G., François P., Matteucci F., Cayrel R., Spite M., 2006, A&A, 448, 557
- Cescutti, G., Matteucci, F., François, P., & Chiappini, C. 2007, A&A, 462, 943
- Cescutti, G., & Matteucci, F. 2011, A&A, 525, A126
- Cescutti G., Chiappini C., Hirschi R., Meynet G., Frischknecht U., 2013, A&A, 553, A51
- Cescutti G., Chiappini C., 2014, A&A, 565, A51
- Cescutti G., Romano D., Matteucci F., Chiappini C., Hirschi R., 2015, A&A, 577, A139
- Cescutti G., Molaro P., 2019, MNRAS, 482, 4372
- Chabrier G., 2003, PASP, 115, 763
- Chang, R.X., Hou, J.L., Shu, C.G., Fu, C.Q. 1999, A&A, 350, 38
- Charbonnel, C., & Primas, F. 2005, A&A, 442, 961
- Chiappini C., 2001, AmSci, 89, 506
- Chiappini, C. 2009, The Galaxy Disk in Cosmological Context, 254, 191

BIBLIOGRAPHY

- Chiappini, C., Matteucci, F., Gratton, R. 1997, *ApJ*, 477, 765
- Chiappini C., Matteucci F., Beers T. C., Nomoto K., 1999, *ApJ*, 515, 226
- Chiappini, C., Matteucci, F., & Romano, D. 2001, *ApJ*, 554, 1044
- Chiosi, C. 1980, *A&A*, 83, 206
- Cirasuolo M., et al., 2014, *SPIE*, 91470N, *SPIE*.9147
- Clarkson, W. I., Sahu, K. C., Anderson, J., et al. 2011, *ApJ*, 735, 37
- Coc, A., Uzan, J.-P., & Vangioni, E. 2014, *J. Cosmology Astropart. Phys.*, 10, 050
- Colavitti E., Cescutti G., Matteucci F., Murante G., 2009, *A&A*, 496, 429
- Combes, F., Debbasch, F., Friedli, D., & Pfenniger, D. 1990, *A&A*, 233, 82
- Côté B., O'Shea B. W., Ritter C., Herwig F., Venn K. A., 2017, *ApJ*, 835, 128
- Côté B., Silvia D. W., O'Shea B. W., Smith B., Wise J. H., 2018, *ApJ*, 859, 67
- Côté B., et al., 2019, *ApJ*, 875, 106
- Cowan J. J., Thielemann F.-K., Truran J. W., 1991, *PhR*, 208, 267
- Cresci, G., Mannucci, F., Maiolino, R., et al. 2010, *Nature*, 467, 811
- Cristallo, S., Straniero, O., Gallino, R., et al. 2009, *ApJ*, 696, 797
- Cristallo, S., Piersanti, L., Straniero, O., et al. 2011, *ApJS*, 197, 17

- Crosby B. D., O'Shea B. W., Beers T. C., Tumlinson J., 2016, *ApJ*, 820, 71
- Cui X.-Q., et al., 2012, *RAA*, 12, 1197
- Dalton G., et al., 2014, *SPIE*, 91470L, *SPIE*.9147
- D'Antona, F., & Matteucci, F. 1991, *A&A*, 248, 62
- da Silveira C. R., et al., 2018, *A&A*, 614, A149
- Debattista, V. P., Ness, M., Gonzalez, O. A., et al. 2017, *MNRAS*, 469, 1587
- Deharveng, L., Peña, M., Caplan, J., & Costero, R. 2000, *MNRAS*, 311, 329
- de Jong R. S., et al., 2014, *SPIE*, 91470M, *SPIE*.9147
- de Laverny, P., Recio-Blanco, A., Worley, C.C., & Plez, B. 2012, *A&A*, 544, A126
- de Laverny, P., Recio-Blanco, A., Worley, C.C., et al. 2013, *The Messenger*, 153, 18
- Delgado Mena, E., Bertrán de Lis, S., Adibekyan, V. Z., et al. 2015, *A&A*, 576, A69
- Delgado Mena E., Tsantaki M., Adibekyan V. Z., Sousa S. G., Santos N. C., González Hernández J. I., Israelian G., 2017, *A&A*, 606, A94
- De Lucia G., Blaizot J., 2007, *MNRAS*, 375, 2
- De Lucia G., 2012, *AN*, 333, 460
- De Pascale, M., Worley, C.C., de Laverny, P., et al. 2014, *A&A*, 570, A68

BIBLIOGRAPHY

- Di Matteo, P., Haywood, M., Combes, F., Semelin, B., & Snaith, O.N. 2013, *A&A*, 553, A102
- Domogatskii, G. V., Eramzhian, R. A., & Nadezhin, D. K. 1978, *Ap&SS*, 58, 273
- Duong L., Asplund M., Nataf D. M., Freeman K. C., Ness M., 2019, *MNRAS*, 486, 5349
- Elmegreen B. G., 1999, *ApJ*, 527, 266
- Esteban, C., García-Rojas, J., Peimbert, M., et al. 2005, *ApJ*, 618, L95
- Ferrini, F., Matteucci, F., Pardi, C., Penco, U. 1992, *ApJ*, 387, 138
- Ferrini, F., Molla, M., Pardi, M.C., & Diaz, A.I. 1994, *ApJ*, 427, 745
- Fontanot F., De Lucia G., Hirschmann M., Bruzual G., Charlot S., Zibetti S., 2017, *MNRAS*, 464, 3812
- Forsberg R., Jönsson H., Ryde N., Matteucci F., 2019, *arXiv*, arXiv:1909.10535
- Fragkoudi, F., Di Matteo, P., Haywood, M., et al. 2018, *A&A*, 616, A180
- Franchini M., et al., 2020, *ApJ*, 888, 55
- François, P., Matteucci, F., Cayrel, R., et al. 2004, *A&A*, 421, 613
- Frankel N., Rix H.-W., Ting Y.-S., Ness M., Hogg D. W., 2018, *ApJ*, 865, 96
- Frebel A., Christlieb N., Norris J. E., Thom C., Beers T. C., Rhee J., 2007, *ApJL*, 660, L117

- Freeman K., et al., 2013, MNRAS, 428, 3660
- Frischknecht U., Hirschi R., Thielemann F.-K., 2012, A&A, 538, L2
- Frischknecht U., et al., 2016, MNRAS, 456, 1803
- Fu X., Bressan A., Molaro P., Marigo P., 2015, MNRAS, 452, 3256
- Fu, X., Romano, D., Bragaglia, A., et al. 2018, A&A, 610, A38
- Gaia Collaboration, Prusti, T., de Bruijne, J.H.J., et al. 2016, A&A, 595, A1
- Gaia Collaboration, Brown, A.G.A., Vallenari, A., et al. 2016, A&A, 595, A2
- Gao, S., Liu, C., Zhang, X., et al. 2014, ApJ, 788, L37
- Gao, S., Zhao, H., Yang, H., & Gao, R. 2017, MNRAS, 469, L68
- Genovali, K., Lemasle, B., da Silva, R., et al. 2015, A&A, 580, A17
- Gilmore G., Reid N., 1983, MNRAS, 202, 1025
- Gilmore, G., Randich, S., Asplund, M., et al. 2012, The Messenger, 147, 25
- Goetz, M., & Koeppen, J. 1992, A&A, 262, 455
- Gonzalez, O. A., Zoccali, M., Monaco, L., et al. 2009, A&A, 508, 289
- Goswami A., Prantzos N., 2000, A&A, 359, 191
- Grand, R.J.J., Kawata, D., & Cropper, M. 2015, MNRAS, 447, 4018
- Grand R. J. J., et al., 2016, MNRAS, 460, L94

BIBLIOGRAPHY

- Grand, R.J.J., Bustamante, S., Gómez, F.A., et al. 2018, MNRAS, 474, 3629
- Grevesse, N., Asplund, M., Sauval, A.J. 2007, SSR, 130, 105
- Grieco, V., Matteucci, F., Pipino, A., & Cescutti, G. 2012, A&A, 548, A60
- Grisoni, V., Spitoni, E., Matteucci, F., et al. 2017, MNRAS, 472, 3637
- Grisoni, V., Spitoni, E., & Matteucci, F. 2018, MNRAS, 481, 2570
- Grisoni V., Matteucci F., Romano D., Fu X., 2019, MNRAS, 489, 3539
- Grisoni V., Cescutti G., Matteucci F., Forsberg R., Jönsson H., Ryde N., 2020, MNRAS, 492, 2828
- Guiglion, G., de Laverny, P., Recio-Blanco, A., et al. 2016, A&A, 595, A18
- Guiglion G., de Laverny P., Recio-Blanco A., Prantzos N., 2018, A&A, 619, A143
- Guiglion G., et al., 2019, A&A, 623, A99
- Guo Q., et al., 2011, MNRAS, 413, 101
- Hansen, T., Hansen, C. J., Christlieb, N., et al. 2014, ApJ, 787, 162
- Hartwick F. D. A., 1987, ASIC, 281, ASIC..207
- Hayden, M.R., Bovy, J., Holtzman, J.A., et al. 2015, ApJ, 808, 132
- Hayden M. R., Recio-Blanco A., de Laverny P., Mikolaitis S., Worley C. C., 2017, A&A, 608, L1
- Hayes C. R., et al., 2018, ApJ, 852, 49

- Haynes C. J., Kobayashi C., 2019, MNRAS, 483, 5123
- Haywood M., 2008, MNRAS, 388, 1175
- Haywood, M., Di Matteo, P., Lehnert, M.D., Katz, D., & Gómez, A. 2013, A&A, 560, A109
- Haywood, M., Di Matteo, P., Snaith, O., Lehnert, M.D. 2015, A&A, 579, A5
- Haywood, M., Di Matteo, P., Snaith, O., & Calamida, A. 2016, A&A, 593, A82
- Haywood, M., Lehnert, M.D., Di Matteo, P. et al. 2016, A&A, 589, A66
- Haywood M., Di Matteo P., Lehnert M., Snaith O., Fragkoudi F., Khoperskov S., 2018, A&A, 618, A78
- Helmi A., 2008, A&ARv, 15, 145
- Hill V., et al., 2002, A&A, 387, 560
- Hill, V., Lecureur, A., Gómez, A., et al. 2011, A&A, 534, A80
- Huang, Y., Liu, X.W., Zhang, H.W., et al. 2015, Research in Astronomy and Astrophysics, 15, 1240
- Hubble E. P., 1926, ApJ, 64, 321
- Ibata R. A., Wyse R. F. G., Gilmore G., Irwin M. J., Suntzeff N. B., 1997, AJ, 113, 634
- Iwamoto K., Brachwitz F., Nomoto K., Kishimoto N., Umeda H., Hix W. R., Thielemann F.-K., 1999, ApJS, 125, 439

BIBLIOGRAPHY

- Izzo, L., Della Valle, M., Mason, E., et al. 2015, *ApJ*, 808, L14
- Johnson C. I., Rich R. M., Kobayashi C., Fulbright J. P., 2012, *ApJ*, 749, 175
- Jönsson H., Ryde N., Nordlander T., Pehlivan Rhodin A., Hartman H., Jönsson P., Eriksson K., 2017, *A&A*, 598, A100
- Jönsson H., Ryde N., Schultheis M., Zoccali M., 2017, *A&A*, 600, C2
- Jørgensen, B. R., & Lindegren, L. 2005, *A&A*, 436, 127
- Kalogera V., et al., 2004, *ApJL*, 614, L137
- Karakas A. I., 2010, *MNRAS*, 403, 1413
- Kennicutt, R. C., Jr, 1998a, *ApJ*, 498, 541
- Kennicutt, R. C., Jr, 1998b, *ARA&A*, 36, 189
- Kirby, E. N., Guhathakurta, P., Zhang, A. J., et al. 2016, *ApJ*, 819, 135
- Kroupa, P., Tout, C.A., Gilmore, G., 1993, *MNRAS*, 262, 545
- Kroupa, P. 2001, *MNRAS*, 322, 231
- Kobayashi C., Umeda H., Nomoto K., Tominaga N., Ohkubo T., 2006, *ApJ*, 653, 1145
- Kobayashi C., Nakasato N., 2011, *ApJ*, 729, 16
- Kobayashi C., Leung S.-C., Nomoto K., 2019, *arXiv*, arXiv:1906.09980
- Komiya Y., Yamada S., Suda T., Fujimoto M. Y., 2014, *ApJ*, 783, 132

- Korobkin O., Rosswog S., Arcones A., Winteler C., 2012, MNRAS, 426, 1940
- Kubryk, M., Prantzos, N., & Athanassoula, E. 2013, MNRAS, 436, 1479
- Kubryk, M., Prantzos, N., & Athanassoula, E. 2015a, A&A, 580, A126
- Kubryk, M., Prantzos, N., & Athanassoula, E. 2015b, A&A, 580, A127
- Kuijken K., Gilmore G., 1991, ApJL, 367, L9
- Lacey, C.G., & Fall, S.M. 1985, ApJ, 290, 154
- Larson R. B., 1976, MNRAS, 176, 31
- Lecureur A., et al., 2007, A&A, 465, 799
- Lemoine, M., Vangioni-Flam, E., & Cassé, M. 1998, ApJ, 499, 735
- Li, W., Chornock, R., Leaman, J., et al. 2011, MNRAS, 412, 1473
- Limongi M., Chieffi A., 2018, ApJS, 237, 13
- Lindegren, L., Lammers, U., Bastian, U., et al. 2016, A&A, 595, A4
- Lodders, K., Palme, H., & Gail, H.-P. 2009, Landolt Börnstein, 712
- Loebman S. R., Roškar R., Debattista V. P., Ivezić Ž., Quinn T. R., Wadsley J., 2011, ApJ, 737, 8
- Loebman, S.R., Debattista, V.P., Nidever, D.L., et al. 2016, ApJ, 818, L6
- Lomaeva M., Jönsson H., Ryde N., Schultheis M., Thorsbro B., 2019, A&A, 625, A141

BIBLIOGRAPHY

- Luck, R.E., Gieren, W.P., Andrievsky, S.M., et al. 2003, *A&A*, 401, 939
- Luck, R.E., & Lambert, D.L. 2011, *AJ*, 142, 136
- Maciel, W.J., & Costa, R.D.D. 2009, *The Galaxy Disk in Cosmological Context*, 254, 38
- Maciel, W.J., & Costa, R.D.D. 2013, *Revista Mexicana de Astronomia y Astrofisica*, 49, 333
- Magrini, L., Sestito, P., Randich, S., & Galli, D. 2009, *A&A*, 494, 95
- Magrini, L., Coccato, L., Stanghellini, L., Casasola, V., & Galli, D. 2016, *A&A*, 588, A91
- Magrini, L., Randich, S., Kordopatis, G., et al. 2017, *A&A*, 603, A2
- Majewski, S.R., Schiavon, R.P., Frinchaboy, P.M., et al. 2015, *arXiv:1509.05420*
- Martig, M., Fouesneau, M., Rix, H.-W., et al. 2016, *MNRAS*, 456, 3655
- Martin, C.L., Kennicutt, R.C., Jr. 2001, *ApJ*, 555, 301
- Masseron, T., & Gilmore, G. 2015, *MNRAS*, 453, 1855
- Matteucci, F. 2001, *The Chemical Evolution of the Galaxy*, ASSL, Kluwer Academic Publisher
- Matteucci F., 2012, *Chemical Evolution of Galaxies*. Springer-Verlag, Berlin
- Matteucci, F., & Greggio, L., 1986, *A&A*, 154, 279
- Matteucci, F., & Francois, P., 1989, *MNRAS*, 239, 885

- Matteucci, F., & Brocato, E. 1990, *ApJ*, 365, 539
- Matteucci, F., & Francois P., 1992, *A&A*, 262, L1
- Matteucci F., Romano D., Molaro P., 1999, *A&A*, 341, 458
- Matteucci, F., Spitoni, E., Recchi, S., Valiante, R. 2009, *A&A*, 501, 531
- Matteucci F., 2010, *IAUS*, 453, *IAUS..268*
- Matteucci F., Romano D., Arcones A., Korobkin O., Rosswog S., 2014, *MNRAS*, 438, 2177
- Matteucci, F., Spitoni, E., & Grisoni, V. 2018, *Rediscovering Our Galaxy*, 334, 298
- Matteucci F., Grisoni V., Spitoni E., Zulianello A., Rojas-Arriagada A., Schultheis M., Ryde N., 2019, *MNRAS*, 487, 5363
- McKee, C.F., Parravano, A., & Hollenbach, D.J. 2015, *ApJ*, 814, 13
- McWilliam, A., & Rich, R. M. 1994, *ApJS*, 91, 749
- Meléndez, J., Casagrande, L., Ramírez, I., Asplund, M., & Schuster, W. J. 2010, *A&A*, 515, L3
- Meneguzzi, M., Audouze, J., & Reeves, H. 1971, *International Cosmic Ray Conference*, 1, 196
- Micali, A., Matteucci, F., Romano, D. 2013, *MNRAS*, 436, 1648
- Mikolaitis, Š., Hill, V., Recio-Blanco, A. et al. 2014, *A&A*, 572, A33
- Mikolaitis, Š., de Laverny, P., Recio-Blanco, A. et al. 2017, *A&A*, 600, A22

BIBLIOGRAPHY

- Minchev, I., Chiappini, C., & Martig, M. 2013, *A&A*, 558, A9
- Minchev I., Chiappini C., Martig M., 2014, *A&A*, 572, A92
- Minchev I., et al., 2018, *MNRAS*, 481, 1645
- Minchev I., et al., 2019, *MNRAS*, 487, 3946
- Minniti, D., Lucas, P. W., Emerson, J. P., et al. 2010, *New Astron.*, 15, 433
- Miranda M. S., et al., 2016, *A&A*, 587, A10
- Mishenina T. V., et al., 2013, *A&A*, 552, A128
- Molaro, P., Bonifacio, P., Castelli, F., & Pasquini, L. 1997, *A&A*, 319, 593
- Molaro, P., Izzo, L., Mason, E., Bonifacio, P., & Della Valle, M. 2016, *MNRAS*, 463, L117
- Mollá, M., & Díaz, A.I. 2005, *MNRAS*, 358, 521
- Monaco P., Fontanot F., Taffoni G., 2007, *MNRAS*, 375, 1189
- Mott, A., Spitoni, E., & Matteucci, F. 2013, *MNRAS*, 435, 2918
- Nandakumar G., et al., 2018, *MNRAS*, 478, 4374
- Navarro J. F., et al., 2018, *MNRAS*, 476, 3648
- Nesti, F., Salucci, P. 2013, *JCAP*, 7, 016
- Nishimura N., Takiwaki T., Thielemann F.-K., 2015, *ApJ*, 810, 109
- Nissen P. E., Gustafsson B., Edvardsson B., Gilmore G., 1994, *A&A*, 285, 440

- Nissen P. E., Schuster W. J., 2010, *A&A*, 511, L10
- Noguchi M., 2018, *Natur*, 559, 585
- Nogueras-Lara, F., Schödel, R., Dong, H., et al. 2018, [arXiv:1809.07627](https://arxiv.org/abs/1809.07627)
- Nomoto, K., Kobayashi, C., & Tominaga, N. 2013, *ARA&A*, 51, 457
- Nordström, B., Mayor, M., Andersen, J., et al. 2004, *A&A*, 418, 989
- Norman, C. A., Sellwood, J. A., & Hasan, H. 1996, *ApJ*, 462, 114
- Obreja A., Stinson G. S., Dutton A. A., Macciò A. V., Wang L., Kang X., 2016, *MNRAS*, 459, 467
- Pagel B. E. J., Patchett B. E., 1975, *MNRAS*, 172, 13
- Pardi M. C., Ferrini F., 1994, *ApJ*, 421, 491
- Pardi M. C., Ferrini F., Matteucci F., 1995, *ApJ*, 444, 207
- Perryman, M. A. C., de Boer, K. S., Gilmore, G., et al. 2001, *A&A*, 369, 339
- Petit P., et al., 2014, *PASP*, 126, 469
- Pezzulli, G., Fraternali, F., & Binney, J. 2017, *MNRAS*, 467, 311
- Philcox O., Rybizki J., Gutcke T. A., 2018, *ApJ*, 861, 40
- Pilkington, K., Few, C.G., Gibson, B.K., et al. 2012, *A&A*, 540, A56
- Piskunov N., Valenti J. A., 2017, *A&A*, 597, A16
- Portinari, L., & Chiosi C., 1999, *A&A*, 350, 827

BIBLIOGRAPHY

- Portinari, L., & Chiosi, C. 2000, *A&A*, 355, 929
- Prantzos, N., & Aubert O., 1995, *A&A*, 302, 69
- Prantzos, N., & Boissier, S. 2000, *MNRAS*, 313, 338
- Prantzos, N. 2012, *A&A*, 542, A67
- Prantzos, N., de Laverny, P., Guiglion, G., Recio-Blanco, A., & Worley, C. C. 2017, *A&A*, 606, A132
- Prantzos, N., Abia, C., Limongi, M., Chieffi, A., & Cristallo, S. 2018, *MNRAS*, 476, 3432
- Rahimi A., Carrell K., Kawata D., 2014, *RAA*, 14, 1406-1414
- Ramírez, I., Fish, J. R., Lambert, D. L., & Allende Prieto, C. 2012, *ApJ*, 756, 46
- Recio-Blanco, A., Bijaoui, A., & de Laverny, P. 2006, *MNRAS*, 370, 141
- Recio-Blanco, de Laverny, P., Kordopatis, G., et al. 2014, *A&A*, 567, A5
- Recio-Blanco, A., de Laverny, P., Allende Prieto, C., et al. 2016, *A&A*, 585, A93
- Reeves, H., Fowler, W. A., & Hoyle, F. 1970, *Nature*, 226, 727
- Renzini, A., Gennaro, M., Zoccali, M., et al. 2018, *ApJ*, 863, 16
- Rizzuti F., Cescutti G., Matteucci F., Chieffi A., Hirschi R., Limongi M., 2019, *MNRAS*, 489, 5244
- Rockosi C., Beers T. C., Majewski S., Schiavon R., Eisenstein D., 2009, *astro*, 14, astro2010

- Rojas-Arriagada, A., Recio-Blanco, A., de Laverny, P., et al. 2017, *A&A*, 601, A140
- Rojas-Arriagada A., et al., 2019, *A&A*, 626, A16
- Romano, D., Matteucci, F., Molaro, P., & Bonifacio, P. 1999, *A&A*, 352, 117
- Romano, D., Matteucci, F., Salucci, P., & Chiappini, C. 2000, *ApJ*, 539, 235
- Romano, D., Matteucci, F., Ventura, P., & D'Antona, F. 2001, *A&A*, 374, 646
- Romano, D., Tosi, M., Matteucci, F., & Chiappini, C. 2003, *MNRAS*, 346, 295
- Romano D., Karakas A. I., Tosi M., Matteucci F., 2010, *A&A*, 522, A32
- Romano D., Starkenburg E., 2013, *MNRAS*, 434, 471
- Romano D., Bellazzini M., Starkenburg E., Leaman R., 2015, *MNRAS*, 446, 4220
- Romano D., Matteucci F., Zhang Z.-Y., Ivison R. J., Ventura P., 2019, *MNRAS*, 490, 2838
- Rosswog S., Liebendörfer M., Thielemann F.-K., Davies M. B., Benz W., Piran T., 1999, *A&A*, 341, 499
- Ryan S. G., Norris J. E., 1991, *AJ*, 101, 1865
- Rybizki J., Just A., Rix H.-W., 2017, *A&A*, 605, A59
- Rudolph, A.L., Fich, M., Bell, G.R., et al. 2006, *ApJS*, 162, 346

BIBLIOGRAPHY

- Sackmann, I.-J., & Boothroyd, A. I. 1992, *ApJ*, 392, L71
- Sackmann, I.-J., & Boothroyd, A. I. 1999, *ApJ*, 510, 217
- Salpeter, E. E. 1955, *ApJ*, 121, 161
- Samland, M., & Gerhard, O. E. 2003, *A&A*, 399, 961
- Sbordone, L., Bonifacio, P., Caffau, E., et al. 2010, *A&A*, 522, A26
- Scalo, J.M. 1986, *Fund. Cosmic Phys.*, 11, 1
- Scannapieco C., White S. D. M., Springel V., Tissera P. B., 2011, *MNRAS*, 417, 154
- Schmidt M., 1959, *ApJ*, 129, 243
- Schönrich, R., & Binney, J. 2009, *MNRAS*, 396, 203
- Schönrich, R., & Weinberg, D. H. 2019, *MNRAS*, 487, 580
- Schultheis, M., Rojas-Arriagada, A., García Pérez, A. E., et al. 2017, *A&A*, 600, A14
- Schultheis, M., Cunha, K., Zasowski, G., et al. 2015, *A&A*, 584, A45
- Selvelli, P., Molaro, P., & Izzo, L. 2018, *MNRAS*, 481, 2261
- Shen, S., Wadsley, J., & Stinson, G. 2010, *MNRAS*, 407, 1581
- Shen S., Cooke R. J., Ramirez-Ruiz E., Madau P., Mayer L., Guedes J., 2015, *ApJ*, 807, 115
- Simonetti P., Matteucci F., Greggio L., Cescutti G., 2019, *MNRAS*, 486, 2896

- Sommer-Larsen J., Yoshii Y., 1989, MNRAS, 238, 133
- Smiljanic, R., Pasquini, L., Bonifacio, P., et al. 2009, A&A, 499, 103
- Snaith O. N., Haywood M., Di Matteo P., Lehnert M. D., Combes F., Katz D., Gómez A., 2014, ApJL, 781, L31
- Snaith, O., Haywood, M., Di Matteo, P., et al. 2015, A&A, 578, A87
- Snedden C., McWilliam A., Preston G. W., Cowan J. J., Burris D. L., Armosky B. J., 1996, ApJ, 467, 819
- Snedden C., Cowan J. J., Gallino R., 2008, ARA&A, 46, 241
- Somerville R. S., Hopkins P. F., Cox T. J., Robertson B. E., Hernquist L., 2008, MNRAS, 391, 481
- Somerville R. S., Davé R., 2015, ARA&A, 53, 51
- Spite, F., & Spite, M. 1982, A&A, 115, 357
- Spite, F., & Spite, M. 1986, A&A, 163, 140
- Spitoni, E., & Matteucci, F. 2011, A&A, 531, A72
- Spitoni, E., Matteucci, F., & Marcon-Uchida, M.M. 2013, A&A, 551, A123
- Spitoni, E., Romano, D., Matteucci, F., & Ciotti, L. 2015, ApJ, 802, 129
- Spitoni, E., Matteucci, F., Jönsson, H., Ryde, N., & Romano, D. 2018, A&A, 612, A16
- Spitoni, E., Silva Aguirre, V., Matteucci, F., Calura, F., & Grisoni, V. 2019, A&A, 623, 60

BIBLIOGRAPHY

- Spitoni E., Verma K., Silva Aguirre V., Calura F., 2020, arXiv, arXiv:1912.04312
- Stanghellini, L., & Haywood, M. 2010, ApJ, 714, 1096
- Stanghellini L., Haywood M., 2018, ApJ, 862, 45
- Starkenbug E., et al., 2013, MNRAS, 429, 725
- Starrfield, S., Truran, J. W., & Sparks, W. M. 1978, ApJ, 226, 186
- Steinmetz M., et al., 2006, AJ, 132, 1645
- Stinson G. S., et al., 2013, MNRAS, 436, 625
- Tajitsu, A., Sadakane, K., Naito, H., Arai, A., & Aoki, W. 2015, Nature, 518, 381
- Tajitsu, A., Sadakane, K., Naito, H., et al. 2016, ApJ, 818, 191
- Talbot R. J., Arnett W. D., 1973, ApJ, 186, 51
- Telting J. H., et al., 2014, AN, 335, 41
- Thygesen A. O., et al., 2012, A&A, 543, A160
- Tinsley B. M., 1976, ApJ, 208, 797
- Tosi M., 1988, A&A, 197, 47
- Travaglio, C., Randich, S., Galli, D., et al. 2001, ApJ, 559, 909
- Truran J. W., 1981, A&A, 97, 391
- Tsikoudi V., 1979, ApJ, 234, 842

- Tsujimoto T., Nomoto K., Yoshii Y., Hashimoto M., Yanagida S., Thielemann F.-K., 1995, MNRAS, 277, 945
- Tsujimoto, T., & Bekki, K. 2012, ApJ, 747, 125
- Tumlinson J., 2006, ApJ, 641, 1
- Tumlinson J., 2010, ApJ, 708, 1398
- Tumlinson J., Peebles M. S., Werk J. K., 2017, ARA&A, 55, 389
- Uttenthaler, S., Schultheis, M., Nataf, D. M., et al. 2012, A&A, 546, A57
- Valenti J. A., Piskunov N., 1996, A&AS, 118, 595
- Valenti, E., Zoccali, M., Renzini, A., et al. 2013, A&A, 559, A98
- Van der Swaelmen M., Barbuy B., Hill V., Zoccali M., Minniti D., Ortolani S., Gómez A., 2016, A&A, 586, A1
- van de Voort F., Quataert E., Hopkins P. F., Kereš D., Faucher-Giguère C.-A., 2015, MNRAS, 447, 140
- Ventura, P., Di Criscienzo, M., Carini, R., & D'Antona, F. 2013, MNRAS, 431, 3642
- Vincenzo F., Kobayashi C., 2018, MNRAS, 478, 155
- Vincenzo F., Spitoni E., Calura F., Matteucci F., Silva Aguirre V., Miglio A., Cescutti G., 2019, MNRAS, 487, L47
- Vogelsberger M., Marinacci F., Torrey P., Puchwein E., 2020, NatRP, 2, 42
- Yates R. M., Henriques B., Thomas P. A., Kauffmann G., Johansson J., White S. D. M., 2013, MNRAS, 435, 3500

BIBLIOGRAPHY

- Yoshii Y., 1982, PASJ, 34, 365
- Yuan, H., Liu, X., Xiang, M., Huang, Y., & Chen, B. 2015, ApJ, 803, 13
- Wang, Y., & Zhao, G. 2013, ApJ, 769, 4
- Wheeler J. C., Sneden C., Truran J. W., 1989, ARA&A, 27, 279
- White S. D. M., Rees M. J., 1978, MNRAS, 183, 341
- Winteler C., et al., 2012, ApJL, 750, L22
- Wong, T., Blitz, L., & Bosma, A. 2004, ApJ, 605, 183
- Worley, C.C., de Laverny, P., Recio-Blanco, A., et al. 2012, A&A, 542, A48
- Wyse, R. F. G., & Gilmore, G. 1992, AJ, 104, 144
- Xiang, M.S., Liu, X.W., Yuan, H.B., et al. 2015, Research in Astronomy and Astrophysics, 15, 1209
- Xiang, M., Liu, X., Shi, J., et al. 2017, ApJS, 232, 2
- Yanny B., et al., 2009, AJ, 137, 4377
- Zasowski G., et al., 2019, ApJ, 870, 138
- Zhang, L., Rix, H.W., van de Ven, G., et al. 2013, ApJ, 772, 108
- Zoccali M., et al., 2006, A&A, 457, L1
- Zoccali M., et al., 2008, A&A, 486, 177
- Zoccali, M., Gonzalez, O. A., Vasquez, S., Hill. V., et al. 2014, A&A, 562,
- 66

BIBLIOGRAPHY

- Zoccali, M., Vasquez, S., Gonzalez, O. A., et al. 2017, *A&A*, 599, A12
- Zucker D. B., de Silva G., Freeman K., Bland-Hawthorn J., Hermes Team, 2012, *ASPC*, 421, *ASPC*..458

Curriculum vitae

Name:	Valeria Grisoni
Born:	23th June 1992 in Trieste, Italy
Citizenship:	Italian
Education:	
2016-today	PhD in Physics, University of Trieste, Italy Thesis supervisor: prof. F. Matteucci
2016	MSc in Physics, University of Trieste, Italy Thesis supervisor: prof. F. Matteucci Final mark: 110/110 <i>cum laude</i>
2014	BSc in Physics, University of Trieste, Italy Thesis supervisor: prof. A. Bassi Final mark: 110/110 <i>cum laude</i>
2011	Diploma, Liceo Classico F. Petrarca, Trieste, Italy Final mark: 100/100 <i>cum laude</i>
Scholarship and awards:	
2016-today	PhD scholarship, University of Trieste, Italy
2016	Merit prizes for MSc results (Enasarco, BCC)
2014	Merit prizes for BSc results (Enasarco, BCC)
2011	Merit prize for Diploma results (MIUR)

Acknowledgements

I would like to start by expressing my sincere gratitude to my super supervisor professor Francesca Matteucci for having introduced me to the wonderful field of Galactic Archaeology, for having taught me and still teaching me a lot about doing research in Astrophysics, and for having depicted to me the way that I want to follow in my life. Thanks for being an example for me not only as a brilliant astrophysicist, but also as a great woman.

Then, I thank my co-supervisor Emanuele Spitoni for his collaboration and for all the useful comments and suggestions which have certainly improved my work.

Moreover, I would like to acknowledge my referees, Chiaki Kobayashi and Benoit Côté, for having read my Thesis and provided their very constructive feedback.

I am also grateful to many other researchers who contributed to my work. I thank Alejandra Recio-Blanco and Patrick de Laverny for their fundamental contribution regarding the observational data and for having invited me at the Observatory of Nice. I warmly thank Donatella Romano for her precious advice on lithium and for having hosted me at the Observatory of Bologna. I also thank Gabriele Cescutti for his important contribution on neutron capture elements. I acknowledge many other researchers in the

ACKNOWLEDGEMENTS

field of Galactic Archaeology for enlightening suggestions. Then, thanks to my colleagues at the Observatory of Trieste and at the Department of Physics of the University of Trieste, and to all my very best friends who accompanied and supported me throughout this wonderful journey called PhD.

Finally, I would like to thank my family for being always by my side. I thank my parents Francesca and Maurizio, for having supported me in doing what I love and for always being curious about my work; my sister Paola, for being my number one fan since childhood; and all my extended family for all the love and support. Last but not least, I thank my love Matteo: the starry sky above me and you by my side make me feel full of wonder and possibility, and I am immensely thankful.